

Deep Learning Based Framework for DTI Parameters  
Estimation and Analysis for Sparse Diffusion MRI data

# SHIV NADAR

INSTITUTION OF EMINENCE DEEMED TO BE  
**UNIVERSITY**  
DELHI NCR

*Ph.D. Thesis*  
*Submitted in partial fulfillment*  
*of the requirements for the degree of*

**Doctor of Philosophy**  
in  
**Computer Science and Engineering**

*by:*

**Abhishek Tiwari**

**Roll No. 2010120961**

*Advisor:*

**Dr. Rajeev Kumar Singh**

**Dr. Saurabh J. Shigwan**

**Shiv Nadar Institution of Eminence, Delhi NCR**

**Computer Science and Engineering**

Gautam Buddha Nagar,

Uttar Pradesh - 201314, India

March, 2024

## **DECLARATION**

This is to declare that the thesis titled **Deep Learning Based Framework for DTI Parameters Estimation and Analysis for Sparse Diffusion MRI data** submitted by me to Shiv Nadar Institution of Eminence, India in partial fulfillment for the award of the degree of Doctor of Philosophy is a record of work carried out by me at Shiv Nadar Institution of Eminence, India. The work, in full or in parts, has not been submitted to any other University/Institute for the award of any other degree. Any information/material used in the thesis from external sources has been appropriately acknowledged.

Abhishek Tiwari [Roll No. 2010120961]

Place

Date

## **CERTIFICATE**

This is to certify that the thesis titled **Deep Learning Based Framework for DTI Parameters Estimation and Analysis for Sparse Diffusion MRI data** submitted by Abhishek Tiwari, Roll number 2010120961 to the Shiv Nadar Institution of Eminence, India for the award of the degree of Doctor of Philosophy is a bonafide record of research work carried out by him/her under my / our supervision. The contents of this thesis, in full or in parts, have not been submitted to any other Institute or University for the award of any degree or diploma.

Place:

Date:

**Dr. Rajeev Kumar Singh**  
Research Advisor  
Associate Professor, Department of CSE  
Shiv Nadar Institution of Eminence, India

Place:

Date:

**Dr. Saurabh J. Shigwan**  
Research Co-Advisor  
Assistant Professor, Department of CSE  
Shiv Nadar Institution of Eminence, India

This thesis is being submitted having met all the requirements of School of Engineering at Shiv Nadar Institution of Eminence, India, and is hereby approved.

Place:

Date:

**Prof. Suneet Tuli**  
Dean, School of Engineering  
Shiv Nadar Institution of Eminence, India

## Acknowledgment

“Gratitude is important not only because it helps people feel good but also because it inspires them to do good”. .....by Dr. APJ Abdul Kalam

My sincere gratitude goes out to my PhD advisors, Dr. Rajeev Kumar Singh and Dr. Saurabh J. Shigwan, for their esteemed guidance. They have improved my perspective with their priceless advice, pointed out my silly errors, greatly encouraged me, and pointed me in the right direction during each conversation. They have taught me how to select problems, think critically, and approach finding a solution. They have provided me with the best training that will enable me to advance in my career as a scholar and researcher. Honestly, it was more than I had ever hoped for in my research life. I am blessed with good luck that I get a chance to work with them. Their passion for research has inspired me to pursue research excellence, even though I may not have fully reached it yet. Without a doubt, they are the best choice I could have made for my advisory panel.

I also express my heartfelt gratitude to Prof. Karmeshu for his invaluable feedback and constructive comments, which have greatly contributed to improving and enhancing the quality of my research work.

I extend my thanks to the Department Head, Prof. Dolly Sharma, for her constant support and guidance. I am also grateful to the Dean of the School of Engineering, Prof. Suneet Tuli, for his kindness and support throughout these years of research.

I would like to express my gratitude to my parents, Mr. Ramesh Tiwari and Mrs. Urmila Tiwari, as well as to other family members, Pranavi Tiwari, Pooja Ashok Mishra, Aviral Pandey, Prakriti Pandey, Priyanka Pandey, and Keshav Pandey. My achievements have been fueled by their unwavering support, unfailing love, and unwavering belief in my abilities. Having them by my side is a true blessing. Last but not least, I would like to thank Ananya Singhal for her assistance with the TBSS analysis and my colleagues for their invaluable advice, support, and encouragement during this academic journey. I am deeply grateful to each and every one of you for your priceless contributions and for playing a crucial role in my success in earning my Ph.D.

**Abhishek Tiwari**

# Abstract

Today, mental health issues are prevalent, which makes the diagnosis and prognosis of neurological diseases crucial from a clinical perspective. Addressing mental health on a broad scale presents challenges in terms of both cost and time. Although psychiatrists typically address mental health through therapy and counseling, the effectiveness of these approaches varies from person to person. Therefore, noninvasive techniques such as diffusion tensor imaging (DTI) play a vital role in providing quantitative measurements that assist in assessing mental health. Understanding the structure of white matter is key to diagnosing and predicting mental health conditions accurately. Moreover, it is essential to have quantitative measurements that are unbiased and can be deployed on a large scale. These DTI quantitative parameters can be acquired in large scale in less amount of time using sparse diffusion MRI.

Sparse diffusion MRI, which can be acquired by small diffusion measurements, presents challenges due to limited diffusion directions and inherent noise. Deep learning has emerged as a promising approach to resolved these problem compare to traditional methods. Our thesis introduces a novel Deep Learning Based Framework for DTI Parameter Estimation and Analysis tailored to sparse diffusion MRI data. This framework, incorporating Transformer Neural Network and Convolutional Neural Network (CNN), aims to overcome the limitations of traditional DTI reconstruction methods.

We conducted experiments on various datasets, including the Human Connectome Project (HCP) which is high resolution, the MICCAI Quad22 Migraine dataset, the National Institute of Mental Health Data (NIFD), and the Alzheimer's Disease Neuroimaging Initiative (ADNI) which are mental health diseases with lower resolution. Our findings show that our framework effectively improves DTI parameter estimation and analysis for sparse diffusion MRI data. These results contribute to advancing our understanding of brain connectivity and neurodegenerative diseases, with implications for future neuroimaging research.

**Keywords:** Diffusion MRI, Deep learning, Tractography, Neurological disorders

# List of Publications

## Accepted:

1. **Abhishek Tiwari**, Rajeev Kumar Singh, and Saurabh J. Shigwan,"SwinDTI: Swin transformer based fast estimation of diffusion tensor parameters from sparse data", **Neural Computing and Applications Springer journal Impact Factor = 6.0 Q1 SCI** (2023) [\[Paper\]](#)
2. Santiago Aja-Fernández, Carmen Martín-Martín, Álvaro Planchuelo-Gómez, Abrar Faiyaz, Md Nasir Uddin, Giovanni Schifitto, **Abhishek Tiwari**, Saurabh J. Shigwan, Rajeev Kumar Singh, Tianshu Zheng, Zuozhen Cao, Dan Wu, Stefano B. Blumberg, Snigdha Sen, Tobias Goodwin-Allcock, Paddy J. Slator, Mehmet Yigit Avci, Zihan Li, Berkin Bilgic, Qiyuan Tian, Xinyi Wang, Zihao Tang, Mariano Cabezas, Amelie Rauland, Dorit Merhof, Renata Manzano Maria, Vinícius Paraniba Campos, Tales Santini, Marcelo Andrade da Costa Vieira, SeyyedKazem HashemizadehKolowri, Edward DiBella, Chenxu Peng, Zhimin Shen, Zan Chen, Irfan Ullah, Merry Mani, Hesam Abdolmalleby, Samuel Eckstrom, Steven H. Baete, Patryk Filipiak, Tanxin Dong, Qiuyun Fan, Rodrigo de Luis-García, Antonio Tristán-Vega, Tomasz Pieciak, "Validation of Deep Learning techniques for quality augmentation in diffusion MRI for clinical studies", **Elsevier NeuroImage: Clinical journal Impact Factor = 4.2 Q1 SCI** (2023) [\[Paper\]](#)
3. **Abhishek Tiwari**, Ananya Singhal, Saurabh J. Shigwan, Rajeev Kumar Singh, "Deep Learning Framework using Sparse Diffusion MRI for Diagnosis of Frontotemporal Dementia", **IEEE/CVF International Conference on Computer Vision ICCV 2023 (Core Rank A\*, h-index 228 ) workshop on BioImage Computing.** [\[ICCV 2023 Paris, Acceptance rate: 2160 / 8068 = 26.8%\]](#) [\[Paper\]](#)
4. **Abhishek Tiwari**, Ananya Singhal, Saurabh J. Shigwan, Rajeev Kumar Singh, "Early Diagnosis of Alzheimer through Swin-Transformer-Based Deep Learning Framework using Sparse Diffusion Measures", **The 15th Asian Conference on Machine Learning (ACML 2023) in Istanbul, Turkey** **Acceptance rate = 26.9%, with just four papers selected from India.** [\[Accepted and Presented\]](#)

# Contents

<b>List of figures</b>	v
<b>List of tables</b>	vi
<b>1 Introduction</b>	1
1.1 Motivation . . . . .	2
1.2 Research Objectives . . . . .	4
1.3 Contribution of the Thesis . . . . .	5
1.4 Overview of the Thesis . . . . .	6
<b>2 Background and Related Work</b>	8
2.1 Introduction to Diffusion Phenomena in Biological Systems . . . . .	8
2.2 Evolution of Diffusion Magnetic Resonance Imaging (dMRI) . . . . .	9
2.3 Diffusion-weighted Imaging (DWI) and Diffusion Tensor Imaging (DTI) . . . . .	10
2.3.1 Positive Aspects of Diffusion Tensor Imaging (DTI) . . . . .	13
2.3.2 Negative Aspects of Diffusion Tensor Imaging (DTI) . . . . .	13
2.4 Advanced Diffusion Imaging Techniques: HARDI, DSI, DKI, and NODDI . . . . .	14
<b>3 DTI parameters estimation using Sparse dMRI Data</b>	19
3.1 Theory . . . . .	19
3.1.1 Diffusion Tensor Imaging . . . . .	19
3.1.2 Investigating the Feasibility of DTI Parameters Estimation over HCP . . . . .	21
3.1.3 Investigating the Feasibility of DTI Parameters Estimation over MICCAI Quad22	23
3.1.4 Investigating the Feasibility of DTI Parameters Estimation over NIFD . . . . .	25
3.1.5 Investigating the Feasibility of DTI Parameters Estimation over ADNI . . . . .	26
3.2 Methods . . . . .	28
3.2.1 Data Preprocessing and Model Training over HCP . . . . .	28
3.2.2 Data Preprocessing and Model Training over MICCAI Quad22 . . . . .	33
3.2.3 Data Preprocessing and Model Training over NIFD . . . . .	36
3.2.4 Data Preprocessing and Model Training over ADNI . . . . .	40

<b>4 Results and Discussion</b>	<b>42</b>
4.1 Experimental findings over HCP . . . . .	42
4.2 Experimental findings over MICCAI Quad22 . . . . .	54
4.3 Experimental findings over NIFD . . . . .	55
4.4 Experimental findings over ADNI . . . . .	58
<b>5 Tract-based spatial statistics(TBSS) Analysis</b>	<b>63</b>
5.1 TBSS analysis over MICCAI Quad22 . . . . .	63
5.2 TBSS analysis over NIFD . . . . .	64
5.3 TBSS analysis over ADNI . . . . .	66
<b>6 Conclusion and Future Directions</b>	<b>69</b>
6.1 Summary of Research Findings . . . . .	69
6.2 Limitations and Potential Improvements . . . . .	72
6.3 Future Research and Applications . . . . .	74
6.4 Conclusion . . . . .	74
<b>References</b>	<b>76</b>

# List of Figures

1.1	General description of the white matter and grey matter that make up the brain's tissue. Neural cell bodies and dendrites are found in the grey matter, whereas axons are found in the white matter and are responsible for connecting distant neurons. Source: <a href="https://www.osmosis.org/learn/Anatomy of the white matter tracts">https://www.osmosis.org/learn/Anatomy of the white matter tracts</a> .	2
1.2	Overview of Thesis with an in-depth look at the proposed architecture outlined in Fig. 3.1.	7
3.1	The proposed framework over HCP dataset consists of two steps: step 1 describes how data are generated, and step 2 concentrates on neural network training and prediction.	29
3.2	Overview of working strategy. Top: Comparative analysis of DTI data processing using 61 and 21 gradient directions, comparing EM to CM based on data acquired with 61 gradient directions. Bottom: Outline of the challenge task, involving the training of a Deep Learning network using healthy controls and the utilization of the trained network to estimate parameters from patients acquired with 21 gradient directions. Image Source: MICCAI 2022 Challenge [1] is QuaD22. I participated in an active part in this challenge as a member of Team 13, which enabled the team to participate successfully.	35
3.3	Proposed model over migraine dataset, in which takes $(64 \times 4)$ input vector and produces $(3 \times 1)$ output vector with FA, AD, and MD score	36
3.4	The proposed model over NIFD dataset architecture for neural network training and prediction.	37
3.5	The proposed model over ADNI dataset architecture for neural network training and prediction.	41
4.1	The diffusion directional signal of 64 DWIs was compared using 3D U-Net16, LLS fitting, and the proposed SwinDTI. Red circles highlight noteworthy areas that show differences from earlier research findings.	43
4.2	The proposed SwinDTI absolute error image, 3D U-Net16, and LLS fitting for 64 DWIs. The range of the AD and MD scales is 0 to $6 \times 10^{-4}$ , whereas the range of the FA scale is 0 to 0.3	43

4.3 Diffusion directional signal of 32 DWIs is compared with 3D U-Net16, LLS fitting, and the proposed SwinDTI. Red circles highlight noteworthy areas that show differences from earlier research findings. . . . .	44
4.4 The proposed SwinDTI absolute error image, 3D U-Net16, and LLS fitting for 32 DWIs. The range of the AD and MD scales is $0$ to $6 \times 10^{-4}$ , whereas the range of the FA scale is $0$ to $0.3$ . . . . .	44
4.5 Diffusion directional signal of 21 DWIs is compared with 3D U-Net16, LLS fitting, and the proposed SwinDTI. Red circles highlight noteworthy areas that show differences from earlier research findings. . . . .	45
4.6 The proposed SwinDTI absolute error image, 3D U-Net16, and LLS fitting for 21 DWIs. The range of the AD and MD scales is $0$ to $6 \times 10^{-4}$ , whereas the range of the FA scale is $0$ to $0.3$ . . . . .	45
4.7 Diffusion directional signal of 5 DWIs is compared with proposed SwinDTI, 3D U-Net16, LLS fitting, and Transformer-DTI. Red circles highlight noteworthy areas that show differences from earlier research findings. For each of the five diffusion directions, SwinDTI outperforms the FA measurement obtained by 3D U-Net16, LLS fitting, and Transformer-DTI. Surprisingly, SwinDTI shows similar performance to LLS fitting when it comes to AD and MD measurements. . . . .	46
4.8 The proposed SwinDTI absolute error image, 3D U-Net16, and LLS fitting for 5 DWIs. The range of the AD and MD scales is $0$ to $6 \times 10^{-4}$ , whereas the range of the FA scale is $0$ to $0.3$ . . . . .	47
4.9 Boxplot of whole brain FA measurement . . . . .	47
4.10 Boxplot of whole brain AD measurement . . . . .	48
4.11 Boxplot of whole brain MD measurement . . . . .	48
4.12 FA measure boxplot of ROI Anterior corona radiata, causes[2] affecting cerebral white matter, including ischemic and multiple sclerosis. . . . .	49
4.13 AD measure boxplot of ROI Anterior corona radiata, causes[2] affecting cerebral white matter, including ischemic and multiple sclerosis. . . . .	49
4.14 MD measure boxplot of ROI Anterior corona radiata, causes[2] affecting cerebral white matter, including ischemic and multiple sclerosis. . . . .	50
4.15 FA measure boxplot of ROI Cingulum, causes[3] Alzheimer's disease, anxiety disorders, addiction, depression, and schizophrenia. . . . .	50
4.16 AD measure boxplot of ROI Cingulum, causes[3] Alzheimer's disease, anxiety disorders, addiction, depression, and schizophrenia. . . . .	50
4.17 MD measure boxplot of ROI Cingulum, causes[3] Alzheimer's disease, anxiety disorders, addiction, depression, and schizophrenia. . . . .	51

4.18 Comparison of 41 diffusion directions: Ground truth vs. Proposed method vs. LLS fitting [4] . . . . .	56
4.19 Comparison of 21 diffusion directions: Ground truth vs. Proposed method vs. LLS fitting [4] and Transformer-DTI [5] . . . . .	56
4.20 Comparison of 5 diffusion directions: Ground truth vs. Proposed method vs. LLS fitting [4] and Transformer-DTI [5] . . . . .	57
4.21 Six diffusion components of diffusion tensor for 5 diffusion directions . . . . .	57
4.22 Six diffusion components of diffusion tensor for 21 diffusion directions . . . . .	58
4.23 The results obtained from the ground truth, the proposed method, and LLS fitting [4] are compared, and it is observed that for 41 diffusion directions, the Proposed method shows comparability with both the ground truth and LLS fitting. . . . .	59
4.24 We compare the results obtained from the ground truth, the proposed method, LLS fitting [4], and Transformer-DTI [5]. We find that, for 21 diffusion directions, the Proposed method outperforms both LLS fitting [4] and Transformer-DTI [5]. . . . .	59
4.25 We compare results obtained from the ground truth, the proposed method, LLS fitting [4], and Transformer-DTI [5]. We find that, for 5 diffusion directions, the proposed method outperforms LLS fitting [4] and Transformer-DTI [5]. . . . .	60
4.26 Six diffusion component of diffusion tensor for 5 diffusion directions . . . . .	60
4.27 Six diffusion component of diffusion tensor for 21 diffusion directions . . . . .	61
 5.1 An axial brain slice showing the Cingulum region; the p-value from the two sample t-test (df=8) is indicated. Green indicates that the tstat1 hypothesis test is a healthy CN > FTD patient; red indicates that the tstat2 hypothesis test is a healthy CN < FTD patient. . . . .	64
5.2 An illustration of the Uncinate fasciculus region in a coronal brain slice is shown with the p-value (df=8) of the two sample t-test. Green hue indicates that tstat1-Healthy CN is the hypothesis being tested. Hypothesis testing tstat2 - Healthy CN < FTD patient, > FTD patient, Red color. . . . .	65
5.3 An axial brain slice showing the Cingulum region; the p-value from the two sample t-test (df=22) is indicated. Green color: hypothesis testing tstat1 - Healthy CN > MCI, Red color: hypothesis testing tstat2 - Healthy CN < MCI. . . . .	66
5.4 Uncinate fasciculus region represented by a coronal brain slice, with a two sample t-test p-value of (df=22) indicated. Green color: hypothesis testing tstat1 - Healthy CN > MCI, Red color: hypothesis testing tstat2 - Healthy CN < MCI. . . . .	67

# List of Tables

4.1	The diffusion direction error for FA measures is $N_{dir} = 5$ . The least amount of error is bolded.	49
4.2	Error ( $\times 10^{-4}$ ) of the AD measure for diffusion direction $N_{dir} = 5$ . The least amount of error is bolded.	51
4.3	Error ( $\times 10^{-4}$ ) of the MD measure for the diffusion direction $N_{dir} = 5$ . The least amount of error is bolded.	52
4.4	The SSIM score[6] compares the quantitative images predicted and Ground Truth. Compared to MD, FA has higher reliability in white matter [7]. The optimum results are shown by the highlighted values, which are the minimum standard deviation (std) and the maximum values for FA, AD, and MD.	53
5.1	The Proposed Model, LLS fitting, and Transformer-DTI are examined for the number of pixels with p-values outside Confidence Intervals (95% and 99%) for the t-statistics (tstat1 and tstat2), where tstat1 compares Healthy CN > FTD patient and tstat2 compares Healthy CN < FTD patient.	65
5.2	Pixel count for t-statistics (tstat1 and tstat2) in the proposed model, LLS fitting, and Transformer-DTI that have p-values outside of the 95% and 99% confidence intervals. There are two hypotheses: tstat1 (healthy CN > MCI) and tstat2 (healthy CN < MCI).	67

# Chapter 1

## Introduction

The correct diagnosis and prognosis of neurological diseases from a clinical perspective is crucial, given the prevalence of mental health issues in today's society[8]. However, access to comprehensive mental health treatment is hampered by significant scheduling and budgetary constraints[9]. Traditional psychotherapy and counseling methods are helpful, but their effectiveness varies widely between individuals[10]. Precise quantitative measurements are essential for the assessment of mental health issues, which makes non-invasive methods such as diffusion tensor imaging (DTI) invaluable [11]. Accurate diagnosis and prognosis of mental health issues require an in-depth understanding of white matter anatomy [12]. Nevertheless, current existing techniques have drawbacks, including limited diffusion directions and intrinsic noise [13].

In response to these challenges, deep learning offers a potential alternative for traditional techniques[13]. This thesis provides a novel Deep Learning Based Framework for DTI Parameter Estimation and Analysis of sparse diffusion MRI data. By merging Transformer Neural Network and Convolutional Neural Network (CNN), our methodology aims to address the shortcomings of traditional DTI reconstruction methods and enable the acquisition of DTI quantitative data on a large scale in a significantly shorter amount of time.

Axons, or nerve fibers coated in myelin, make up the majority of white matter, a vital component of the central nervous system[14]. The myelin sheath, which promotes effective signal transmission between various brain and spinal cord regions, gives it, its white matter[15]. Understanding white matter is crucial because it offers valuable applications and crucial insights into the workings of the brain. Several neurological and mental disorders, such as depression, schizophrenia, and Alzheimer's disease, have been linked to white matter abnormalities[16]. Examining[17] the composition and role of white matter in various diseases can provide insight into the underlying degenerative mechanisms, potentially paving the way for the discovery of improved treatment strategies.

## 1.1 Motivation

The tissue found in the central nervous system is mainly made up of nerve fibers (axons) and the fatty material known as myelin, which envelops and insulates these fibers, is referred to as white matter[18]. The myelin coating, which gives it a white look, is the reason it is termed white. Signals can be transmitted more easily between various parts of the brain and spinal cord due to the communication network that is white matter[19]. The development of connections between neurons facilitates the transmission of information between different parts of the brain, enabling the coordination of motor and sensory activities, as well as higher cognitive processes.

The exploration of brain white matter holds significant importance for two key reasons: first, it can help us understand how the human brain works, and second, it has clinical implications. A wide range of neurological and psychiatric conditions, including schizophrenia, multiple sclerosis, Alzheimer's disease, depression, and anxiety disorders, have been linked to abnormalities in white matter[20, 21]. Assessing the composition and capabilities of white matter under these circumstances can shed light on the fundamental processes leading to degeneration and facilitate the creation of more effective therapies[22, 23].

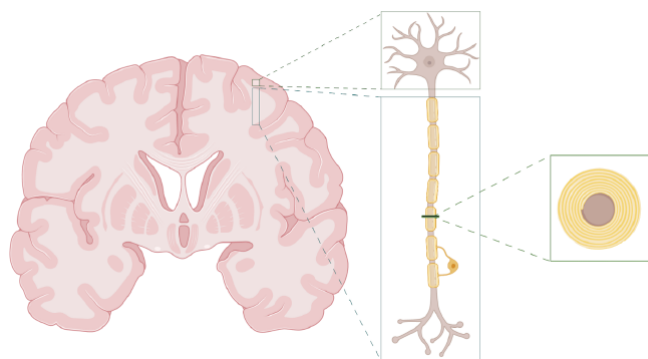


Figure 1.1: General description of the white matter and grey matter that make up the brain's tissue. Neural cell bodies and dendrites are found in the grey matter, whereas axons are found in the white matter and are responsible for connecting distant neurons. Source: [https://www.osmosis.org/learn/Anatomy of the white matter tracts](https://www.osmosis.org/learn/Anatomy%20of%20the%20white%20matter%20tracts).

Furthermore, understanding of brain white matter is essential to understanding normal brain function and the underlying mechanisms of brain activity. For example, white matter changes significantly during the early stages of brain development, from infancy to childhood. We can learn a great deal about brain development and normal brain function by monitoring and measuring these changes[24, 25]. Later, with this knowledge, it will be easier to create more successful treatments that target white matter pathways in order to improve cognitive abilities and quality of life.

Numerous methods can be used to study the white matter of the brain. Among the most popular techniques are:

**Tracer**[26] One of the more established methods of identifying the white matter pathways is the use of tracers, which are chemicals injected into the brain that label specific nerve fibers with a particular

color. Once the brain has been dissected, the connections indicated by the tracer can be seen. Over the years, the mapping of brain connections for several species has benefited greatly from the use of tracers. Although the tracer approach is a direct means of observing connections, it is severely limited by artifacts caused by leaks, intrusiveness, and the excessive sacrifices required.

**Histology**[27]: Examining tissue under a microscope is known as histology, and it is one more way to look into white matter. Similar to tracers, chemicals can be used to "stain" white matter samples in order to identify specific materials such as myelin, microglia, Nissl bodies, etc. Histology is particularly useful for researching how diseases and pathologies affect the microstructure of white matter. However, due to its invasiveness, small sample size, and difficulties with quantification, its application is limited in many circumstances.

**Structural Magnetic Resonance Imaging (MRI)**[28]: Images of the structures of the brain are obtained by using specific MRI modalities, such as T1, T2, and FLAIR acquisitions. Due to their ability to detect a wide range of brain abnormalities, such as tumors, white matter lesions, and other abnormalities, these modalities have become indispensable in clinical practice. The ability to obtain comprehensive measurements of the entire brain and the non-invasive nature of these MRI techniques are their main advantages. Their sensitivity, which typically only permits the detection of significant alterations, is a notable drawback, as it frequently leads to diagnoses in the later stages of disease progression.

**Diffusion MRI (dMRI)**[29]: This type of magnetic resonance imaging (MRI) is sensitive to the movement of water molecules within tissue as a result of diffusion. This method detects the direction and velocity of water molecules to provide information about the local orientation and strength of white matter connections at every location throughout the brain. The benefit of dMRI is that it is non-invasive and has the capacity to scan the entire brain simultaneously; however, its drawback is that it is noisy.

Understanding and diagnosing neurodegenerative diseases are greatly aided by the complex dynamics of water flow within the brain[30, 31]. One non-invasive technique that has gained popularity is Diffusion Tensor Imaging (DTI), which provides information about white matter pathways. However, because of its precision, lengthy scan times are required, which can be problematic for some patient populations, especially pediatric patients[5, 32]. In order to tackle this issue, researchers have investigated deep learning methodologies to expedite the DTI parameter estimation from diffusion-weighted images, an essential task for neurological diagnosis[33, 34].

In order to quickly estimate diffusion tensor parameters, this thesis presents a novel method that makes use of a transformer model based on neural networks. Despite sparse measurements, the suggested approach performs exceptionally well in managing scalable and generalized estimation, outperforming earlier attempts to tackle this problem. Our model outperforms conventional methods in terms of mean diffusivity (MD), axial diffusivity (AD), and fractional anisotropy (FA) in experiments conducted on the Human Connectome Project (HCP) Young Adult benchmark dataset.

By concentrating on particular neurodegenerative illnesses, our work makes a substantial contribution

to early diagnosis of frontotemporal dementia (FTD). Since FTD affects the frontal and temporal lobes, an accurate diagnosis is crucial to timely intervention. Using sparse diffusion measures, our research proposes a novel deep learning framework for the estimated 1.2 to 1.8 million affected people worldwide. This novel method effectively differentiates between healthy people and those who have FTD, providing encouraging findings for improving FTD diagnosis and opening the door for more research in this important area.

Now, turning to Alzheimer's disease, a common neurodegenerative disease that affects 6.2 million people in the US alone, this research addresses the difficulties associated with early diagnosis. The Diffusion Weighted Imaging (DWI) process is a major bottleneck because it takes more than three hours to complete. Our proposed Transformer-based deep learning model, incorporating an attention mechanism, drastically reduces scanning time and generates accurate quantitative measures of MD, AxD, and FA. Our model offers a viable path for the early diagnosis and treatment of Alzheimer's disease, having proven its superiority over traditional techniques. Finally, our ground-breaking work has the potential to significantly improve the early detection and treatment of several neurodegenerative diseases. In this crucial field of medical research, the open-access repository offers a useful tool for additional investigation and collaboration.

## 1.2 Research Objectives

- **Development of Efficient DTI Estimation from sparse data**

We aim to create a transformer neural network-based novel method (SwinDTI) for the quick and accurate estimation of diffusion tensor parameters from sparse DWI data. The objective is to tackle persistent issues such as longer scan times, lower resolution, noise sensitivity, and limited ability to generalize in different diffusion directions.

- **Improving Quality of quantitative measure using sparse measurement**

Determining how well deep learning methods improve quantitative measure using sparse measurement for clinical applications was the next goal. The assessment of the influence of angular resolution on dMRI was our main focus, and we also examined the possibility of losing important clinical information or creating false information when using AI techniques in medical images. Using deep learning to improve diffusion metrics and yield results that were on par with those obtained from more gradient directions was the goal.

- **Enhancing FTD Diagnosis**

Our next goal was to improve Frontotemporal Dementia (FTD) diagnosis by implementing a deep learning framework. The goal of this framework is to increase the diagnostic accuracy of FTD by utilizing sparse diffusion measures that are extracted from neuroimaging data. By using the Swin-Transformer, the method is able to reduce scanning time compared to traditional methods and existing deep learning techniques, and achieve higher diagnostic precision for FTD.

- **Accelerating Alzheimer's Disease Diagnosis**

The centers around expediting the diagnosis of Alzheimer's disease through the introduction of a deep learning model based on Swin-Transformer attention. The goal is to derive quantitative measures (FA, AxD, MD) utilizing sparse diffusion directions data, allowing for efficient clinical diagnosis with decreased scanning time, all the while ensuring precise identification of early-stage Alzheimer's disease.

In summary, the research objectives involve the creation of novel methods, frameworks, and models to tackle particular difficulties in neuroimaging and clinical diagnosis. The ultimate goal is to enhance the accuracy, efficiency, and applicability of these approaches in actual medical environments.

### 1.3 Contribution of the Thesis

The thesis contributes significantly to the field of neuroimaging and clinical diagnosis. The key contributions can be outlined as follows:

**Innovative DTI Estimation Method (SwinDTI):** The thesis introduces a novel approach, SwinDTI, for efficiently estimating diffusion tensor parameters from sparse DWI data using a transformer neural network. This method addresses the limitations of existing techniques, such as long scan times and limited generalization across different diffusion directions. SwinDTI leverages advanced attention mechanisms and patch-based processing, making a notable contribution to the field of neuroimaging by enabling fast and accurate DTI estimation.

**Advancements of quantitative measure using sparse measurement:** The thesis evaluates the efficacy of deep learning techniques in enhancing the quality of quantitative measure for help in biomarker decision making over chronic migraine and episodic migraine. By investigating the impact of angular resolution in diffusion MRI and challenging multiple teams to utilize deep learning for improving diffusion metrics, the thesis contributes to the understanding of the role of AI methods in medical imaging and the potential challenges associated with such applications. Additionally, it provides insights into maintaining data integrity and accuracy in clinical settings while employing advanced AI methodologies.

**Enhanced FTD Diagnosis Framework:** The thesis proposes a deep learning framework, leveraging Swin-Transformer, for improving the diagnosis of Frontotemporal Dementia (FTD). By utilizing sparse diffusion measures from neuroimaging data, the framework enhances the accuracy of FTD diagnosis while significantly reducing scanning time compared to conventional methods and existing deep learning techniques. This contribution is particularly valuable in the realm of neurodegenerative disorder diagnostics.

**Accelerated Alzheimer's Disease Diagnosis Model:** The thesis introduces a Swin-Transformer

attention-based deep learning model designed to expedite the diagnosis of Alzheimer's disease. By extracting quantitative measures, including fractional anisotropy (FA), axial diffusivity (AxD), and mean diffusivity (MD), from sparse diffusion directions, the model facilitates rapid and accurate early-stage diagnosis, thereby significantly contributing to the effective management and treatment of this prevalent neurodegenerative disorder.

In summary, the thesis makes significant contributions to the advancement of neuroimaging techniques, deep learning applications in clinical diagnostics, and the understanding of the impact of AI methodologies on medical imaging data. Its contributions significantly enhance the accuracy, efficiency, and reliability of neuroimaging analysis, thereby paving the way for improved diagnostic capabilities and better treatment outcomes in the field of neurodegenerative disorders.

## 1.4 Overview of the Thesis

The thesis offers a comprehensive overview of the development and application of innovative techniques in neuroimaging and clinical diagnostics. The following summarizes the major contributions:

The Innovative DTI Estimation Method (SwinDTI), which employs a transformer neural network to efficiently estimate diffusion tensor parameters from sparse DWI data, is a novel approach presented in the thesis. This approach addresses the drawbacks of earlier techniques, including long scan times and limited generalization in different diffusion directions. SwinDTI, which uses sophisticated attention mechanisms and patch-based processing to provide a fast and accurate estimation of DTI, is a major advancement in neuroimaging.

Assessment of Deep Learning Methods to improve the quantitative measure using sparse measurement: Furthermore, the thesis assesses how well deep learning methods work to improve the quality of quantitative measure using sparse measurement for decision making over chronic migraine and episodic migraine. By concentrating on the dMRI's angular resolution and the possible applications of AI techniques in medical imaging. The thesis also provides a critical analysis of how well different teams performed in comparison to traditional methods, based on a thorough evaluation of the outcomes they achieved by utilizing deep learning techniques to improve diffusion metrics.

Improved Framework for Deep Learning-Based FTD Diagnosis: The thesis then explores the difficulties in diagnosing frontotemporal dementia (FTD) and presents a deep learning framework that makes use of Swin-Transformer to improve the accuracy of FTD diagnosis. This highlights the framework's ability to use neuroimaging data's sparse diffusion measures, which improves diagnostic capabilities while cutting scanning time, and offers insights into its possible uses in clinical settings.

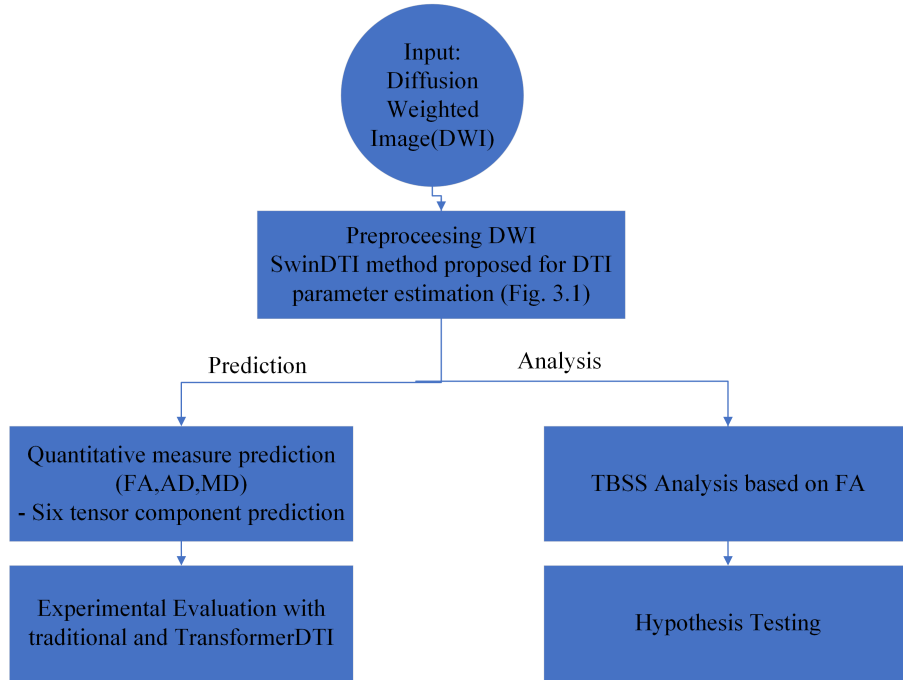


Figure 1.2: Overview of Thesis with an in-depth look at the proposed architecture outlined in Fig. 3.1.

**Faster Diagnosis of Alzheimer's Disease with Deep Learning Model:** This thesis presents an attention-based deep learning model based on Swin-Transformer and delves deeper into the difficulties associated with Alzheimer's disease diagnosis. This model is intended to enable quick and precise early-stage diagnosis by extracting critical quantitative measures from sparse diffusion directions. By offering an in-depth understanding of the model's applications in actual clinical settings, the highlights the model's potential impact on improving the management and treatment of Alzheimer's disease.

In conclusion, the thesis offers a thorough analysis of the difficulties and constraints associated with neuroimaging and clinical diagnostics, along with cutting-edge approaches and solutions to these problems. It highlights how sophisticated deep learning techniques can transform the field and how they can improve data quality, efficiency, and accuracy in a variety of clinical applications.

# Chapter 2

## Background and Related Work

### 2.1 Introduction to Diffusion Phenomena in Biological Systems

Botanist Robert Brown[35] first proposed the idea of diffusion in 1828 after he used a microscope to record the erratic movement of pollen particles suspended in water. The principles of diffusion were later formalized by Albert Einstein in 1905, when he defined it as the unrestricted motion of particles[36]. However, barriers and cell structures impose restrictions on the movement of water molecules in biological tissues, resulting in categories such as hindered and restricted diffusion[16, 37].

Although physics and chemistry were the original fields in which the principles of diffusion were conceived, applying these concepts to biological systems presents special difficulties. Water molecules in biological tissues are subject to restrictions imposed by cell structures and other impediments. As a result, various diffusion patterns, including limited and impeded diffusion, have been identified[16, 37]. Deciphering these subtleties is crucial to understanding the intricacies of diffusion in living things.

Because of their complex cellular structure, biological tissues give rise to phenomena other than the traditional unrestricted diffusion. The restricted movement of molecules inside cellular compartments, like organelles or cellular membranes, is referred to as restricted diffusion. Conversely, hindered diffusion refers to barriers in the extracellular matrix or closely spaced cellular environments that impede the movement of molecules[16, 37]. Significant ramifications flow from these classifications for understanding diffusion phenomena in biological settings.

Technological developments in imaging have been essential in explaining diffusion processes in biological systems. Non-invasive methods to investigate the mobility of water molecules in living tissues include diffusion-weighted magnetic resonance imaging (DW-MRI) and diffusion tensor

imaging (DTI)[37, 38]. These instruments enhance our comprehension of physiological and pathological processes by providing insightful information about the temporal and spatial dynamics of diffusion.

Diffusion in biological systems is a subject with practical applications in biology and medicine, going beyond theoretical comprehension. A wide range of medical conditions, such as cancer, neurological disorders, and cardiovascular diseases, are diagnosed and tracked with diffusion-weighted imaging[37]. Furthermore, the principles of diffusion are important in the delivery of drugs and have implications for the design of focused therapeutic approaches.

The understanding of diffusion in biological systems has advanced significantly, but difficulties still exist. Sufficient spatial and temporal resolution in imaging techniques, the dynamic nature of living organisms, and the variability in tissue properties[16]. By tackling these issues, we will be able to gain a deeper understanding of diffusion phenomena and make this knowledge more useful in diverse scientific and medical fields.

## 2.2 Evolution of Diffusion Magnetic Resonance Imaging (dMRI)

Prior to the development of magnetic resonance imaging (MRI) in the 1970s, water diffusion in a variety of media samples was the primary focus of groundbreaking nuclear magnetic resonance (NMR) experiments carried out in the 1950s[39]. When Stejskal and Tanner presented the first diffusion-weighted sequence in 1965[40], they achieved a major breakthrough by incorporating gradient pulses into the spin-echo sequence. This novel method not only made measuring diffusion coefficients in NMR signals easier, but it also set the stage for the development of diffusion MRI. A significant turning point in this trajectory was the introduction of the b-value, a critical parameter quantifying diffusion sensitization[41, 42].

Numerous studies have highlighted the age-related decline in the trajectory of cognitive functions, particularly fluid intelligence and memory[43, 44]. Multiple orders of magnitude of structural changes in the brain are closely associated with this decline. Traditional structural MRI studies provide macroscopic insights into these age-related changes, showing a significant decrease in both white and grey matter volume after the fifth decade of life[30, 45]. These macroscopic alterations surpass the direct resolution limit of current MRI technologies and intricate details are hard to capture[46].

Fortunately, diffusion MRI (dMRI) has emerged as an effective modality that offers insights at the micrometric scale for the *in vivo* investigation of water diffusion. Using the microscopic displacements of water molecules brought about by diffusion, dMRI overcomes the limitations of image voxels' typical resolution [47, 48].

Numerous methods[49] have been developed to extract fine-grained microstructural details from dMRI maps due to the wealth of information contained in these images. DTI is a notable and impactful dMRI technique among these methodologies[50]. Since diffusion is restricted in some directions by barriers like axon membranes and myelin sheaths, diffusive transfer imaging (DTI) aims to measure the anisotropy of diffusion in biological tissues. Hence, decreases in diffusion anisotropy function as markers of microstructural degenerative processes, such as fiber demyelination and axonal loss.

In addition, DTI allows 3D maps to be reconstructed, showing the main paths taken by white matter fibers. Through a relationship between the orientation of individual fiber axons and the direction of maximum diffusion, tractography is a technique that has been widely used to examine the complex structure of white matter connections in the brain[51, 52]. Such efforts make a substantial contribution to the detailed understanding of the microstructural modifications that underlie age-related changes in brain connectivity and cognitive decline.

## 2.3 Diffusion-weighted Imaging (DWI) and Diffusion Tensor Imaging (DTI)

Diffusion-weighted images (DWIs) become an effective tool by combining the Stejskal and Tanner sequence with an MRI space-encoding gradient, identifying changes in signal intensity that correspond to different diffusion rates. Brain DWIs demonstrate low signal intensities in areas where diffusion is unrestricted, such as the cerebral ventricles. Diffusion coefficient estimation is made possible by acquiring DWIs at various b-values, which provides important information about tissue microstructure. However, it is important to remember that the formalism of Stejskal and Tanner does not take into account the complex effects of diffusion in biological tissues. As a result, diffusion estimates depend on acquisition parameters, which is particularly obvious when considering diffusion anisotropy in brain images.

Basser et al. (1994) introduced diffusion tensor imaging (DTI), a groundbreaking diffusion magnetic resonance imaging (dMRI) technique that significantly advances brain water diffusion anisotropy modeling[50]. With the use of the diffusion tensor, a second-order tensor that provides detailed information about tissue microstructure, DTI represents diffusion. The eigenvectors and eigenvalues of the tensor provide information about the direction and intensity of diffusion, which allows rotationally invariant measurements like mean diffusivity (MD), radial diffusivity (RD), and axial diffusivity (AD) to be calculated.

Within the context of cognitive aging, in which memory and fluid intelligence show a noticeable degradation with aging, the brain suffers structural changes on several levels. Traditional structural MRIs indicate large decreases in both white and grey matter volume after a certain threshold age,

indicating macroscopic changes. But prior microstructural alterations, such as cell loss, fiber loss, and demyelination, which go beyond the direct resolution limits of traditional MRI methods, remain unnoticed by these outwardly visible alterations.

Diffusion tensor imaging (DTI) and diffusion-weighted imaging (DWI) become essential techniques in this regard for exploring and understanding the subtle aspects of microstructural alterations in biological tissues. DWI is a technique that is used in conjunction with magnetic resonance imaging (MRI) to detect the diffusion of water molecules in tissues. This modality goes beyond the traditional resolution of image voxels by taking advantage of the micrometric scale displacements of water molecules.

A number of methods have been developed to extract different microstructural details from DWI maps because of the abundance of information they contain. Within DTI, it measures the anisotropy of diffusion inside biological tissues based on the hypothesis that diffusion meets barriers along certain directions, like axon membranes and myelin sheaths[50]. Decreases in diffusion anisotropy, therefore, can be used as markers for underlying microstructural degradation processes like axonal loss and fiber demyelination.

Additionally, by connecting the orientation of individual fiber axons with the direction of maximum diffusion, DTI makes it easier to reconstruct three-dimensional maps that show the principal trajectories of white matter fibers. Examining the complex architecture of white matter connections in the brain is made possible by the use of a method called tractography. These developments greatly aid in the process of identifying the microstructural basis of age-related changes in brain connectivity as well as cognitive decline. The physical structure of the tissues is directly correlated with the diffusion coefficient. Since each anatomical region of the brain has an underlying structure that can be inferred[53], researching the DTI parameters can provide excellent details about any anomalies that may be present.

Recently, the field of diffusion tensor imaging (DTI) has moved towards parameter estimation using deep learning techniques[1, 54]. Q-space deep learning was the first deep learning technique applied to a comparable task[55]. This technique reduced the number of measurements by a factor of twelve by estimating diffusion kurtosis using a dense neural network consisting of three layers. After the q-space deep learning method proved to be successful, scientists started concentrating on other voxel-level diffusion parameter estimations[56]. Deep neural networks outperform traditional linear least square methods in the estimation of fiber orientations, as many researchers have successfully demonstrated[5, 32, 57, 58, 59, 60, 61]. However, they have limitations when it comes to spherical deconvolution[62]. The number of fiber orientations is one of the other estimated voxels [63, 64]. It is clear from the literature review that stronger and more precise estimations are needed to comprehend spatial correlations between DTI parameters and diffusion-weighted images in nearby voxels. Researchers[65, 66] used basic convolution neural networks on patches of diffusion-weighted images to estimate fiber orientation because deep learning models can learn complex patterns.

They discovered that this method produced a more accurate estimation of diffusion kurtosis than the q-space deep learning method, which is based only on dense layers. Other convolutional neural network-based methods for fast DTI and fiber tractography with a restricted number of diffusion-weighted images have been proposed, including DeepDTI[34] and SuperDTI[33]. Transformer-DTI[5] uses a recently published multi-head self attention mechanism[67] to take advantage of the spatial correlation between the diffusion signal and the diffusion tensor parameter in the nearby slices and voxels. 25 million trainable parameters were used by Transformer-DTI[5] to meet its high memory and processing requirements. For six diffusion directions, the original Transformer-DTI[5] model is employed. We predict the output of the Transformer-DTI model for a reduced number of diffusion directions  $N_{dir} = 5$  in order to compare it with the proposed model.

Transformer model[5, 67] is highly promising, but because it may result in larger trainable parameters, which require more memory and training time, it is not scalable for a larger number of diffusion directions. As a result, it became challenging to train a single model to handle numerous diffusion-directional signals. The exceptional ability of the Swin Transformer model[68] to manage larger input sizes has attracted a lot of attention[5, 67]. Recent developments in deep neural network architecture have shown that it performs well in a variety of computer vision tasks, such as semantic segmentation, object detection, and image classification. By using a hierarchical structure, the Swin-Transformer[68] divides input feature maps into non-overlapping patches and processes them simultaneously using multiple transformer layers, enabling efficient parallelization and lowering the computational cost of the self-attention mechanism. This is in contrast to traditional transformer models, which process input data sequentially[5, 67]. As a consequence, this method produces fewer parameters, which is essential for developing a more generalized model that can manage multiple diffusion-directional signals. A Swin Transformer-based method known as the SwinDTI framework has been proposed for the estimation of DTI measures.

A comparative study of various deep learning architectures for diffusion tensor imaging (DTI) is presented. We specifically combine the architecture of DeepDTI[34], which uses a 3D convolutional neural network (CNN) with input patch  $64 \times 64 \times 64$ , and SuperDTI[33], which uses a 2D U-Net with input patch  $21 \times 21$ . This combination of architectures is called 3D U-Net16 because it uses 3D U-Net of  $16 \times 16 \times 16$  patches. In order to lower the computational and memory costs of U-Net, we selected a patch size of  $16 \times 16 \times 16$ . A closer alignment with the proposed model objectives for estimating quantifying measures FA, AD, and MD is the justification for merging DeepDTI[34] and SuperDTI[33] into a modified 3D U-Net[69] architecture. In contrast to the original 3D U-Net [69], the problems under consideration for 3D U-Net16 are entirely different. Regression problem is solved by the suggested method, whereas segmentation problem is solved by the original.

We also observe that, because SwinDTI has fewer trainable parameters than Transformer-DTI[5], our suggested model uses windowing-based Swin Transformer[68], which results in a significantly lower computation cost. In patch-based image processing tasks, Swin Transformer[68] has

demonstrated promising results. Moreover, scalability with larger 3D-patches is possible with patch-based processing using Swin Transformer[68], without a significant increase in memory and computational costs. Consequently, to handle larger 3D patch sizes, our suggested model makes use of the computational efficiency and scalability of windowing-based Swin Transformer[68].

### 2.3.1 Positive Aspects of Diffusion Tensor Imaging (DTI)

**Visualization of Microstructural Changes without Invasive Procedures:** DTI offers a non-invasive way to see microstructural changes in tissues, especially the brain. This is crucial for figuring out how the white matter tracts are organized and for spotting anomalies[70].

**Quantitative Evaluation of Fiber Integrity:** DTI makes it possible to evaluate white matter fiber tract integrity quantitatively. This is important because pathology can be indicated by changes in the connectivity of brain regions, as is the case with conditions like neurodegenerative diseases[71].

**Mapping Connectivity in the Brain:** By monitoring the direction and amount of water diffusion, the method makes it easier to map the structural connectivity of the brain. Understanding neural circuitry and functional networks is aided by diffusion tensor imaging[58, 72].

**Clinical Applications:** DTI has been widely used in clinical settings for a variety of neurological disorders, including Alzheimer's disease, multiple sclerosis, and traumatic brain injury. It is also used for the diagnosis and ongoing monitoring of these disorders. It offers useful data for prognosis and treatment planning[33, 73].

**Research Advancements:** DTI has been essential to the progress of neuroscience studies. Researchers have gained a deeper understanding of neural plasticity, brain connectivity, and the anatomical foundations of cognitive processes[34, 74].

### 2.3.2 Negative Aspects of Diffusion Tensor Imaging (DTI)

**Motion Artifact Sensitivity:** DTI is very susceptible to motion artifacts, which may affect the accuracy of the findings. Images can be distorted by patients, especially those who may find it difficult to remain motionless during scanning[75].

**Limited Spatial Resolution:** Because the spatial resolution of DTI is intrinsically low, it can be difficult to precisely see smaller structures. This restriction may affect the accuracy of monitoring particular routes or identifying minute alterations in microstructure[76].

**Water Diffusion Complexity:** The actual complexity of water diffusion in biological tissues may be oversimplified by the assumption that it follows a Gaussian distribution. Non-Gaussian diffusion is a common feature of biological tissues, which can cause errors when interpreting DTI data[74].

**Incapacity to Differentiate Between Intra-axonal and Extra-axonal Diffusion:** DTI gives information about the general diffusion of water molecules, but it is unable to discern between the two types of diffusion. This lack of precision may make it more difficult to interpret the cellular microstructural alterations[77].

**Difficulties in Crossing Fiber Regions:** DTI encounters difficulties in precisely resolving the intricate fiber architecture in areas known as crossing fiber regions, which are areas where multiple fiber orientations intersect. The accuracy of tractography in these areas may be impacted by this limitation[78].

## 2.4 Advanced Diffusion Imaging Techniques: HARDI, DSI, DKI, and NODDI

The purpose of high-angular-resolution diffusion imaging (HARDI), a magnetic resonance imaging (MRI) method, is to obtain comprehensive data regarding the diffusion of water molecules in biological tissues, with a focus on the brain[79]. By collecting data at several gradient directions, HARDI avoids the constraint of conventional diffusion tensor imaging (DTI), which is predicated on a single Gaussian diffusion model. As a result, complex tissue microstructure can be represented with greater accuracy.

### **Advantage of HARDI:**

Higher Angular Resolution: HARDI offers a more accurate characterization of tissue orientation and structure than DTI because it has a higher angular resolution than the latter.

Increased accuracy in the handling of cross-fibers: HARDI's ability to capture multiple diffusion directions makes it more accurate in handling regions where multiple fiber orientations intersect[80, 81].

### **Drawbacks of HARDI:**

Increased Acquisition Time: The increased acquisition time associated with higher angular resolution makes it less appropriate for certain clinical applications where scan time is a crucial consideration.

Sensitivity to Motion Artifacts: Due to its longer acquisition time, HARDI is more susceptible to motion artifacts, which could result in data quality degradation and image distortions[82].

### **Limitations of HARDI:**

Difficult Data Analysis: In order to extract useful information from the acquired datasets, HARDI data analysis can be computationally demanding and require the use of sophisticated algorithms.

Restricted Usability in Clinical Settings: Extended acquisition durations and increased complexity could potentially hinder the extensive integration of HARDI in standard clinical environments[83].

A q-space imaging method called Diffusion Spectrum Imaging (DSI) uses a 3D Fourier transform of signal attenuations to measure the diffusion propagator directly[78]. This method makes it possible to estimate the diffusion orientation distribution function (ODF), which offers spatial data regarding diffusion in three-dimensional space along particular directions.

**Advantages of DSI:**

Accurate Representation of Complex Tissue Microstructure: DSI provides a more accurate depiction of the tissue microstructure by capturing detailed angular information without the need for simplified models.

Strong Management of Crossing Fibers: DSI can handle crossing fibers, much like HARDI, making it suitable for areas with intricate fiber layouts[84].

**Disadvantages of DSI:**

High Data Requirements: The application of DSI in clinical research may be limited due to its typical requirement for a large number of signal measurements, which can result in longer acquisition times.

Resource-Intensive Data Processing: DSI data analysis and processing can be computationally challenging and require sophisticated algorithms and significant computer resources[85].

**Limitations of DSI:** Limited Clinical Adoption: DSI's practicality in clinical settings is hindered by its need for a large number of signal measurements, which are often critical in short scan times.

Standardization challenges: It can be difficult to standardize DSI protocols across various imaging systems and sites, which may limit the protocol's applicability in multicenter settings[86, 87].

In summary, diffusion imaging techniques have advanced with HARDI and DSI, offering significant insight into tissue microstructure. They are not as applicable in routine settings or clinical research, though, because they have trade-offs with respect to acquisition time, data complexity, and computational demands.

**Diffusion Kurtosis Imaging (DKI):** DKI is a precise magnetic resonance imaging (MRI) method used in neuroimaging to evaluate the microstructural complexity of various tissues, including brain tissues[88, 89]. Traditional diffusion MRI measures the diffusion of water molecules; DKI measures the diffusion of water molecules as well as their non-Gaussian distribution, which can reveal information about the microstructure of the tissue. In the context of DKI, kurtosis denotes the statistical measure of the shape of a probability distribution. It measures the amount that water diffusion in DKI deviates from a Gaussian distribution, suggesting the existence of intricate tissue architectures like cell membranes, myelin sheaths, and microcapillaries. Researchers[88, 89] can obtain more information on tissue microarchitecture using DKI to analyze diffusion data and derive parameters such as mean kurtosis (MK) and kurtosis anisotropy (KA), which are not available via conventional diffusion magnetic resonance

imaging. DKI can help with the diagnosis, prognosis and treatment planning of a variety of neurological disorders, such as stroke, traumatic brain injury, and neurodegenerative diseases[90].

#### **Advantages of DKI:**

**Enhanced Sensitivity:** DKI offers more information than diffusion tensor imaging (DTI), especially in areas with complex microstructural features such as tissue heterogeneity or crossing fibers[74].

**Characterization of Non-Gaussian Diffusion:** DKI provides information on tissue microstructure and pathology by simulating the non-Gaussian distribution of water diffusion in biological tissues[90].

**Measurement of Tissue Microstructural Changes:** DKI metrics, like fractional anisotropy (FA) and mean kurtosis (MK), can be sensitive indicators of microstructural changes linked to a range of neurological conditions, such as tumors, neurodegenerative diseases, and white matter injury[91].

#### **Drawbacks of DKI:**

**Complexity of Interpretation:** It can be difficult for non-experts to interpret DKI metrics because they require a sophisticated understand of diffusion physics and the biological basis of kurtosis[92, 92].

**Sensitivity to Image Acquisition Parameters:** DKI metrics are susceptible to variations in acquisition parameters, like b-values, which may cause disparities and complicate the process of contrasting the outcomes of various investigations[92].

**Greater Data Requirements and Acquisition Times:** Compared to DTI, DKI typically has higher data requirements and acquisition times. This can limit its clinical viability, especially in applications that are time sensitive or in populations that are more vulnerable[92].

#### **Limitations of DKI:**

**Tissue Heterogeneity:** In highly heterogeneous tissues, DKI may have difficulties precisely characterizing diffusion properties due to kurtosis model assumptions.

**Limited Clinical Validation:** Although DKI appears to have promise as a research tool, more studies are required to fully comprehend its clinical utility and ensure that it is widely used. To achieve this, a variety of patient populations and pathologies will need to validate the technology[93, 94].

**Processing Challenges:** DKI data analysis requires the application of complex postprocessing methods, which may lead to mistakes or inconsistencies if not performed correctly or standardized[92, 94].

**Neurite Orientation Dispersion and Density Imaging (NODDI):** Diffusion MRI (dMRI) uses a neuroimaging technique called Neurite Orientation Dispersion and Density Imaging (NODDI) to characterize the microstructural features of brain neural tissue. Unlike traditional diffusion tensor imaging (DTI), NODDI aims to provide more accurate information regarding the underlying neuronal architecture[80, 95].

The NODDI model sources the diffusion signal in each voxel from three compartments: isotropic diffusion (representing the cerebrospinal fluid CSF); intracellular diffusion (representing the diffusion of water molecules within neurites, such as axons and dendrites); and extracellular diffusion (representing the diffusion of water in the extracellular space)[80].

By estimating neurite density and orientation dispersion parameters, NODDI can provide insights into the composition and intricacy of neural tissue. The total density of neurites within a voxel is indicated by the neurite density index (NDI), while the orientation dispersion index (ODI) characterizes the degree of coherence or dispersion in the orientations of the neurites within the voxel[80, 95].

#### **Advantages of NODDI:**

**Microstructural Specificity:** By measuring neurite density and orientation dispersion independently, NODDI offers novel insights into tissue microstructure that are more closely linked to the underlying neuroanatomy than traditional diffusion metrics[96].

**Sensitivity to Pathological Changes:** NODDI metrics have shown sensitivity to a number of neuropathologies, such as brain tumors, white matter disorders, and neurodegenerative diseases, allowing for the early identification and tracking of the disease's progression[97].

**Possibility for Clinical Translation:** Because NODDI can detect microstructural changes linked to neurological conditions, it may be able to provide biomarkers for the diagnosis, prognosis, and evaluation of response to treatment[97, 98].

#### **Consequences of the NODDI:**

**Dependency on Model Assumptions:** Because the NODDI is predicated on certain assumptions about the microstructure of tissue, such as the existence of distinct compartments that represent neurites and extracellular space, it may not adequately capture the complexity of biological tissue[99].

**Challenges in Parameter Approximation** Accurate NODDI parameter estimation requires robust modeling and fitting algorithms, which may be sensitive to noise, artifacts, and image quality[100].

**Limited Spatial Resolution:** NODDI may have problems resolving microstructural features at the sub-voxel level in regions with complex fiber configurations or low signal-to-noise ratios[101].

#### **Limitations of NODDI:**

**Validation Across Populations:** Although NODDI has shown promise in research settings, more validation is required to ensure the reliability and reproducibility of its clinical utility in a variety of patient populations and imaging protocols[97, 100].

**Interpretation Complexity:** Because interpreting NODDI metrics requires an understanding of the underlying biological processes and potential confounding factors, clinicians and researchers may find it challenging to do so without specialized training[97].

It is still challenging to integrate NODDI with other imaging modalities, such as structural or functional magnetic resonance imaging, which restricts its ability to provide comprehensive information on the connections between brain structure and function. NODDI provides valuable microstructural information despite its limitations.

# Chapter 3

## DTI parameters estimation using Sparse dMRI Data

### 3.1 Theory

#### 3.1.1 Diffusion Tensor Imaging

Diffusion weighted images (DWIs) are a type of magnetic resonance imaging (MRI) that quantifies the brain's water molecule diffusion. With the use of the Diffusion Tensor Imaging (DTI) technique[50], it can be used to evaluate the damage caused by neurological diseases[102, 103] as well as the structural integrity of white matter[104] tracts. Since DTI offers quantitative measurements of the brain's structural construct, it is especially helpful in the investigation of brain development[105]. Additionally, it aids in assessing how lifestyle and environmental factors, like eating habits, physical activity, and drug use, affect the brain[65, 73]. DTI is also utilized in the study of the heart, muscles, nerve fiber development, and the digestive tube[106]. While the majority of MRI techniques produce univariate scalar images[107], DTI yields multivariate tensor-valued images that are useful for detailed image visualization[5, 55]. Under Gaussian assumption[50], the diffusion tensor, a 3x3 matrix as stated in equation 3.11, represents the diffusion rates in each combination of directions.

$$D = \begin{bmatrix} D_{xx} & D_{xy} & D_{xz} \\ D_{yx} & D_{yy} & D_{yz} \\ D_{zx} & D_{zy} & D_{zz} \end{bmatrix} \quad (3.1)$$

Multiple sclerosis, Alzheimer's disease, traumatic brain injury, stroke, and other neurological conditions can all be diagnosed and tracked with the help of DTI, which offers precise images of

the white matter structure of the brain. Moreover, the efficacy of various therapies and treatments for these conditions can be assessed using DTI[108]. DTI measures three key parameters that are indicative of the structural integrity and function of the brain: mean diffusivity (MD), axial diffusivity (AD), and fractional anisotropy (FA)[109]. Comprehending these values can be beneficial for both neurological disorder diagnosis and treatment[110].

Voxel diffusion[4, 50, 111] is measured at each image along a set of distinctly gradient directions  $u_1, u_2, \dots, u_n$ , and the corresponding diffusion signal  $s = [s_1, s_2, \dots, s_n]^T$ . Equation 3.2, with simplified assumptions, represents the diffusion tensor model for voxels containing a diffusion pattern[50, 112, 113]. Here, the diffusion signal with  $b = 0$  is represented by  $s_0$ .

$$s_i = s_0 e^{-bu_i^T Du_i} \quad (3.2)$$

The symmetric matrix  $D$  describes the diffusion rates in all directions. The eigenvalues  $\lambda_1, \lambda_2$ , and  $\lambda_3$  represent the three positive principal effective diffusivities, and the eigenvectors  $\mathcal{E}_1, \mathcal{E}_2$ , and  $\mathcal{E}_3$  represent the three orthogonal principal coordinate directions.

$$D\mathcal{E}_i = \lambda_i \mathcal{E}_i, i = \{1, 2, 3\} \quad (3.3)$$

These equations are based on[50, 111].  $DE = E\Lambda$  where  $E = (\mathcal{E}_1 | \mathcal{E}_2 | \mathcal{E}_3)$  and  $\Lambda = \text{diag}(\lambda_1, \lambda_2, \lambda_3)$ . The eigenvalues are contained in the diagonal matrix  $\Lambda$ , and the orthonormal eigenvectors are contained in the columns of the matrix  $E$ .

We discuss the quantitative measures—Fractional Anisotropy (FA), Axial Diffusivity (AD), and Mean Diffusivity (MD)—that are particularly important in this field within the framework that has been suggested.

The directionality or degree of anisotropy of water diffusion in biological tissues, especially white matter, is measured by fractional anisotropy.

$$FA = \sqrt{\frac{3}{2} \frac{\sqrt{(\lambda_1 - \hat{\lambda})^2 + (\lambda_2 - \hat{\lambda})^2 + (\lambda_3 - \hat{\lambda})^2}}{\sqrt{\lambda_1^2 + \lambda_2^2 + \lambda_3^2}}} \quad (3.4)$$

where,

$$\hat{\lambda} = MD = \frac{(\lambda_1 + \lambda_2 + \lambda_3)}{3} \quad (3.5)$$

According to equations 3.11 and 3.5,  $\hat{\lambda}$  denotes the average of the eigenvalues  $\lambda_1, \lambda_2$ , and  $\lambda_3$  derived from the diffusion tensor  $D$ . The average apparent diffusion along each of the three diffusion axes is represented by the mean diffusivity, or MD. The amount of apparent diffusion along the primary diffusion axis is known as apparent diffusivity (AD).  $AD = \lambda_1$ .

For HCP dataset, the operation of the deep transformer neural network can be seen in Figure 3.1, which generates a nonlinear mapping between  $5 \times 5 \times 5$  DWI patch inputs and quantitative measures

of FA, AD, and MD (output) in the proposed approach. One way to represent the suggested neural network is as  $[FA_{predict}, AD_{predict}, MD_{predict}] = F(X; w)$ , where traditional tensor fitting is not necessary because nonlinear function  $F$ , which maps input  $X$  and trainable parameters  $w$  to output quantitative measures, is learned and optimized through training a deep neural network[4]. We want to extract the diffusion tensor  $D$  from the signal for the NIFD and ADNI datasets, thus rewrite equation 3.2.

$$s_i = s_0 e^{(-b_{xx} D_{xx} - b_{yy} D_{yy} - b_{zz} D_{zz} - 2b_{xy} D_{xy} - 2b_{xz} D_{xz} - 2b_{yz} D_{yz})} \quad (3.6)$$

The function of diffusion directions  $\mathbf{g} = \{g_i\}_{i=1}^N$  is represented here by  $b_{jk}$ , for  $j, k \in \{x, y, z\}$ , where each  $g_i = [g_{ix}, g_{iy}, g_{iz}]$  is a unit direction vector. In addition, the zero diffusion signal is represented by  $s_0$ . The best estimate of the diffusion coefficient  $D$  is provided by the equation  $s_i/s_0 = e^{-bg_i^T D g_i}$ , which is obtained by simplifying the b-matrix as described in [112]. For every  $g_i$ , the apparent diffusion coefficient  $K_i$  can be computed as follows:  $K_i = g_i^T D g_i = (-1/b) \ln(s_i/s_0)$ .

The linear mapping between the diffusion tensor  $D$  and the apparent diffusion coefficient estimates  $K = [K_1, \dots, K_N]^T$  using  $K = \alpha \bar{D}$ , where  $\bar{D} = [D_{xx}, D_{yy}, D_{zz}, D_{xy}, D_{xz}, D_{yz}]$ , is represented by the design matrix  $\alpha = [\alpha_1, \dots, \alpha_N]^T \cdot 2g_{ix}g_{iy}, 2g_{ix}g_{iz}, 2g_{iy}g_{iz}$ , and  $\alpha_i = [g_{ix}^2, g_{iy}^2, g_{iz}^2]^T$ .  $\bar{D} = (\alpha^T \alpha)^{-1} \alpha^T K$  is used in the conventional linear least squares fitting (LLS) method [4], but it is sensitive to noise and sparse measurements.

We suggest solving for  $D$  directly using Equation 3.6 as an inverse map  $\bar{D} = F(\mathbf{X}, \mathbf{g})$ , where the input  $\mathbf{X} = [s_1/s_0, \dots, s_N/s_0]$  per voxel, in place of using the linear model for sparse measurements. Using a neural network based on Swin-transformers, we have formulated  $F$  [68]. We present a more general modeling framework in which a single model (e.g., 41, 21, 5) can effectively learn from diffusion signals with varying numbers of diffusion directions.

Multiple attention heads are frequently used in real-world applications to learn various input representations. With just six diffusion-weighted images, the Transformer-DTI [5] model used multi-head self-attention to estimate diffusion tensor imaging parameters.

### 3.1.2 Investigating the Feasibility of DTI Parameters Estimation over HCP

The Human Connectome Project (HCP) dataset is a cornerstone of neuroimaging research because of its large collection of high-quality data[114]. This literature review aims to examine current research investigating the feasibility of estimating DTI parameters using the HCP dataset, with a focus on methods, challenges, and advancements in the area[115, 116].

**Methods of Estimation for DTI Parameters:** Mean diffusivity (MD), fractional anisotropy (FA), axial and radial diffusivity, and other DTI measurements can be used to describe the organization

and integrity of white matter[117, 118]. In recent investigations, sophisticated algorithms have been applied for DTI processing, including as enhanced tensor fitting methods, diffusion model-based approaches, and machine learning techniques[5, 34, 119]. These methods aim to extract comprehensive information from diffusion-weighted MRI data in order to properly estimate microstructural features.

With the help of the HCP dataset, which includes diffusion and structural MRI images from a large cohort of healthy individuals, studying brain connectivity and organization has never been easier. Utilizing the enormous HCP dataset, studies on individual variability in white matter architecture, brain network topology, and the influence of genetic factors on diffusion metrics have been conducted recently. Considerable progress in neuroscience and neuroimaging has been made possible by the richness and diversity of the dataset.

**HCP Dataset-Based Feasibility Studies for Estimating DTI Parameters:** Utilizing cutting-edge image processing pipelines and computational techniques, recent research has shown that predicting DTI parameters over the HCP dataset is feasible. In order to assure the precision and dependability of DTI parameter estimation, these investigations have tackled issues such motion artifacts, eddy current distortions, and image registration problems. In addition, initiatives have been taken to improve the reproducibility of results by standardizing analysis pipelines and establishing quality control protocols.

**Limitations and Challenges:** Although there has been a lot of advancement, there are still a number of difficulties with DTI parameter estimation using the HCP dataset. Data harmonization and analysis are restricted by subject-specific characteristics, variations in scanner technology, and variability in acquisition techniques. Furthermore, it is still difficult to understand complicated diffusion measures in the context of underlying biological processes, which calls for interdisciplinary cooperation and methodological developments.

The Human Connectome Project (HCP) gathered a significant amount of behavioral, demographic, and brain imaging data that is available to the public in the form of the HCP Young Adult dataset. Data from 1200 healthy young adults, aged 22 to 35, are included in the Young Adult dataset. Diffusion-weighted magnetic resonance imaging (DW-MRI) data obtained using a multi-shell acquisition protocol and having multiple b-values are included in the HCP Young Adult dataset. The b-value is directly related to how strong the diffusion-sensitizing gradients were used in the MRI scan. The random movement of water molecules in tissue, or diffusion, is measured using diffusion-sensitizing gradients. The dataset comprises three distinct b-values for DW-MRI data acquisition:  $1000s/mm^2$ ,  $2000s/mm^2$ , and  $3000s/mm^2$ . In the course of data processing and analysis, several images not diffusion weighted ( $b = 0$ ) from the acquisition protocol are also included. These images serve as a reference for diffusion-weighted images. We only take into account DW-MRI scans with  $b = 1000$  for the estimation of DTI. There are 90 diffusion encoding directional signals available for  $b = 1000$  image volumes. These signals are

uniformly distributed on a unit sphere.

In conclusion, new research has shown that it is feasible to estimate DTI parameters over the HCP dataset, opening up currently uncommon possibilities for understanding brain connection and microstructure. In spite of obstacles, the discipline is moving forward thanks to collaborative efforts and continuous methodological improvements, which open up new avenues for understanding the complex structure of the human brain. In the ongoing effort to solve the mysteries of the brain, the HCP dataset continues to be a vital resource for neuroimaging research.

### **3.1.3 Investigating the Feasibility of DTI Parameters Estimation over MICCAI Quad22**

The purpose of this research was to evaluate the validity of Deep Learning-based reconstructed dMRI images for migraine pathology in a real clinical setting. The primary disabling disorder known as migraine is common and more common in young and middle-aged women. It is characterized by recurrent episodes of headache. Currently, there are no biomarkers for migraine, and the pathophysiological mechanisms are poorly understood despite the high prevalence of the disease. The International Headache Society's Headache Classification Committee[120] has classified migraine patients into two groups: episodic migraine (EM) and chronic migraine (CM). The two groups are distinguished by the number of days of headache each month (15 or more days for patients with chronic migraine).

Migraine is useful because the results of dMRI are not as dramatic as those of healthy controls (HC). On the contrary, with disorders such as schizophrenia or Alzheimer's disease, where it is relatively easy to find statistically significant results with traditional methods based on DTI, T1, and T2-weighted magnetic resonance imaging, it becomes difficult to appreciate techniques or parameters that can better define pathophysiological properties.

There have been several dMRI studies evaluating migraine, and the most popular method for assessing microstructural properties is DTI. Studies comparing migraine patients with healthy controls[121, 122, 123] and between EM and CM patients[123, 124] have reported differences in DTI-related scalars such as fractional anisotropy (FA), mean diffusion (MD), and axial diffusivity (AD). When evaluating microstructural properties, DTI has been the most often used method. Variations have been observed between EM and CM patients, as well as between migraine patients and controls. The finding reported most frequently in these investigations is that MP had reduced FA compared to controls. Many studies have reported higher and lower AD values in MP compared to controls. Like AD, there have been trends in both MD and radial diffusivity with higher and lower values in MP compared to controls; however, more studies have reported higher values in MP. Somewhere else[125] is a more thorough explanation of these findings and additional comparisons with a larger number of references.

The individuals involved in this study were taken from a prior clinical trial on migraine[126]. A data set was constructed with patients with EM and CM and healthy controls (HC).

Snowball and convenience sampling were used to find HC. Exclusion criteria applied to controls who had a history of migraine, other headache conditions other than infrequent tension-type headaches (less than one attack per month), or a history of other neurological or psychiatric conditions. HC's age ranged from 18 to 65. Furthermore, controls received a questionnaire to determine whether they experienced headaches similar to migraines. Migraine patient(MP) was examined for the first time by a neurologist specialized in headache disorders. Patients with migraine had been referred to the Hospital Clínico Universitario de Valladolid (Valladolid, Spain) Headache Unit.

The assessment of the microstructural characteristics of the brain and other organs is made possible by diffusion magnetic resonance imaging (dMRI), a non-invasive imaging method that provides information about the diffusion of water molecules in biological tissues[127, 128]. At different stages of the dMRI data pipeline, the application of deep learning techniques in this modality has demonstrated great potential and is a rapidly expanding field. Among these methods are automatic detection and elimination of artifacts[129, 130], phase error correction in multi-shot dMRI acquisitions[131], and noise filtering[34, 132]. Data harmonization from various sources has also made extensive use of artificial intelligence (AI) techniques. This is especially crucial when it comes to MRIs, since the data obtained from various vendors' scanners or with varying parameters can differ greatly. Harmonizing such databases is essential to allow multisite studies. In order to improve the statistical power of the analysis and generalize results across different sites, DL techniques have demonstrated the ability to integrate data from multiple sources[133, 134, 135, 136]. It is anticipated that the use of DL in the harmonization process will have a major impact as it can standardize data collected under different circumstances.

Our goal is to find out if DTI parameters generated from volumes acquired with a reduced number of data and processed by deep learning techniques can match the statistical results obtained from standard quality acquisitions, considering the potential benefits of using DL on incomplete data in dMRI. Our goal is to confirm in actual clinical trials the value of deep learning-based reconstruction methods.

To be clear, the study has concentrated on one important dMRI component, namely the angular resolution. In dMRI, this parameter is a critical design component that is proportional to the inverse of diffusion sensitizing gradient directions[137, 138]. Several dozens or even hundreds of gradient directions are needed to fit the basis in High Angular Resolution Diffusion Imaging (HARDI) techniques, while DTI methods only require a minimum of six gradient directions[139, 140, 141]. To reduce examination time and guarantee patient comfort, the number of gradient directions must be optimized in clinical settings. Conversely, decreasing the number of gradient directions might cause[142] to eliminate small variations in the angular properties of dMRI data, which could result in inaccurate quantitative measures from a fitted model. Clinical research may therefore yield

varying outcomes with varying numbers of gradient directions.

To enhance the number of gradient directions, or to increase angular sampling, one can either decompose the dMRI signal into orthogonal basis and reconstruct the angular information under a different gradient configuration[143, 144, 145] or average the local angular neighborhood using the representation of the spherical radial basis functions[146]. Although other AI-based approaches have been applied in[147, 148, 149], the efficacy of these methods was assessed by applying numerical metrics such as the RMSE, PSNR, or SSIM indexes. Recent research, however, has demonstrated that fewer gradients may lead to a loss of clinically meaningful data and complicate the identification of variations in a range of medical conditions[150, 151]. It has been established that the number of diffusion gradient orientations plays a significant role in determining the diffusion and DTI descriptor values as well as the outcomes of their statistical comparisons between clinical groups.

Patients with episodic migraine (EM) and chronic migraine (CM), in particular, comprised the evaluated clinical groups in this investigation. The following criteria led to the selection of this disorder:

With an appropriate acquisition scheme that permits downsampling the number of gradient directions without sacrificing the coverage of the q-space, a unique and comprehensive database of migraine patients (MP) was accessible. The brain regions with statistically significant differences have been identified by previous studies using the same database using fully sampled data, which makes them the perfect benchmark for reduced acquisitions.

Patients with episodic migraine (EM) and chronic migraine (CM), in particular, comprised the evaluated clinical groups in this investigation. With an appropriate acquisition scheme that permits downsampling the number of gradient directions without sacrificing the coverage of the q-space, a unique and comprehensive database of migraine patients (MP) was accessible.

We used 160 dMRI volumes, all of which included a special q-space coverage scheme that allows us to subsample the data with ease by just choosing 21 of the 61 gradient directions that are appropriate, eliminating the need to use interpolation algorithms. Using the available reduced dMRI dataset, we aimed to replicate a realistic scenario in a clinical setting. We found that when only 21 gradient directions were used, 60% of the statistically significant differences between EM and CM patients that had been found in a white matter study using 61 gradient directions were no longer present as mentioned in Fig 3.2.

### 3.1.4 Investigating the Feasibility of DTI Parameters Estimation over NIFD

Frontotemporal dementia (FTD) is a serious neurodegenerative disease that mainly affects the frontal and temporal lobes of the brain, resulting in behavioral abnormalities and cognitive decline. To begin the intervention and for patients to receive proper care, an early and accurate diagnosis

of FTD is essential. About 12–22 people out of every 100,000 people, according to the experts, suffer from FTD. This indicates that 1.2 million to 1.8 million individuals globally are affected. To help with the early diagnosis of frontotemporal dementia, this research study proposes a novel deep learning framework that makes use of sparse diffusion measures taken from neuroimaging data. The proposed framework successfully distinguishes between people who are healthy and those who have FTD by utilizing deep learning techniques to automatically extract pertinent features from the data. The results of the experiment show how promising the suggested method is for enhancing FTD diagnosis and opening up opportunities for future research in this field.

The neurodegenerative condition known as frontotemporal dementia (FTD) affects millions of individuals worldwide [152, 153]. Time-consuming diffusion weighted imaging (DWI) used for the current clinical diagnosis requires at least 40 diffusion directions and can result in scanning times longer than three hours [154, 155]. For management and treatment to be effective, an accurate and timely diagnosis is essential [156, 157]. A potent neuroimaging method called diffusion tensor imaging (DTI) offers important insights into the white matter of the brain, which is frequently damaged in patients with frontotemporal dementia (FTD) [108, 158, 159]. This presents problems for patients and diagnostic laboratories because conventional linear methods for DTI processing call for multiple diffusion directions. In terms of speeding up DTI processing and improving quantitative measures for FTD diagnosis, recent developments in deep learning [1, 54, 160, 161, 162, 163] appear promising. By focusing on pertinent brain regions, attention-based deep learning techniques such as Transformer-DTI [5] allow efficient processing with fewer diffusion directions. However, because of the larger trainable parameters, longer training times, and higher memory requirements, scalability becomes an issue with more diffusion directions.

We suggest a novel attention-based deep learning model called Swin-Transformer to tackle this. Input feature maps are processed efficiently by the hierarchical structure of the Swin Transformer by being divided into non-overlapping patches, which lowers the number of parameters and computational expenses. Using our proposed model on the frontotemporal lobar degeneration neuroimaging initiative (NIFD) dataset, we aim to accurately diagnose early FTD incidence by extracting quantitative measures such as Fractional Anisotropy (FA), Axial Diffusivity (AD), and Mean Diffusivity (MD). We evaluate its performance for various diffusion directions against both Transformer-DTI and conventional linear methods.

### 3.1.5 Investigating the Feasibility of DTI Parameters Estimation over ADNI

With an estimated 6.2 million cases in the US, Alzheimer's disease is one of the most prevalent neuro-degenerative diseases. In order to improve the early diagnosis of Alzheimer disease (AD) using

sparse data, this research study explores the potential of Transformer-based deep learning techniques to speed up the processing of diffusion tensor imaging (DTI) measures. Diffusion Weighted Imaging (DWI) is a laborious procedure that requires more than three hours of scanning time per patient. Each diffusion direction takes two to five minutes to complete, and a minimum of forty diffusion directions are required for the standard clinical diagnosis. Our proposed model, which reduces the scanning time by more than half, makes use of the attention mechanism to generate quantitative measures of mean diffusivity (MD), axial diffusivity (AxD), and fractional anisotropy (FA) using 5 and 21 diffusion directions. We show that our proposed model, which uses sparse diffusion directions to achieve accurate quantitative measurement of FA, AxD, and MD scores for early diagnosis of AD patients from healthy controls, outperforms the conventional linear least square method on the Alzheimer's Disease Neuroimaging Initiative (ADNI) dataset.

Alzheimer disease (AD) is a neurodegenerative disease that affects millions of people worldwide [152, 153]. DWI is used in the routine clinical diagnosis of AD. It is a laborious procedure that requires at least 40 diffusion directions and takes two to five minutes for each direction. As a result, the scanning time for every patient is longer than three hours [155]. Early and accurate diagnosis is critical to effective treatment and management of AD [156, 157]. The brain's white matter microstructural integrity is often compromised in Mild Cognitive Impairment (MCI), an early stage of Alzheimer's disease (AD) [108, 158, 159]. Diffusion tensor imaging (DTI) is a powerful neuroimaging technique that can offer useful information on this topic. However, the patient and the diagnostic laboratory face difficulties because the conventional linear least squares method for DTI processing requires many diffusion directions.

Current developments in deep learning have demonstrated great promise for speeding up the processing of DTI measures and enhancing the quantitative measures of AD and MCI diagnosis [1, 54, 160, 162]. Attention-based [5] deep learning is an effective method that extracts quantitative measures from diffusion tensor imaging, namely fractional anisotropy (FA), axial diffusivity (AxD) and mean diffusivity (MD), by focusing on pertinent brain regions of interest. Even with six diffusion directions, it is possible to process DTI measures more accurately and efficiently by using the attention mechanism [5]. Transformer-DTI [5] makes use of the multihead self-attention mechanism, which was first presented in the work by Vaswani et al. on attention [67], to take advantage of the spatial correlation found in diffusion tensor parameters and the diffusion signals between adjacent slices and voxels. Although transformer models have great potential, issues with scalability arise when handling more diffusion directions. This is mainly because there are more trainable parameters, which means that training takes longer and requires more memory. As a result, it becomes difficult to train a single model that can handle multiple diffusion directional signals. In contrast to conventional transformer models, the Swin transformer model has attracted a great deal of attention due to its remarkable capacity to handle larger input sizes [68]. With its recent introduction, this deep neural network architecture has shown

remarkable performance in a range of computer vision tasks, including semantic segmentation, object detection, and image classification. The Swin Transformer utilises a hierarchical structure in contrast to traditional transformer models, which process input data sequentially [67].

The input feature maps are split into non-overlapping patches in the Swin Transformer, and several transformer layers are used to process these patches concurrently. This method lowers the self-attention mechanism's computational cost and permits effective parallelization. As a result, fewer parameters are needed, which is essential for creating a more comprehensive model that can handle several diffusion-directional signals. To precisely diagnose early incidence of AD in this context, we present a novel attention-based deep learning model called Swin-Transformer that is based on deep learning and can extract quantitative measures like FA, AxD, and MD. We utilize the publicly available Alzheimer's Disease Neuroimaging Initiative (ADNI) dataset to assess the efficacy of our suggested model. For 41 diffusion directions, we compare the performance of our model with that of a conventional linear least squares method [4]. Additionally, we compare our model with Transformer-DTI [5] and the conventional linear least square method [4] for 21 and 5 diffusion directions, respectively. Our goal in making these comparisons is to show how much better our suggested model is at correctly identifying AD in its early stages.

## 3.2 Methods

### 3.2.1 Data Preprocessing and Model Training over HCP

Robust estimation of DTI parameters depends extensively on compactly capturing correlation information between neighboring voxels. Conventional techniques such as LLS fitting estimates only depend on a single voxel. To capture correlations between nearby voxels, the following layers have previously been used in deep neural based approaches[5, 33, 34, 164, 165].

**A. Convolution Layer:** To discover local correlation structures within a layer, convolutional neural networks (CNNs) are frequently employed[164]. This is done by using the input image's small neighborhoods, or kernel sizes, which are convolved with a weight matrix that has been learned to generate the feature maps that are output. With height  $h$ , width  $w$ , and  $d_{in}$  input channels, let  $x \in \mathbb{R}^{h \times w \times d_{in}}$  be the input image. A region with shape  $k \times k \times d_{in}$  is obtained by extracting a local neighborhood  $\mathcal{N}_k$  with spatial extent  $k$  for each pixel  $x_{ij}$ . By spatially summing the product of depthwise matrix multiplications of the input values with a learned weight matrix  $W \in \mathbb{R}^{k \times k \times d_{out} \times d_{in}}$ , the output  $y_{ij} \in \mathbb{R}^{d_{out}}$  for position  $ij$  is obtained; The following can be used to represent the output  $y_{ij}$ :

$$y_{ij} = \sum_{a,b \in \mathcal{N}_k(i,j)} W_{i-a,j-b} x_{a,b} \quad (3.7)$$

where  $\mathcal{N}_k(i,j) = (a, b) \mid |a - i| \leq k/2, |b - j| \leq k/2$  is the set of indices within the neighborhood of

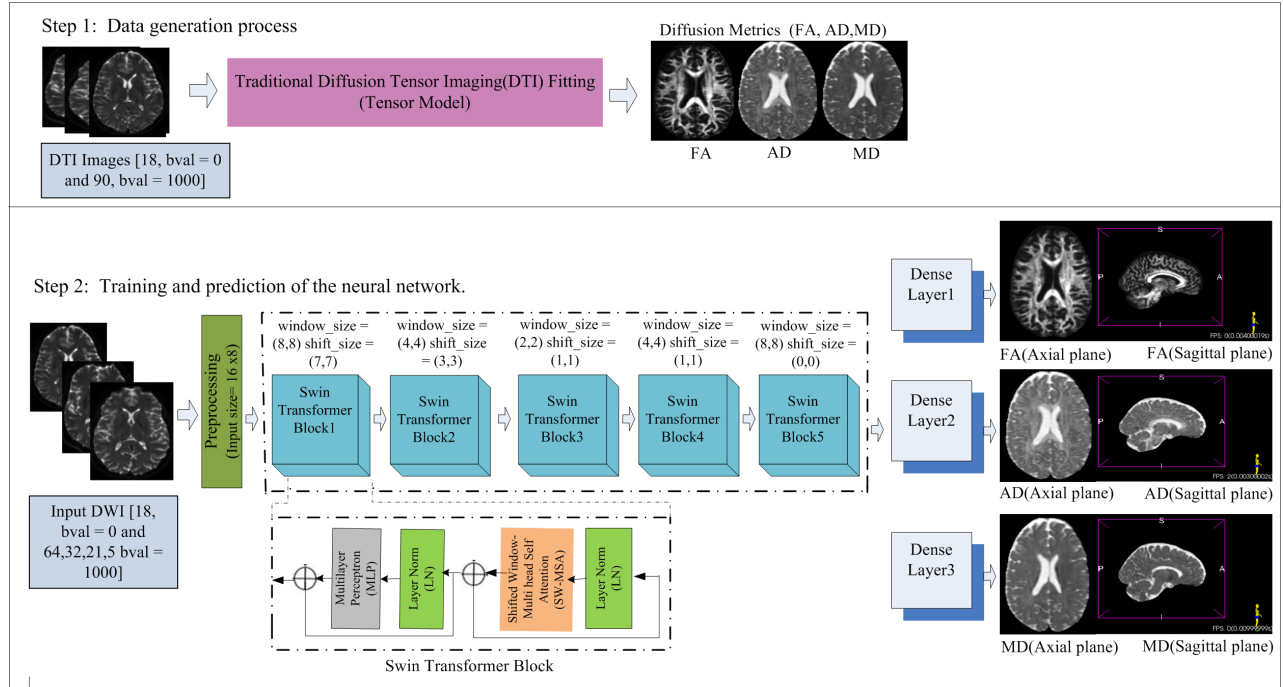


Figure 3.1: The proposed framework over HCP dataset consists of two steps: step 1 describes how data are generated, and step 2 concentrates on neural network training and prediction.

pixel  $x_{ij}$ . A convolutional layer was used by 3D U-Net16[33, 34, 69]. Although the Convolution Layer uses parameters efficiently, it has trouble capturing non-local features and its parameter size increases quickly as the number of filters and filter size increase.

**B. Self-attention :** The local region of the pixels is extracted at positions  $a, b \in \mathcal{N}_k(i, j)$  with spatial extent  $k$  centered around  $x_{ij}$ , just as convolution does with a pixel  $x_{ij} \in \mathbb{R}^{d_{in}}$ . In contrast to earlier studies on attention in vision, which carried out global attention between every pixel, this type of local attention is distinct. Global attention is computationally costly, which makes it difficult to use it for all layers in a fully attention model. To compute the output of pixels  $y_{ij} \in \mathbb{R}^{d_{out}}$ , the single head attention[164] is used as follows:

$$y_{ij} = \sum_{a,b \in \mathcal{N}_k(i,j)} \text{softmax}_{ab}(q_{ij}^\top k_{ab}) v_{ab} \quad (3.8)$$

where the neighborhood pixels and the pixel in position  $ij$  are linearly transformed by the queries  $q_{ij} = W_Q x_{ij}$ , the keys  $k_{ab} = W_K x_{ab}$ , and the values  $v_{ab} = W_V x_{ab}$ . A softmax applied to all logits computed in the surrounding area of  $ij$  is indicated by the notation  $\text{softmax}_{ab}$ . The learned transforms are  $W_Q$ ,  $W_K$ , and  $W_V \in \mathbb{R}^{d_{out} \times d_{in}}$ .

Although self-attention considers global features by applying data from all pixels at once, it has the drawback of having more parameters because it is global. However, this limitation can be mitigated by carefully using self-attention or downsampling data to reduce computational complexity. Stronger than convolution, self-attention ensures global relationships and long-range

dependencies within the input data. It allows for flexibility in modeling complex interactions while maintaining computational efficiency and performance, but careful management of the parameter requirements is necessary.

**C. Multi-head self attention:** The input data is represented along the depth of the data as a diffusion signal. In the context of local self-attention[164], spatial information is aggregated over neighborhoods convolutions through the use of a convex combination of value vectors with mixing weights ( $\text{softmax}_{ab}(\cdot)$ ) that are influenced by content interactions. For each pixel  $ij$ , this computation is performed again. To learn multiple distinct representations of the input, multiple attention heads are used in practice. The method involves splitting the pixel features  $x_{ij}$  depthwise into  $N$  groups  $x_{ij}^n \in \mathbb{R}^{d_{in}/N}$ . Then, for each group, separate single-headed attention is computed using distinct transforms  $W_Q^n$ ,  $W_K^n$ , and  $W_V^n \in \mathbb{R}^{d_{out}/N \times d_{in}/N}$  per head. Finally, the output representations are concatenated to produce the final output  $y_{ij} \in \mathbb{R}^{d_{out}}$ .

$$x_{ij} = [x_{ij}^1, x_{ij}^2, \dots, x_{ij}^w]; y_{ij}^n = \sum_{a,b \in \mathcal{N}_k(i,j)} \text{softmax}_{ab}(q_{ij}^{n\top} k_{ab}^n) v_{ab}^n \quad (3.9)$$

$\text{softmax}_{ab}$  is the result of applying a softmax function to the logits computed in the neighborhood of  $ij$  in order to capture the relationship between the pixels in the neighborhood. This softmax operation gives a probabilistic interpretation of each pixel's importance in the neighborhood and guarantees that the attention weights sum to 1. Multi-head self-attention was used by Transformer-DTI[5].

**D. Spatial relative attention:** Spatial relative attention calculates the spatial relation between a target pixel  $p_{ij} = [i, j]$  and a pixel  $p_{ab} = [a, b]$  within its position scope as follows[164, 165]:

$$y_{ij}^n = \sum_{a,b \in \mathcal{N}_k(i,j)} \text{softmax}_{ab}(q_{ij}^{n\top} k_{ab}^n + f_{\theta_g}^n(p_{ab} - p_{ij})) v_{ab}^n;$$

$$y_{ij} = [y_{ij}^1, y_{ij}^2, \dots, y_{ij}^n] \quad (3.10)$$

where, depending on a geometric prior,  $f_{\theta_g}(p_{ab} - p_{ij})$  defines the composability of a pixel pair  $(p_{ij}, p_{ab})$ . Our method is based on patches; the input image is divided into patches, and each patch is given a different amount of spatial relative attention. This enables us to model long-range spatial relations in large images and lower the computational cost of spatial relative attention.

#### E. Window Self attention:

The concept of window self-attention, which is derived from the Swin-Transformer[68], is integrated into our proposed SwinDTI model. In order to reduce the number of parameters and simultaneously increase non-linearity, we apply specific modifications. Using a predetermined stride, our model systematically moves adjacent windows, building upon the Swin Transformer[68] architecture. The

purposeful modification results in areas where windows overlap with each other. By allowing tokens to form connections despite belonging to separate windows, this strategic overlap aims to promote inter-token attention. A wider range of possibilities for mutual influence is introduced by the dynamic interplay between the tokens, which encourages the development of more detailed and complex representations. Key to our model is the window self-attention mechanism in SwinDTI, which provides several advantages over conventional self-attention mechanisms[68].

**Window Size and Direction Vector:** We use  $5 \times 5 \times 5$  as the fixed patch size in SwinDTI. Rather than applying the learned weights to the diffusion direction, we concatenate the direction vector into the input signal. This improves the model’s non-linearity and enables it to represent more intricate relationships between the input data. See subsection 2.2 for more information.

**Shared Triplets:** Self-attention traditionally applies distinct triplets of (query, key, value) to each position in the input [5, 67]. On the other hand, we use window self-attention in SwinDTI, where all windows in a patch receive the same triplets. By doing this, the needed number of parameters is greatly decreased without compromising the non-linearity of the model.

**Compact Parameter Space:** SwinDTI achieves a more compact parameter space than conventional self-attention mechanisms because it makes use of shared triplets. Because of its compactness, the model can learn more complicated functions while still operating effectively and efficiently.

**Shifting Mechanism:** In order to overcome the restriction of only learning local features shared by all windows, SwinDTI integrates a shifting mechanism into the architecture of the Swin Transformer. By applying various shift sizes across several Swin Transformer blocks, this mechanism produces shifted windows that are different from the original windows. Because there are several layers in the Swin-transformer block with varying shift sizes, SwinDTI is able to efficiently capture both global and local features. Through this mechanism, a thorough correlation of the diffusion signals between and within patches is captured. Enhancing predictive performance, SwinDTI strikes a balance between capturing local and global features by merging the window self-attention mechanism and the shifting mechanism. Moreover, SwinDTI is a more effective and efficient model for DTI prediction tasks due to its increased non-linearity and fewer parameters.

The three stages of the proposed model are as follows: producing training data is the first step, training a neural network is the second, and predicting quantitative measures of FA, AD, and MD is the last stage. Algorithm 1 describes the Dataset in detail, as does the Model Training procedure.

**Data Preprocessing and Model Training:** We have applied Qball-based interpolation to generate sub-datasets of the original dataset that have fewer diffusion directions [146, 166].  $N_{dir}$  represents the number of diffusion directions. We specifically interpolated to  $N_{dir} = \{64, 32, 21, 5\}$ , where the unit sphere’s diffusion directions are uniformly sampled. These

sub-datasets are denoted as  $HCP - N_{dir}$ .

---

**Algorithm 1** An algorithm for preprocessing data for HCP dataset

An algorithm to generate preprocessed training datasets  $HCP - 90$ ,  $HCP - 64$ ,  $HCP - 32$ ,  $HCP - 21$ , and  $HCP - 5$  by preprocessing DWI images of the HCP dataset.

**Step 1:** Apply the DTI model fit from the DIPY Python package[166] to each DWI image separately to create FA, AD, and MD images.

**Step 2:** Select  $100K$  voxels that are uniformly distributed in the range of  $(0, 1)$ , excluding 0, from each DWI image in accordance with their FA score.

**Step 3:** Obtain  $100K$  tuples of (input, ground-truth), where each tuple contains the ground-truth, which is a  $5 \times 5 \times 5$  voxel patch with  $3 \times 1$  vector per voxel of corresponding FA, AD, and MD scores, and the input, which is a  $5 \times 5 \times 5$  voxel patch with a 90 diffusion directions per voxel. This process should be repeated for each DWI image.

**Step 4:** For each input voxel, concatenate the diffusion signal of the neighboring  $5 \times 5 \times 5$  patch to obtain a  $125 \times 90$  matrix.

**Step 5:** To obtain a  $128 \times 90$  matrix for each input voxel, concatenate the diffusion direction ( $3 \times 90$ ) with the diffusion signal.

**Step 6:** To create a  $128 \times 100$  matrix, zero-pad each tuple's input; the resulting  $125 \times 3$  matrix will be the ground truth. Let  $HCP - 90$  be the name of the resulting training dataset.

**Step 7:** Using Qball-based[146, 166] interpolation in the DIPY package, interpolate 64, 32, 21, and 5 directional diffusion signals from the 90-directional input of the  $HCP - 90$  dataset.

**Step 8:** Create inputs of size  $125 \times 64$ ,  $125 \times 32$ ,  $125 \times 21$ , and  $125 \times 5$  vectors, as well as ground truth of size  $125 \times 3$  matrix, by concatenating the diffusion direction with the diffusion signal of each tuple.

**Step 9:** Each tuple's input should be zero-padded to create a  $128 \times 100$  matrix.

**Step 10:** The resulting training datasets for  $N_{dir} = \{64, 32, 21, 5\}$  should be called to as  $HCP - 64$ ,  $HCP - 32$ ,  $HCP - 21$ , and  $HCP - 5$ , respectively.

---

The original  $HCP - 90$ ,  $HCP - 64$ ,  $HCP - 32$ ,  $HCP - 21$ , and  $HCP - 5$  images each contained one million tuples, which we used to train our neural network. It came from a subset of ten DWI images that had undergone pre-processing with the help of **Algorithm 1**. From a different set of 5 DWI images, we selected 500K tuples from the same  $HCP - N_{dir}$  datasets for the validation set. We selected an additional 500K tuples from each of the same  $HCP - N_{dir}$  datasets derived from a distinct set of 5 images for the testing set. We trained two identical models on the two sets of 10 images each using 20 images from the  $HCP$  dataset in order to assure consistency and robustness of the model. Our neural network uses a swin-transformer block, which is well known for its ability to identify correlation in input signals, as seen in Figure 3.1. The diffusion signals and the diffusion directions, as supplementary information, are the input signals in our scenario. Our model took into account diffusion signals in the adjacent  $5 \times 5 \times 5$  patch, in addition to the diffusion signal within a voxel. This will increase the prediction robustness with minimal computational overhead. The nonlinearity in the DTI parameter estimation is learned by the swin-transformer block through matrix multiplication within the attention mechanism.

We performed experiments in the SwinDTI framework, collecting data on diffusion signals from 3D patches and reformulating them into a 2D matrix. We employed relative position indexing based on the 3D row-major order to maintain the spatial information of the original 3D patch. The input of size  $16 \times 8 \times 100$ , where  $16 \times 8$  is the input size of the outer window and 100 is the input size

of the channels, is used by each of the five swin-transformer blocks in our model in order. Figure 3.1 illustrates the various inner window and shift sizes of each swin-transformer block, which are determined through empirical means. It also removes all dependence on the diffusion signals' order and directions in the input due to the linear embedding in the swin-transformer block. Three sets of two dense layers, each with a separate absolute loss and varying scaling, processed the swin transformer output to adjust to the various ranges of values of the FA, AD, and MD output. Since the values of all three parameters fall between 0 and 1, the Sigmoid activation was used in the final layers. The Gelu activation was used in the Swin-transformer block, while the Relu activation was used in all other layers. We employed the loss function L1 since the ranges for mean diffusivity (MD), axial diffusivity (AD), and fractional anisotropy (FA) all fall between 0 and 1. Scaling factors for each output were set to  $10^3$ ,  $10^5$ , and  $10^5$  for FA, AD, and MD, respectively. The model was trained using only augmentations for 100 epochs, as indicated in **Algorithm 1**.

### 3.2.2 Data Preprocessing and Model Training over MICCAI Quad22

Neural Network Training using preprocessed Healthy Control (HC) data: We trained our neural network on a dataset comprising two million tuples each from *HC* and *HC – 21* obtained from 20 DWI images. To create the validation set, we selected 500K tuples from *HC* and *HC – 21* from a separate set of 5 images. For the testing set, we also chose another 500K tuples each from *HC* and *HC – 21* from a different set of 5 images. To ensure the consistency of the model predictions, we trained two identical models separately on the 30 images in the *HC* and *HC – 21* datasets. The transformer architecture of our neural network is illustrated in Figure 3.3.

We used the transformer block[5] in our neural network architecture, which is a novel neural network that has gained recognition for its proficiency in discerning the correlation between diffusion signals and diffusion directions. By utilizing the attention mechanism's matrix multiplication in the transformer block, we anticipate that the non-linearity of the DTI model fit can be learned. Additionally, we expect that the linear embedding inside the transformer block[5] will eliminate any dependency on the order of the diffusion signals and their corresponding directions within the input.

Finally, we passed the transformer output through two dense layers to split the data into three parts and adjust to their different value ranges. In our implementation, we utilized the *Sigmoid* activation in the final layers and the *Gelu* activation in the transformer layers and *Relu* activation in all other layers. We used the L1 loss function with different scaling for each output since the ranges of fractional anisotropy (FA), axial diffusivity (AD), and mean diffusivity (MD) are different within the range of 0 to 1.

$$Loss_{FA} = C_{FA} \|FA_{GT} - FA_{predict}\|_1 \quad (3.11)$$

$$Loss_{AD} = C_{AD} \|AD_{GT} - AD_{predict}\|_1 \quad (3.12)$$

$$Loss_{MD} = C_{MD} \|MD_{GT} - MD_{predict}\|_1 \quad (3.13)$$

$$Loss_{Total} = Loss_{FA} + Loss_{AD} + Loss_{MD} \quad (3.14)$$

The ground truth of FA is represented by  $FA_{GT}$ , the ground truth of AD is represented by  $AD_{GT}$ , and the ground truth of MD is represented by  $MD_{GT}$ , in equations 3.11, 3.12, 3.13. Correspondingly, the scaling factors for losses for FA, AD, and MD are indicated as  $C_{FA}$ ,  $C_{AD}$ , and  $C_{MD}$ , respectively. We have trained our model with 100 epochs. Data augmentation was not used during the neural network training process. During the training process, we have used the loss function as indicated by equation 3.14.

FA, AD, and MD volume predictions for Migraine Patient (MP) data: We employed our method to predict fractional anisotropy (FA), axial diffusivity (AD), and mean diffusivity (MD) scores voxel by voxel for each individual Migraine volume in MP dataset. Prior to making the predictions, we have generated diffusion signal in  $(64 \times 4)$  vector form as input to the model using the same preprocessing procedure used for training dataset. It is worth noting that we did not perform any post-processing on the predicted volumes after their generation.

**Training:** There were 60 healthy control(HC) in this dataset. In the MICCAI Quad22 Challenge participants received all the diffusion weighted volumes, or 61 directions, as well as a non-diffusion weighted volume ( $b = 0$ ). The sampling plan makes it simple to subsample the 61 gradient directions into 21 gradients.

**Test:** 50 patients with EM and 50 patients with CM were included in this dataset. The challenge participants received a subsample consisting of 21 diffusion gradient directions along with each subject's baseline volume. The participant was unable to determine if a volume belonged to EM or CM because the datasets were shuffled. The organizers, not the participants, had access to the full acquisition with all 61 gradient directions in order to verify the findings.

Since our goal was to evaluate the impact of applying a general machine learning method to increase the number of diffusion gradient orientations in the statistical relationships between clinical groups, there were no migraine patients in the training dataset. The goal was to prevent the emergence of a migraine classifier or a "migraine-specific" method.

**Diffusion MRI Preprocessing** Preprocessing was done on the training and test datasets provided in the challenge to mitigate any bias resulting from the various preprocessing pipelines used by the various participant groups. The Marchenko-Pastur Principal Component Analysis (MP-PCA) method of denoising[167], the correction of motion and eddy currents[168], and the B1 field inhomogeneity[169, 170] comprised the dMRI preprocessing. The MRtrix3 program was used for each of these procedures[171].

An extraction mask was made from the preprocessed dMRI volumes[172]. Using FSL software's ordinary least squares approach, the diffusion tensor (DT) was estimated at the voxels defined within the brain mask[173]. As contrast to the original study comparing the CM, EM, and HC groups[126], no potential bias was present in the extraction of the diffusion tensor or its descriptors. Instead, the FA, MD, and AD maps of the training dataset were obtained using the FSL estimation methods.

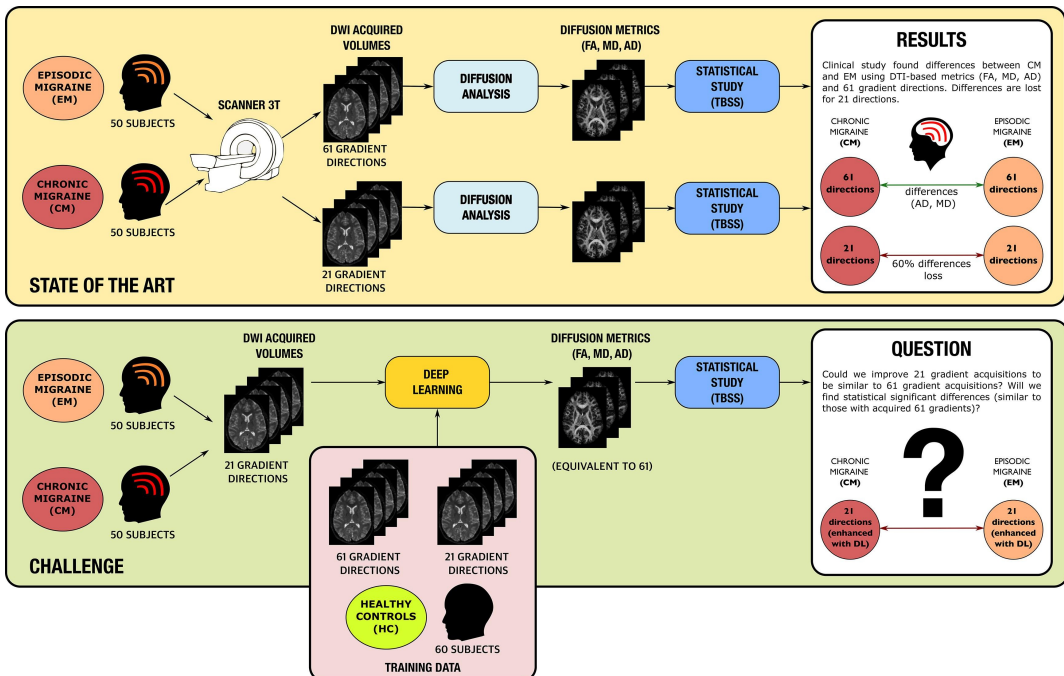


Figure 3.2: Overview of working strategy. Top: Comparative analysis of DTI data processing using 61 and 21 gradient directions, comparing EM to CM based on data acquired with 61 gradient directions. Bottom: Outline of the challenge task, involving the training of a Deep Learning network using healthy controls and the utilization of the trained network to estimate parameters from patients acquired with 21 gradient directions. Image Source: MICCAI 2022 Challenge [1] is QuaD22. I participated in an active part in this challenge as a member of Team 13, which enabled the team to participate successfully.

**Task: Quality enhancement** Only three DTI-derived metrics are taken into consideration for the analysis conducted in this study: FA, AD, and MD. After initial investigations with migraine patients, AD and MD were chosen because they were the ones who were able to identify significant differences. An additional metric called FA was also computed. Using the migraine dataset that was acquired with 21 diffusion gradient directions at  $b = 1000 \text{ s/mm}^2$ , participants were asked to estimate these three metrics in an attempt to approximate the parameters of 61 gradient directions with a similar quality level. Having that in consideration:

- They trained an AI-based system using the training data set to be able to angularly augment the dMRI data from 21 to 61 gradient directions. DL methods were advised to ensure the most accurate representation of the signal and, by extension, the quantitative parameters, such as FA, MD, and AD.

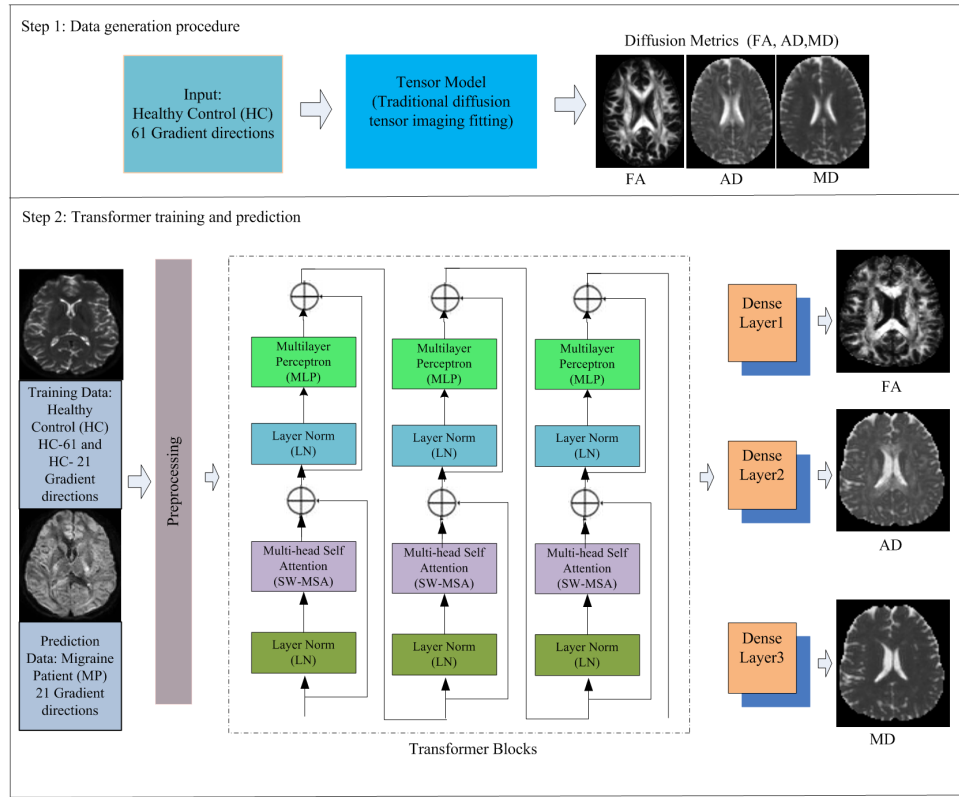


Figure 3.3: Proposed model over migraine dataset, in which takes  $(64 \times 4)$  input vector and produces  $(3 \times 1)$  output vector with FA, AD, and MD score

2. Next, using the migraine dataset, the participants used the enhancement method. Regarding each of the 50 EM and 50 CM subjects, each participant group submitted three volumes (FA, MD, and AD).

### 3.2.3 Data Preprocessing and Model Training over NIFD

To improve nonlinearity and reduce parameter count, we incorporate a modified version of window self-attention in our suggested model. This window self-attention mechanism is an essential part because it provides various benefits over conventional self-attention mechanisms. We concatenate the direction vector as part of the input signal rather than implicitly embedding the diffusion directions using learned weights. This improvement strengthens the non-linearity of the model and makes it capable of capturing more complex relationships in the input data. Traditionally, self-attention assigns different triplets to each input position: query, key, and value. On the other hand, we use window self-attention in our proposed model, where all windows in the same patch receive the same triplets. By splitting the input matrix into patches and applying spatial relative attention to each patch independently, this patch-based approach reduces the computational load associated with spatial relative attention and enables the modeling of long-range spatial relationships in large images.

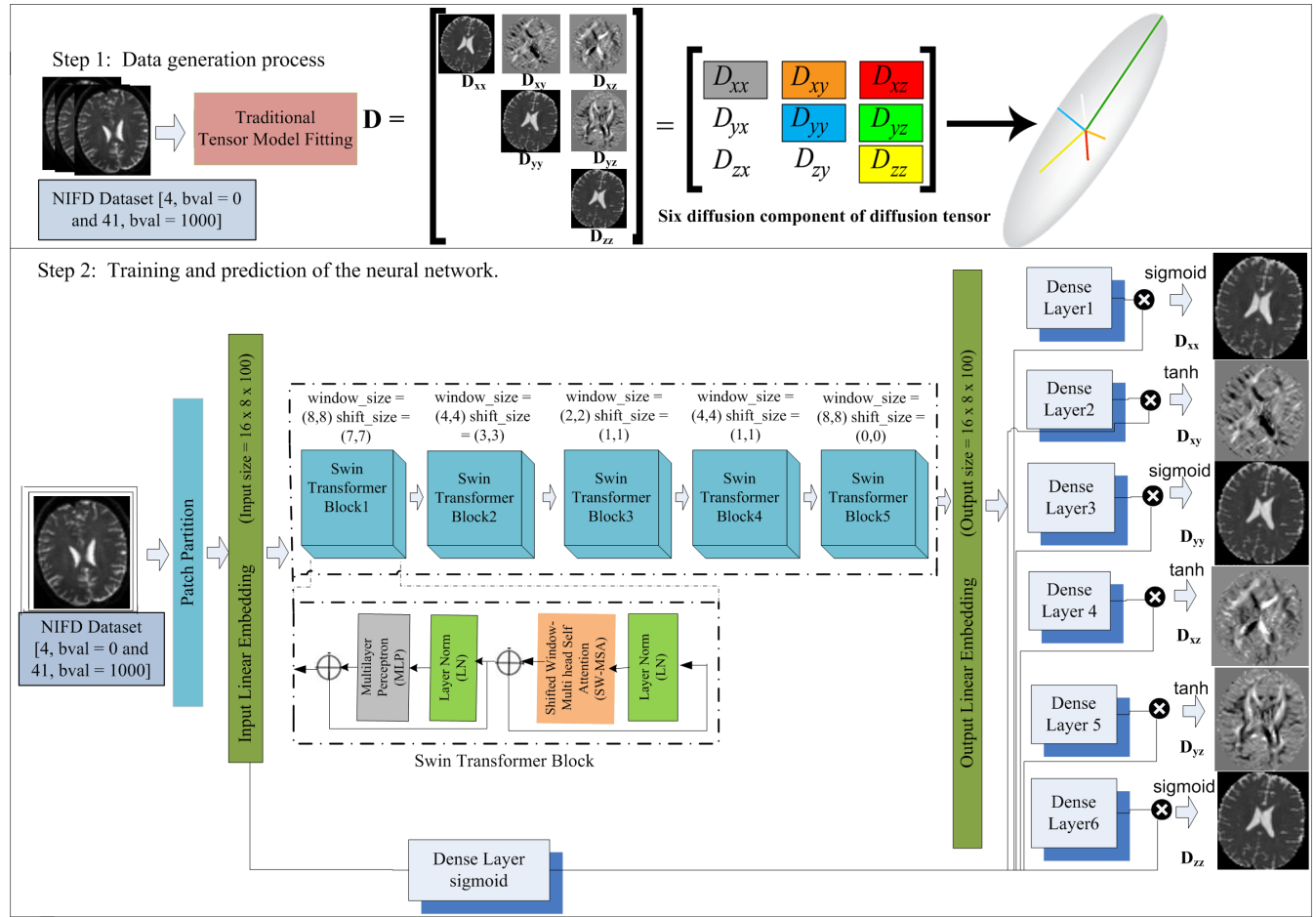


Figure 3.4: The proposed model over NIFD dataset architecture for neural network training and prediction.

---

**Algorithm 2** Preprocessing the data for the proposed model over NIFD dataset

---

*NIFD – 41*, *NIFD – 21*, and *NIFD – 5* are the three preprocessed training datasets that are created as part of the preprocessing algorithm for DWI images from the NIFD dataset.

---

**Step 1:** To process each DWI image independently, use the DTI model fitting procedure found in the DIPY Python package[166]. Six different diffusion components are produced by this process:  $D_{xx}$ ,  $D_{xy}$ ,  $D_{yy}$ ,  $D_{xz}$ , and  $D_{yz}$ . These components together make up the diffusion tensor.

**Step 2:** From each DWI image, select 20,000 voxels by calculating their fractional anisotropy (FA) score. Zero values should be ignored in voxel selection in order to preserve a uniform distribution throughout the interval (0, 1).

**Step 3:** Gather a dataset of 20,000 pairs of (input, ground-truth) where the input is a  $5 \times 5 \times 5$  voxel patch for each pair. 41 diffusion directions per voxel are characteristics of this patch. The matching ground-truth component consists of a  $5 \times 5 \times 5$  voxel patch, in which each voxel is connected to a  $6 \times 1$  vector that symbolizes the six diffusion components of the diffusion tensor.

**Step 4:** Combine the diffusion signals from the neighboring  $5 \times 5 \times 5$  patch to create a matrix with dimensions  $125 \times 41$  for each input voxel.

**Step 5:** For every input voxel, concatenate the diffusion directions ( $3 \times 41$ ) with the diffusion signal to produce a matrix with dimensions  $128 \times 41$ .

**Step 6:** Apply zero-padding to each tuple's input to create a  $128 \times 100$  matrix. The corresponding ground truth is represented by a  $125 \times 6$  matrix. *NIFD – 41* is the name given to the resulting training data set.

**Step 7:** Apply Qball-based interpolation [146, 166] to the 41-directional input from the *NIFD – 41* dataset using the DIPY package. Diffusion signals with 41, 21, and 5 directions will be produced by this process, in that order.

**Step 8:** To create input vectors with dimensions of  $125 \times 41$ ,  $125 \times 21$ , and  $125 \times 5$ , as well as a ground truth matrix with size  $125 \times 6$ , concatenate the diffusion directions and diffusion signals within each tuple.

**Step 9:** To create a matrix with dimensions of  $128 \times 100$ , apply zero-padding to each tuple's input.

**Step 10:** The resulting training datasets are designated as *NIFD – 41*, *NIFD – 21*, and *NIFD – 5*, which correspond to the respective specific diffusion directions of 41, 21, and 5.

---

As a consequence of neighboring windows being deliberately moved using a predetermined stride, our suggested model which is based on the Swin Transformer architecture creates window overlapping regions. By allowing tokens to connect with one another even though they are part of separate windows, this strategic overlap helps to promote inter-token attention. By creating a wider range of opportunities for reciprocal influence, this dynamic interaction between tokens fosters the growth of more complex and richer representations.

We have included a novel activation function based on element-wise multiplication as part of our proposed model. To be more precise, within our system, the values of  $D_{xx}$ ,  $D_{yy}$ , and  $D_{zz}$  can only fall within the range of 0 and 1, while the values of  $D_{xy}$ ,  $D_{yz}$ , and  $D_{xz}$  can only fall within the range of -1 and 1. We used the *sigmoid* activation function for the first set and the *tanh* activation function for the second set to deal with these different ranges. Furthermore, the DWI signals magnitude and the outputs magnitude  $\bar{D}$  function nonlinearly together. We multiplied the final outputs by the output of a Sigmoid-activated dense layer on the DWI signal in order to account for this knowledge. We were able to modulate the estimates output magnitude because to this innovative method, which also shortened the training period and increased the overall accuracy of our suggested framework.

We created three preprocessed training datasets, *NIFD* – 41, *NIFD* – 21, and *NIFD* – 5, by developing an algorithm to preprocess diffusion-weighted imaging (DWI) images from the NIFD dataset. Specifically, Algorithm 2 [146, 166] describes the preprocessing algorithm.

We trained our neural network using three separate datasets: *NIFD* – 41, *NIFD* – 21, and *NIFD* – 5 [146, 166]. Each dataset contained 20,000 tuples per image. Following preprocessing with *Algorithm 2*, these tuples were obtained from a subset of 24 diffusion-weighted imaging (DWI) images. We use a Swin-transformer block, which is well-known for its capacity to detect correlations in input signals [68]. The architecture of our neural network is shown in Figure 3.4. Diffusion signals and their directions make up the input signals in our scenario, and our model takes into account both the current voxel diffusion signal and the diffusion signals inside a nearby  $5 \times 5 \times 5$  patch.

To improve non-linearity and reduce parameter measure, we incorporate a modified version of window self-attention in our suggested model. A key component of our model is the window self-attention mechanism, which has several advantages over conventional self-attention mechanisms. We concatenate the direction vector as part of the input signal rather than integrating the diffusion direction using learned weights. This improvement strengthens the non-linearity of the model and makes it capable of capturing more complex relationships in the input data. Traditionally, self-attention assigns different triplets to each input position: query, key, and value. On the other hand, we use window self-attention in our proposed model, where all windows in the same patch receive the same triplets. Using a patch-based approach, the input image is divided into patches, and each patch is given distinct spatial relative attention. By using this method, modeling long-range spatial relationships in large images is made possible while also lessening the computational load associated

with spatial relative attention.

### 3.2.4 Data Preprocessing and Model Training over ADNI

We created three preprocessed training datasets, *ADNI* – 41, *ADNI* – 21, and *ADNI* – 5, by developing an algorithm to preprocess the DWI images from the ADNI dataset. Algorithm 3 provides an overview of the algorithm.

---

**Algorithm 3** Data Preprocessing of Proposed Model over ADNI dataset
 

---

The preprocessed training datasets *ADNI* – 41, *ADNI* – 21, and *ADNI* – 5 are produced using the preprocessing algorithm for the DWI images in the ADNI dataset.

---

**Step 1:** Utilize the DTI model fit from the DIPY Python package [166] for every DWI image separately. This will yield six diffusion components of the diffusion tensor:  $D_{xx}$ ,  $D_{xy}$ ,  $D_{yy}$ ,  $D_{xz}$ ,  $D_{yz}$ , and  $D_{zz}$ .

**Step 2:** From each DWI image, choose 100,000 voxels that are uniformly distributed within the range (0, 1), based on their fractional anisotropy (FA) score, excluding zero.

**Step 3:** Acquire 100,000 tuples of (input, ground-truth) such that each tuple contains an input  $5 \times 5 \times 5$  voxel patch with 41 diffusion directions per voxel and the ground-truth is a  $5 \times 5 \times 5$  voxel patch with a  $6 \times 1$  vector per voxel, which expresses the corresponding six diffusion components of the diffusion tensor.

**Step 4:** For each input voxel, concatenate the diffusion signals of the adjacent  $5 \times 5 \times 5$  patch to create a  $125 \times 41$  matrix.

**Step 5:** To obtain a  $128 \times 41$  matrix per input voxel, concatenate the diffusion directions ( $3 \times 41$ ) with the diffusion signal.

**Step 6:** The ground truth is represented as a  $125 \times 6$  matrix, and each tuple's input is zero-padded to create a  $128 \times 100$  matrix. The training dataset that is produced is called *ADNI* – 41.

**Step 7:** Apply the DIPY package to the 41 directional input of the *ADNI* – 41 dataset and perform Qball-based interpolation [146, 166] to obtain 41 directional, 21 directional, and 5 directional diffusion signals.

**Step 8:** Diffusion directions are concatenated with the diffusion signals of each tuple to produce inputs of vector sizes  $125 \times 41$ ,  $125 \times 21$ , and  $125 \times 5$ , as well as a ground truth matrix of size  $125 \times 6$ .

**Step 9:** To generate a  $128 \times 100$  matrix, zero-pad each tuple's input.

**Step 10:** The training datasets that are obtained are denoted *ADNI* – 41, *ADNI* – 21, and *ADNI* – 5, which correspond to the corresponding diffusion directions = 41, 21, 5.

---

Three separate datasets, *ADNI* – 41, *ADNI* – 21, and *ADNI* – 5, each containing one million tuples per image, were used to train our neural network. *Algorithm 3* was used to preprocess a subset of 10 DWI images, from which these tuples were obtained. Figure 3.5 shows the architecture of our neural network, which uses a Swin-transformer block, which is well known for its ability to detect correlations in input signals. In our scenario, the input signals are diffusion signals plus diffusion directions, and our model takes into account both the current voxel diffusion signal and the diffusion signals inside a neighboring patch  $5 \times 5 \times 5$ .

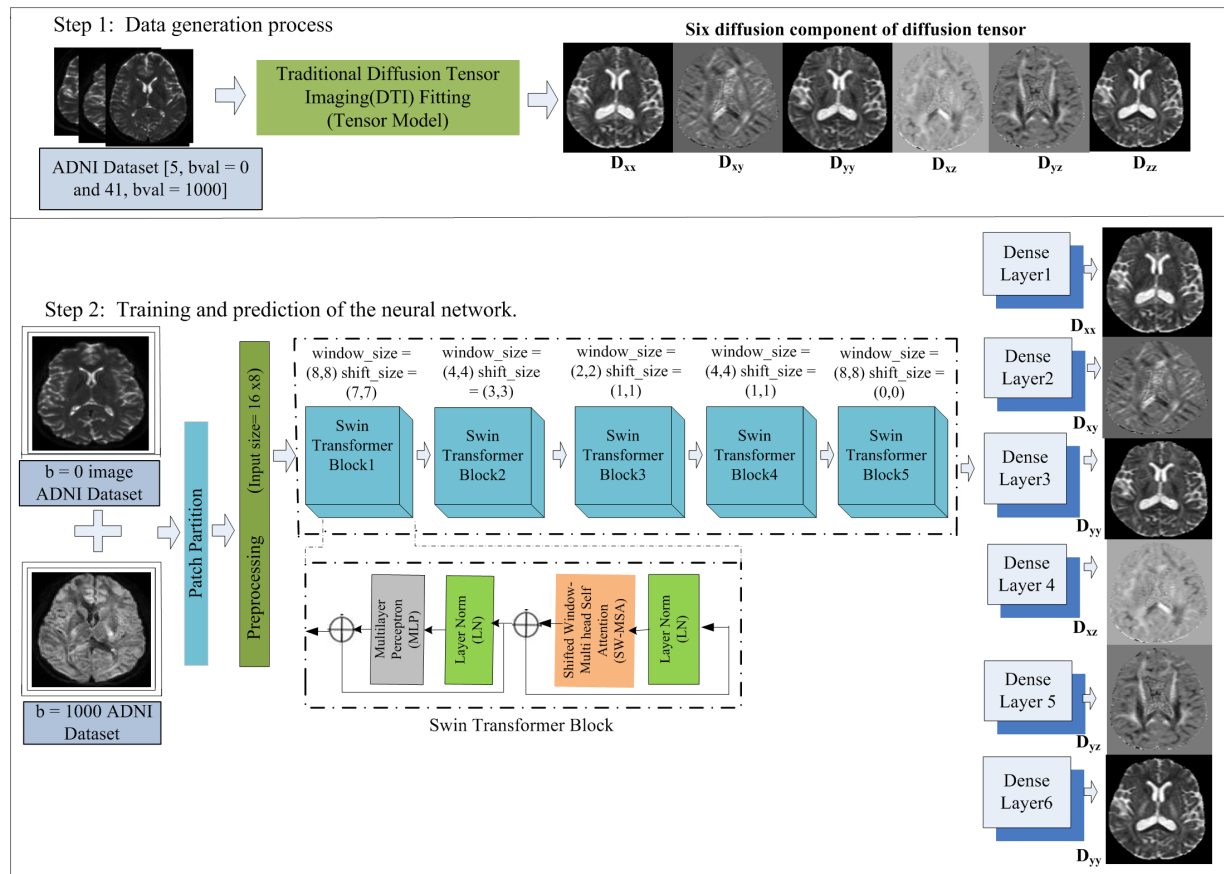


Figure 3.5: The proposed model over ADNI dataset architecture for neural network training and prediction.

# Chapter 4

## Results and Discussion

### 4.1 Experimental findings over HCP

In an experiment, we compared our results to Ground Truth and those obtained with traditional LLS fitting[4] and 3D U-Net16[33, 34, 69] on four different numbers of diffusion directional signal ( $N_{dir} = 64, 32, 21, 5$ ). In a follow-up experiment, we contrast our predictions with those from Transformer-DTI[5] on the same data for a diffusion directional signal ( $N_{dir} = 5$ ). While 3D U-Net16[33, 34, 69], which requires an input size of  $16 \times 16 \times 16$  patch, used 8.1 million trainable parameters, the approach we propose only uses 0.66 million. Transformer-DTI[5] employs an input size of  $5 \times 5 \times 5$  patch and 25 million trainable parameters. We trained the model using Adam optimizer with a batch size of 100 and an initial learning rate of  $10^{-4}$ . When the validation loss did not go down for an epoch, we reduced the learning rate, and if the validation loss did not go down for two epochs, we terminated the training. Utilizing an NVIDIA GeForce RTX A4000 GPU, training and validation were performed out. Furthermore, as shown in figures 4.9, 4.10, and 4.11, we have carried out error analysis on FA, AD, and MD predictions for the entire brain. We conducted experiments to compare the performance of our proposed model, SwinDTI, with the 3D U-Net16[33, 34, 69] model and with the similarly comparable LLS fitting[4] model across various diffusion directions ( $N_{dir} = 21, 32, 64$ ). When evaluating quantitative metrics like fractional anisotropy (FA), axial diffusivity (AD), and mean diffusivity (MD), our results consistently show that SwinDTI performs better than the 3D U-Net16 model[33, 34, 69] and equally comparable LLS fitting[4] model. Moreover, we found that SwinDTI outperforms not only the 3D U-Net16 model[33, 34, 69] but also the Transformer-DTI[5] model and similarly good LLS fitting[4] methods, in particular for the diffusion direction  $N_{dir} = 5$ . These results offer compelling evidence for the SwinDTI model’s superior ability to capture and analyze diffusion tensor imaging data with accuracy.

Additionally, we registered the predictions non-linearly to the Dipy framework template[166],

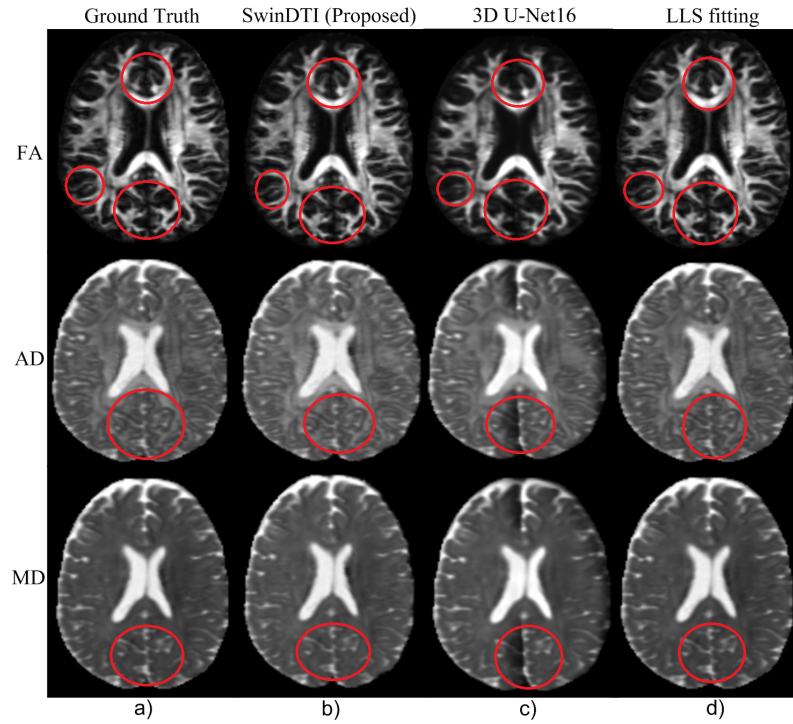


Figure 4.1: The diffusion directional signal of 64 DWIs was compared using 3D U-Net16, LLS fitting, and the proposed SwinDTI. Red circles highlight noteworthy areas that show differences from earlier research findings.

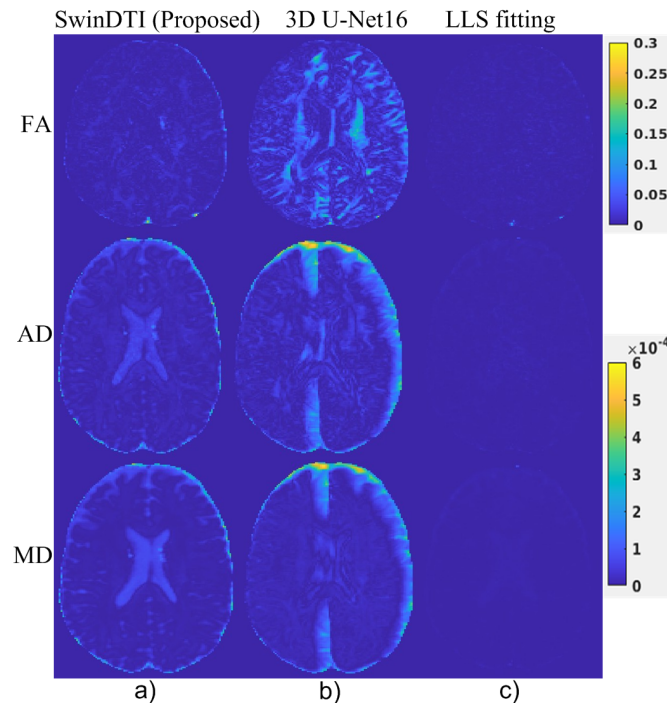


Figure 4.2: The proposed SwinDTI absolute error image, 3D U-Net16, and LLS fitting for 64 DWIs. The range of the AD and MD scales is  $0 \text{ to } 6 \times 10^{-4}$ , whereas the range of the FA scale is 0 to 0.3

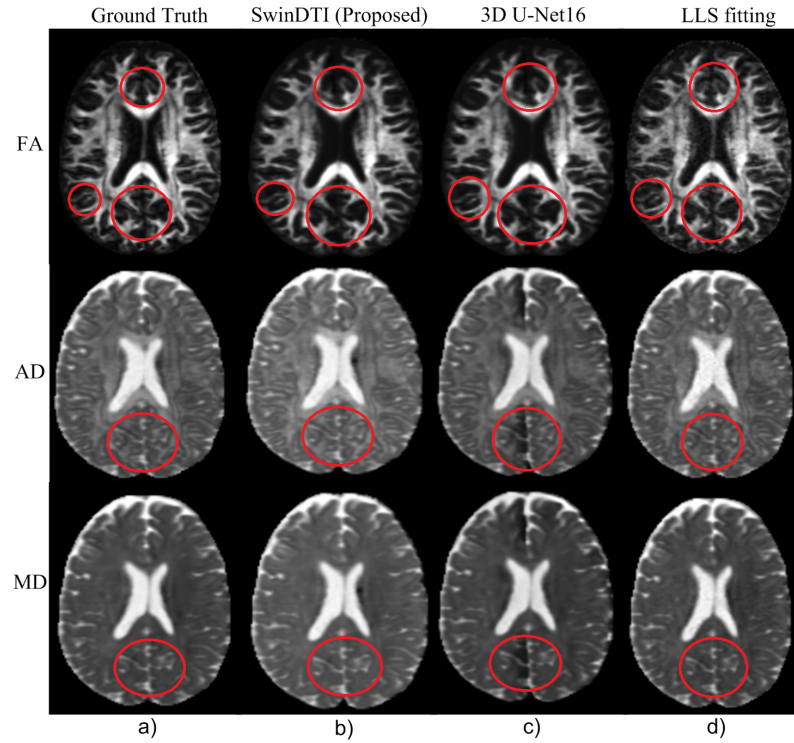


Figure 4.3: Diffusion directional signal of 32 DWIs is compared with 3D U-Net16, LLS fitting, and the proposed SwinDTI. Red circles highlight noteworthy areas that show differences from earlier research findings.

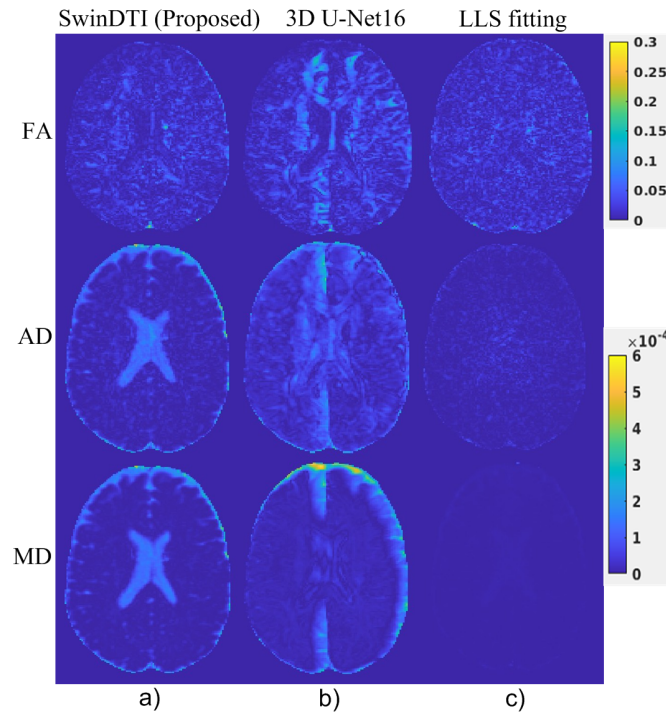


Figure 4.4: The proposed SwinDTI absolute error image, 3D U-Net16, and LLS fitting for 32 DWIs. The range of the AD and MD scales is 0 to  $6 \times 10^{-4}$ , whereas the range of the FA scale is 0 to 0.3

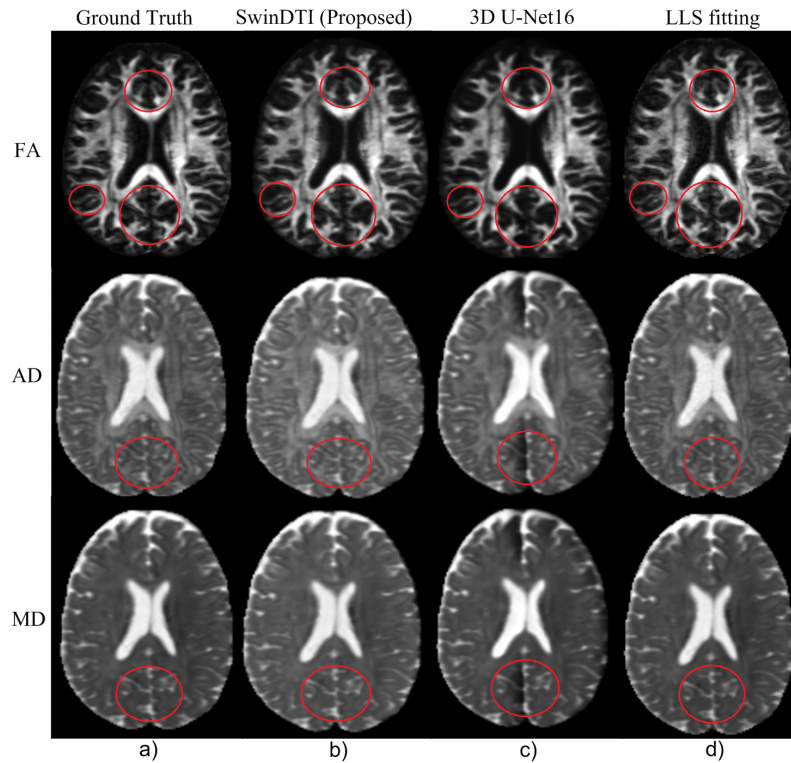


Figure 4.5: Diffusion directional signal of 21 DWIs is compared with 3D U-Net16, LLS fitting, and the proposed SwinDTI. Red circles highlight noteworthy areas that show differences from earlier research findings.

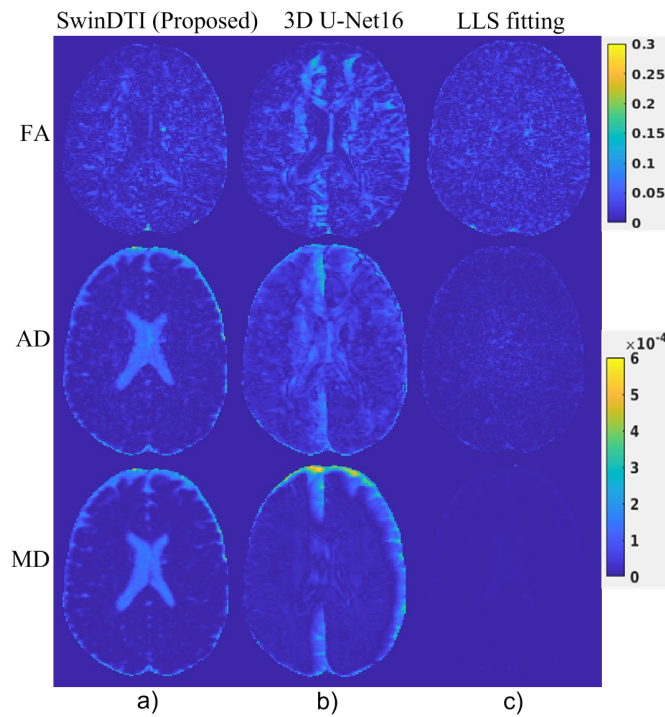


Figure 4.6: The proposed SwinDTI absolute error image, 3D U-Net16, and LLS fitting for 21 DWIs. The range of the AD and MD scales is 0 to  $6 \times 10^{-4}$ , whereas the range of the FA scale is 0 to 0.3

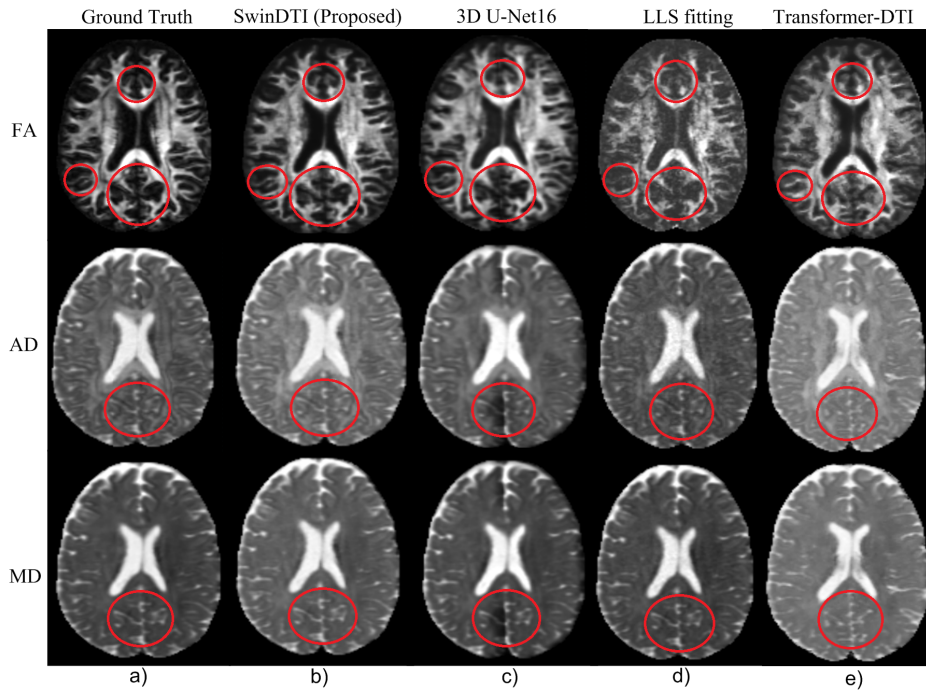


Figure 4.7: Diffusion directional signal of 5 DWIs is compared with proposed SwinDTI, 3D U-Net16, LLS fitting, and Transformer-DTI. Red circles highlight noteworthy areas that show differences from earlier research findings. For each of the five diffusion directions, SwinDTI outperforms the FA measurement obtained by 3D U-Net16, LLS fitting, and Transformer-DTI. Surprisingly, SwinDTI shows similar performance to LLS fitting when it comes to AD and MD measurements.

utilizing the JHU DTI-based white-matter atlases template[174] to perform a region-of-interest(RoI) analysis. Figures 4.12–4.17 depict the region-specific predictions of the FA, AD, and MD scores. This method helps diagnose neurological conditions and provides support and guidance during surgical procedures. Two-dimensional slices of our predictions for all diffusion measurements  $N_{dir} = 5, 21, 32, 64$  are shown in Figures 4.1–4.8, along with the associated error images. Moreover, for  $N_{dir} = 5$ , the most sparse measurement in our framework, tables 4.1, 4.2, and 4.3 display the mean, median, and standard deviation of errors for our predictions. For directional diffusion, the Structural Similarity Index (SSIM) score[6] between the Ground Truth and the predicted quantitative images is displayed in Table 4.4 ( $N_{dir} = 5, 21$ ). A key metric for assessing the accuracy and reliability of the predictions is the SSIM score[6], which offers a quantitative assessment of the similarity between the two images. A low score suggests that there may be significant differences between the two images and that the predictions may need more research or improvement. A high score indicates that the predicted images are similar to the Ground Truth.

### Quantitative Parameter Prediction

For our test dataset, the diffusion tensor parameters are estimated using the proposed Swin-DTI model. We compare the ground truth parameters derived from the fully sampled data with these estimated diffusion tensor parameters. Predicting FA, MD, and AD values for every  $5 \times 5 \times 5$  patch

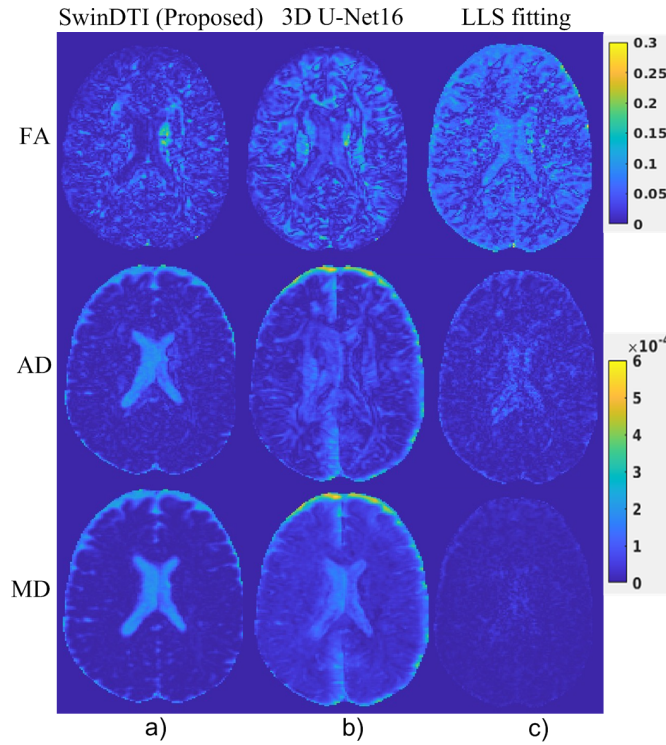


Figure 4.8: The proposed SwinDTI absolute error image, 3D U-Net16, and LLS fitting for 5 DWIs. The range of the AD and MD scales is 0 to  $6 \times 10^{-4}$ , whereas the range of the FA scale is 0 to 0.3

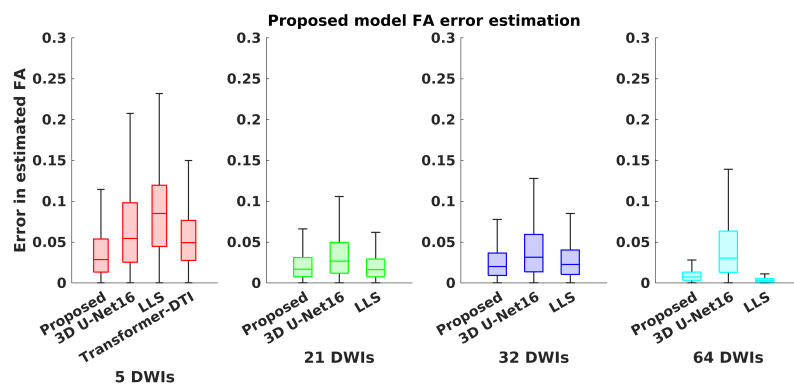


Figure 4.9: Boxplot of whole brain FA measurement

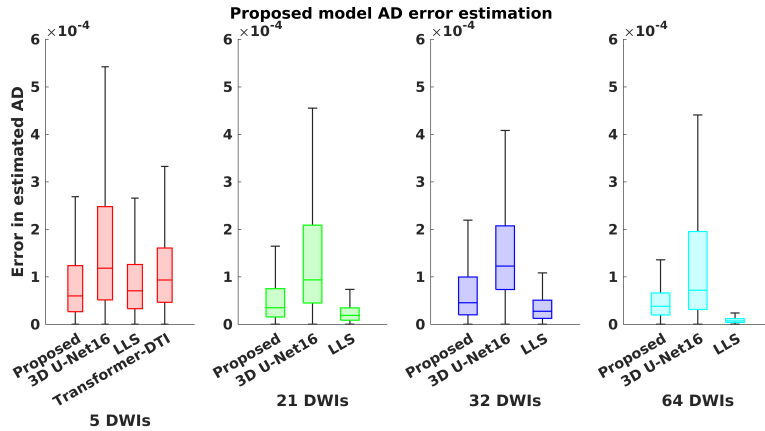


Figure 4.10: Boxplot of whole brain AD measurement

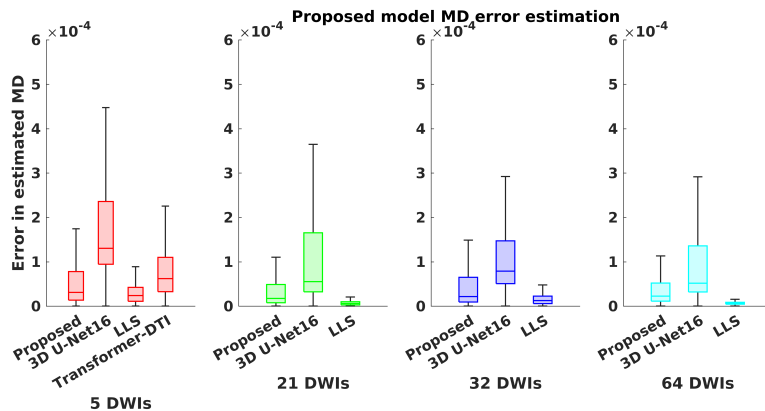


Figure 4.11: Boxplot of whole brain MD measurement

in a DWI test image is how we proceed about our approach. We take the average prediction to get the final value because these predictions overlap. This averaging method has improved the predictions' robustness and helped minimize artifacts.

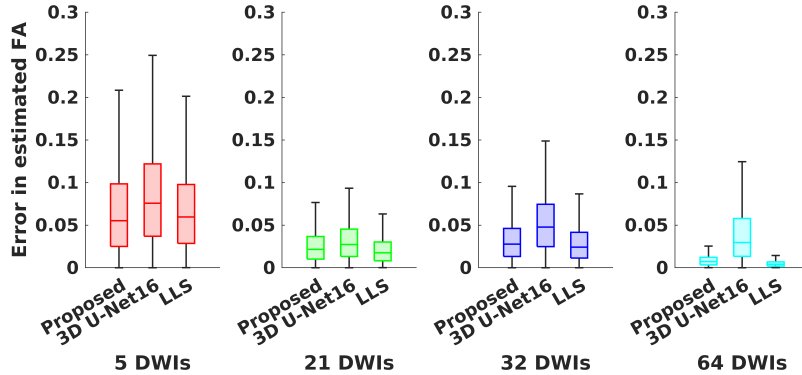


Figure 4.12: FA measure boxplot of ROI Anterior corona radiata, causes[2] affecting cerebral white matter, including ischemic and multiple sclerosis.

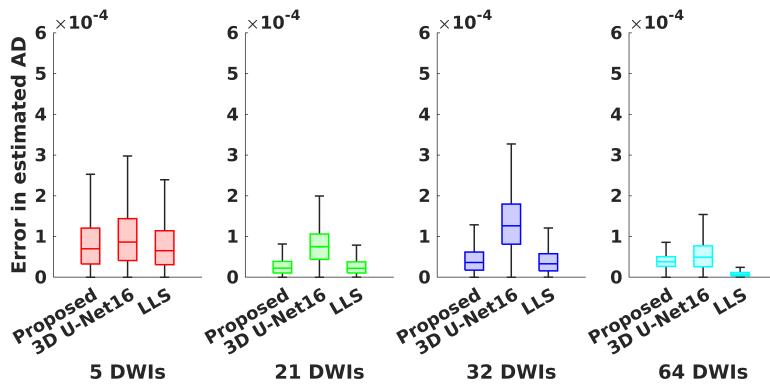


Figure 4.13: AD measure boxplot of ROI Anterior corona radiata, causes[2] affecting cerebral white matter, including ischemic and multiple sclerosis.

Table 4.1: The diffusion direction error for FA measures is  $N_{dir} = 5$ . The least amount of error is bolded.

ROIs	Proposed Model			3D U-Net16			LLS fitting method		
	Mean	Median	Std	Mean	Median	Std	Mean	Median	Std
Middle cerebellar peduncle	<b>0.074</b>	<b>0.060</b>	<b>0.059</b>	0.093	0.082	0.066	0.085	0.071	0.065
Pontine crossing	0.066	<b>0.055</b>	0.052	<b>0.065</b>	0.057	<b>0.050</b>	0.074	0.062	0.060
Genu of corpus callosum	<b>0.050</b>	<b>0.040</b>	<b>0.042</b>	0.073	0.057	0.060	0.071	0.056	0.060
Cerebral peduncle	<b>0.075</b>	<b>0.060</b>	0.063	0.093	0.087	<b>0.057</b>	0.087	0.075	0.065
Posterior limb of internal	<b>0.071</b>	<b>0.058</b>	<b>0.057</b>	0.106	0.104	0.063	0.088	0.076	0.064
Anterior corona radiata	<b>0.066</b>	<b>0.054</b>	0.053	0.082	0.074	0.057	<b>0.066</b>	0.058	<b>0.048</b>
Cingulum	<b>0.057</b>	<b>0.046</b>	<b>0.046</b>	0.075	0.062	0.057	0.070	0.059	0.055
Uncinate fasciculus	0.061	0.052	0.046	<b>0.058</b>	<b>0.047</b>	<b>0.044</b>	0.063	0.048	0.054
Whole brain	<b>0.039</b>	<b>0.028</b>	<b>0.037</b>	0.068	0.054	0.054	0.085	0.085	0.051

The outcomes of our experiments show that our suggested SwinDTI model works well for diffusion tensor imaging applications. In the anterior corona radiata and cingulum regions, box plots of

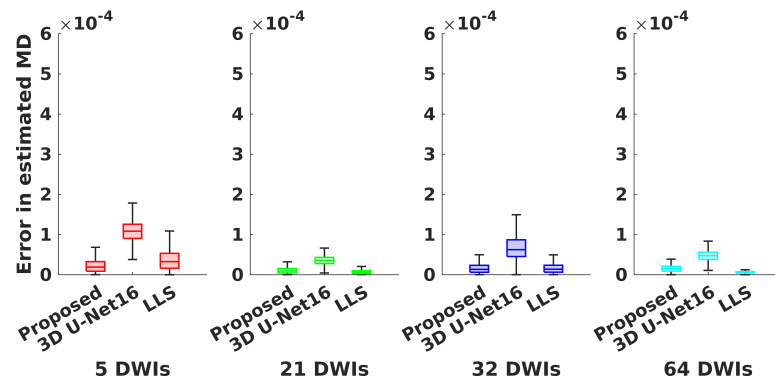


Figure 4.14: MD measure boxplot of ROI Anterior corona radiata, causes[2] affecting cerebral white matter, including ischemic and multiple sclerosis.

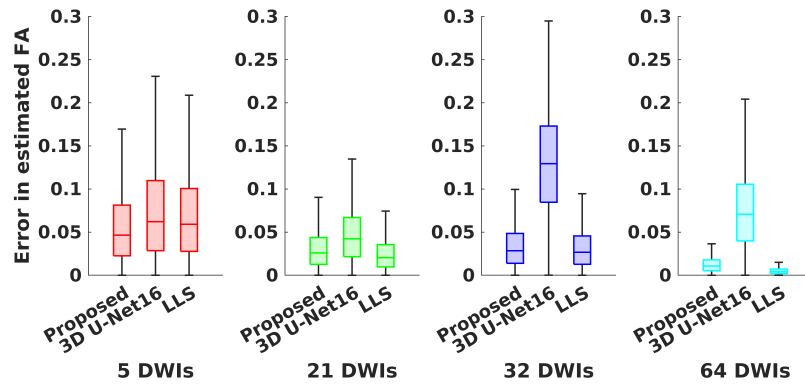


Figure 4.15: FA measure boxplot of ROI Cingulum, causes[3] Alzheimer's disease, anxiety disorders, addiction, depression, and schizophrenia.

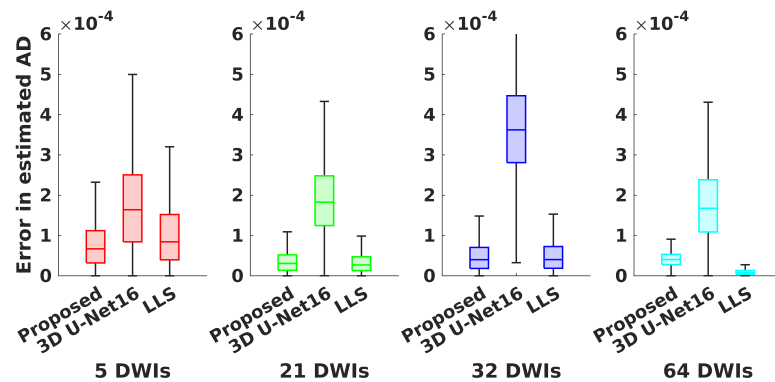


Figure 4.16: AD measure boxplot of ROI Cingulum, causes[3] Alzheimer's disease, anxiety disorders, addiction, depression, and schizophrenia.

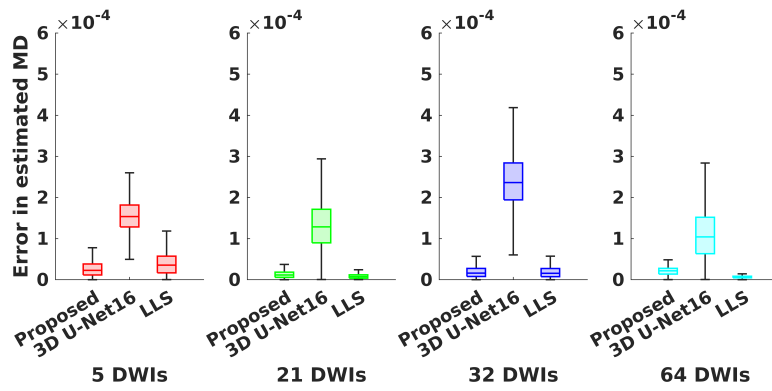


Figure 4.17: MD measure boxplot of ROI Cingulum, causes[3] Alzheimer's disease, anxiety disorders, addiction, depression, and schizophrenia.

Table 4.2: Error ( $\times 10^{-4}$ ) of the AD measure for diffusion direction  $N_{dir} = 5$ . The least amount of error is bolded.

ROIs	Proposed Model			3D U-Net16			LLS fitting method		
	Mean	Median	Std	Mean	Median	Std	Mean	Median	Std
Middle cerebellar peduncle	<b>1.059</b>	0.894	<b>0.820</b>	1.518	1.121	1.321	1.196	<b>0.874</b>	1.123
Pontine crossing	<b>0.812</b>	<b>0.670</b>	<b>0.626</b>	1.160	1.052	0.791	0.974	0.817	0.751
Genu of corpus callosum	<b>0.931</b>	<b>0.725</b>	<b>0.815</b>	1.956	1.679	1.436	1.369	1.093	1.113
Cerebral peduncle	<b>1.182</b>	<b>0.891</b>	1.062	2.548	2.552	1.379	1.244	1.062	<b>0.930</b>
Posterior limb of internal	<b>0.891</b>	<b>0.738</b>	<b>0.701</b>	2.268	2.328	1.355	1.113	0.953	0.829
Anterior corona radiata	0.837	0.700	0.641	0.991	0.863	0.715	<b>0.796</b>	<b>0.652</b>	<b>0.627</b>
Cingulum	<b>0.780</b>	<b>0.669</b>	<b>0.580</b>	1.734	1.641	1.100	1.047	0.843	0.835
Uncinate fasciculus	<b>0.795</b>	<b>0.686</b>	<b>0.577</b>	1.776	1.740	0.957	0.999	0.752	0.909
Whole brain	1.136	<b>0.600</b>	1.505	1.955	1.184	2.340	<b>0.934</b>	0.706	<b>0.859</b>

Table 4.3: Error ( $\times 10^{-4}$ ) of the MD measure for the diffusion direction  $N_{dir} = 5$ . The least amount of error is bolded.

ROIs	Proposed Model			3D U-Net16			LLS fitting method		
	Mean	Median	Std	Mean	Median	Std	Mean	Median	Std
Middle cerebellar peduncle	0.391	0.321	0.365	1.089	0.974	0.544	<b>0.328</b>	<b>0.278</b>	<b>0.247</b>
Pontine crossing	<b>0.240</b>	<b>0.203</b>	<b>0.184</b>	0.971	0.959	0.309	0.334	0.276	0.261
Genu of corpus callosum	<b>0.401</b>	<b>0.258</b>	0.520	1.244	1.141	0.628	0.406	0.348	<b>0.295</b>
Cerebral peduncle	0.377	0.318	0.248	0.911	0.854	0.334	<b>0.240</b>	<b>0.222</b>	<b>0.118</b>
Posterior limb of internal	0.458	<b>0.316</b>	0.499	1.168	1.121	0.539	<b>0.384</b>	0.319	<b>0.297</b>
Anterior corona radiata	<b>0.228</b>	<b>0.190</b>	<b>0.177</b>	1.083	1.086	0.264	0.369	0.328	0.255
Cingulum	<b>0.271</b>	<b>0.227</b>	<b>0.208</b>	1.578	1.535	0.443	0.400	0.354	0.289
Uncinate fasciculus	<b>0.277</b>	<b>0.240</b>	<b>0.205</b>	1.037	1.053	0.251	0.301	0.255	0.231
Whole brain	0.941	0.313	1.544	2.145	1.305	2.262	<b>0.308</b>	<b>0.240</b>	<b>0.276</b>

the error measures of FA, AD, and MD indicate that SwinDTI performs better than the 3D U-Net16[33, 34, 69] and equally comparable LLS fitting[4] methods. These regions have been related to cerebral white matter disorders and diseases, including Alzheimer, anxiety, addiction, depression, and schizophrenia. Comparing FA, AD, and MD measures for diffusion directions  $N_{dir} = 5$ , the analysis's quantitative findings are shown in Tables 4.1, 4.2, and 4.3. Even though  $N_{dir} = 5$  is an extreme case that is hardly ever employed in a clinical setting, it is used in the demonstration to show the accuracy and robustness of the SwinDTI model. SSIM scores[6] were used to measure the similarity between the ground truth and predicted quantitative images. Our proposed SwinDTI model, along with three other models (3D U-Net16[33, 34, 69], Transformer-DTI[5], and equally comparable LLS fitting[4]), were evaluated. A summary of the findings is provided in Table 4.3.

There are several figures and tables that show the experiment results. We present the results of the proposed SwinDTI model with 64 DWIs diffusion directional signal against the 3D U-Net16[33, 34, 69] and LLS fitting[4] in Figures 4.1, 4.2, 4.9, 4.10, and 4.11. Range for the AD and MD scales are 0 to  $6 \times 10^{-4}$ , and for the FA scale, 0 to 0.3. We present a comparative analysis of the SwinDTI model (proposed) with 3D U-Net16[33, 34, 69] and LLS fitting[4] for 32 DWIs diffusion directional signal in Figures 4.3, 4.4, 4.9, 4.10, and 4.11. The range of the FA scale is still 0 to 0.3, and the range of the AD and MD scales is 0 to  $6 \times 10^{-4}$ . Figures 4.5, 4.6, 4.9, 4.10, and 4.11 show a detailed comparison of the performance of the 3D U-Net16[33, 34, 69], and LLS fitting[4] using 21 DWIs diffusion directional signal. The proposed SwinDTI model is evaluated using 5 DWIs diffusion directional signals against three different models: 3D U-Net16[33, 34, 69], LLS fitting[4], and Transformer-DTI[5]. The results are shown in Figures 4.7, 4.8, 4.9, 4.10, and 4.11. Whole-brain FA (figure 4.9), AD (figure 4.10), and MD (figure 4.11) measurements are included in the boxplot analysis.

Figures 4.12, 4.13, and 4.14 display Anterior corona radiata measure (RoI) boxplots of error for patients with cerebral white matter disorders, such as multiple sclerosis and ischemic stroke, respectively. According to the findings, SwinDTI outperforms the 3D U-Net16 method[33, 34, 69], and is on par with LLS fitting[4] in terms of accuracy in capturing the microstructural changes in

Table 4.4: The SSIM score[6] compares the quantitative images predicted and Ground Truth. Compared to MD, FA has higher reliability in white matter [7]. The optimum results are shown by the highlighted values, which are the minimum standard deviation (std) and the maximum values for FA, AD, and MD.

Patient ID $N_{dir} = 5$	Proposed Model			3D U-Net16			LLS fitting method			Transformer-DTI		
	FA	AD	MD	FA	AD	MD	FA	AD	MD	FA	AD	MD
103010	<b>0.965</b>	0.972	0.979	0.937	0.951	0.959	0.899	<b>0.981</b>	<b>0.996</b>	0.941	0.957	0.961
103111	<b>0.958</b>	0.968	0.978	0.928	0.939	0.948	0.905	<b>0.980</b>	<b>0.996</b>	0.937	0.952	0.959
103212	<b>0.964</b>	0.973	0.980	0.930	0.951	0.959	0.893	<b>0.981</b>	<b>0.996</b>	0.938	0.957	0.962
103414	<b>0.970</b>	0.977	0.985	0.943	0.943	0.952	0.924	<b>0.983</b>	<b>0.996</b>	0.951	0.964	0.971
103515	<b>0.965</b>	0.972	0.980	0.937	0.946	0.954	0.908	<b>0.980</b>	<b>0.996</b>	0.945	0.961	0.968
Mean	<b>0.964</b>	0.972	0.980	0.935	0.946	0.955	0.906	<b>0.981</b>	<b>0.996</b>	0.942	0.958	0.964
Std	<b>0.004</b>	0.003	0.002	0.006	0.005	0.004	0.011	<b>0.001</b>	<b>0.0001</b>	0.005	0.004	0.005
Patient ID $N_{dir} = 21$	Proposed Model			3D U-Net16			LLS fitting method					
	FA	AD	MD	FA	AD	MD	FA	AD	MD			
103010	<b>0.972</b>	0.970	0.972	0.954	0.953	0.956	0.979	<b>0.988</b>	<b>0.990</b>			
103111	<b>0.965</b>	0.967	0.969	0.946	0.947	0.952	0.980	<b>0.984</b>	<b>0.986</b>			
103212	<b>0.972</b>	0.970	0.972	0.954	0.952	0.955	0.976	<b>0.985</b>	<b>0.987</b>			
103414	<b>0.975</b>	0.973	0.975	0.961	0.954	0.956	0.985	<b>0.986</b>	<b>0.988</b>			
103515	<b>0.970</b>	0.969	0.970	0.956	0.952	0.955	0.976	<b>0.983</b>	<b>0.985</b>			
Mean	0.971	0.970	0.972	0.954	0.951	0.955	<b>0.979</b>	<b>0.985</b>	<b>0.987</b>			
Std	<b>0.003</b>	0.002	0.002	0.005	0.002	0.001	0.003	<b>0.001</b>	<b>0.001</b>			
Patient ID $N_{dir} = 32$	Proposed Model			3D U-Net16			LLS fitting method					
	FA	AD	MD	FA	AD	MD	FA	AD	MD			
103010	<b>0.972</b>	0.979	0.982	0.959	0.974	0.978	0.966	<b>0.995</b>	<b>0.998</b>			
103111	<b>0.967</b>	0.977	0.982	0.951	0.971	0.976	0.978	<b>0.995</b>	<b>0.998</b>			
103212	<b>0.972</b>	0.978	0.981	0.961	0.977	0.982	0.968	<b>0.995</b>	<b>0.998</b>			
103414	<b>0.978</b>	0.984	0.986	0.966	0.974	0.979	0.985	<b>0.996</b>	<b>0.998</b>			
103515	<b>0.971</b>	0.977	0.979	0.963	0.976	0.981	0.972	<b>0.995</b>	<b>0.998</b>			
Mean	0.972	0.979	0.982	0.960	0.974	0.979	<b>0.974</b>	<b>0.995</b>	<b>0.998</b>			
Std	<b>0.003</b>	0.002	0.002	0.005	0.002	0.002	0.007	<b>0.0004</b>	<b>0.0001</b>			
Patient ID $N_{dir} = 64$	Proposed Model			3D U-Net16			LLS fitting method					
	FA	AD	MD	FA	AD	MD	FA	AD	MD			
103010	0.988	0.988	0.987	0.946	0.958	0.963	<b>0.998</b>	<b>0.999</b>	<b>0.999</b>			
103111	0.985	0.987	0.986	0.938	0.953	0.961	<b>0.998</b>	<b>0.999</b>	<b>0.999</b>			
103212	0.986	0.986	0.985	0.948	0.960	0.966	<b>0.998</b>	<b>0.999</b>	<b>0.999</b>			
103414	0.987	0.988	0.987	0.954	0.961	0.966	<b>0.998</b>	<b>0.999</b>	<b>0.999</b>			
103515	0.985	0.985	0.984	0.951	0.961	0.967	<b>0.9987</b>	<b>0.9998</b>	<b>0.9999</b>			
Mean	0.986	0.986	0.985	0.947	0.958	0.964	<b>0.998</b>	<b>0.999</b>	<b>0.999</b>			
Std	0.001	0.001	0.001	0.006	0.003	0.002	<b>0.0003</b>	<b>0.0003</b>	<b>0.0004</b>			

this region. The ROI Cingulum's FA, AD, and MD measure boxplots of error for people with neurodegenerative and psychiatric disorders and is shown in Figures 4.15, 4.16, and 4.17. When it comes to accurately representing the microstructural alterations in the area that are connected with the pathology of these illnesses, the SwinDTI model performs better. The ranges of the ROI

AD and MD scales are 0 to  $6 \times 10^{-4}$ , and 0 to 0.3, respectively, for the ROI FA scale. In summary, the suggested SwinDTI approach outperforms previous approaches in terms of accuracy and robustness for DTI-based measurements. The results unequivocally show that SwinDTI can measure the white matter regions of the brain with accuracy and reliability, which can help with the diagnosis and treatment of a variety of diseases and disorders of the brain. For the diffusion direction numbers of  $N_{dir} = 21, 32, 64$ , our suggested model performs better than the 3D U-Net16[33, 34, 69] and similar comparable LLS fitting[4] models. Moreover, SwinDTI outperforms the Transformer-DTI[5] models, the LLS fitting[4], and the 3D U-Net16[33, 34, 69] models specifically for 5 diffusion directions when measuring FA. Notably, in terms of measurements for AD and MD, SwinDTI performs comparably to LLS fitting[4]. These results imply that the SwinDTI model has a great potential to enhance the precision and effectiveness of diffusion tensor imaging, with possible uses in neurological disease diagnosis and treatment planning.

## 4.2 Experimental findings over MICCAI Quad22

A slice from a patient with chronic migraine (CM) was used to perform an initial visual evaluation of the various techniques. The metrics (FA, AD, and MD) that were taken into account were computed using both the initial data and various AI-enhancement techniques. Visual inspection indicated that most of the images had a similar overall appearance. No appreciable differences were found in structural features, despite minor variations in intensity levels.

Comparisons in quality metrics are made between AI-enhanced scalar values (FA, AD, MD) derived from 21 gradients and the original scalar values calculated from 61 gradients. The structural similarity index measure (SSIM) and the peak signal-to-noise ratio (PSNR) are computed. "REF (21 grad)" denotes metrics directly derived from 21 gradient directions without employing any AI algorithms. The results show the average of 100 reconstructed volumes, with cases that did not improve on the reference highlighted in red. When evaluating the quality of reconstructed images in medical imaging, visual references and different error or noise metrics are frequently used. We can assess the degree of similarity between the original and reconstructed images through this method. Thus, we started by calculating two image-based metrics: peak signal to noise ratio (PSNR) and structural similarity index measure[175]. For each team, the 100 enhanced volumes for the three metrics (FA, MD and AD) were taken into account in this regard. The same metrics have been computed using the original data, which were reconstructed from 61 gradient directions. The metric has only been calculated on a white matter mask, determined for those points where  $FA > 0.2$  with the FA calculated with 61 gradient directions.

In terms of the SSIM metric, the majority of the techniques demonstrated enhancement or were on par with the reference. The results obtained by Team 9 are the only ones that suggest a

notable difference between the reference and the reconstructed signal. Not only that, but Team 13 outperformed the reference by a small margin. Team 9 once more showed a significant departure from the reference in terms of PSNR, while the other teams showed results that were marginally better or marginally worse than the reference. With the exception of Team 9, the majority of the teams' results showed a high degree of similarity with the original data. In the following sections, we will investigate whether these results agree with the statistical findings of the clinical investigation. False positives can have detrimental effects, including misdiagnosis and decreased reliability of results. They can also have major implications. Because they may restrict the applicability of these techniques, it is crucial to carefully examine the existence of these results in the studies conducted with AI-enhanced volumes. The number of voxels with notable variations found by TBSS for each approach is displayed. The TPs found by the 21-gradient reference are shown in blue; the TPs found by the 61-gradient reference but not by the 21-gradient reference are shown in green; and the FPs are shown in red in our color-coding scheme. Each method yields new TPs, which are represented by values indicated in green. FA finds no significant differences, so for the sake of simplicity, we only display results for AD and MD.

### 4.3 Experimental findings over NIFD

We used 54 DWI images from the NIFD dataset for our experiments, 27 of which were from the Cognitively Normal (CN) group and 27 from the FTD patient group. We used 3 images from each group for validation and 12 images from CN and FTD patients to train our model. Testing was carried out on the 12 CN and 12 of the FTD patients that were left. For our experiments, we used the results of the LLS fitting on NIFD-41 as the ground truth.

We compared the outcomes of our suggested method with LLS fitting and Transformer-DTI in order to assess its effectiveness. Comparisons between ground truth, the suggested method, and the LLS fitting for 41 diffusion directions are shown in Figure 4.18. The outcomes show that, in terms of accurately estimating diffusion tensor parameters, the suggested method is comparable to LLS fitting. Diffusion measures for 21 diffusion-directed signals are shown in Figure 4.19, and the results for 5 diffusion-directed signals using the suggested method, LLS fitting and the Transformer-DTI are shown in Figure 4.20. For 21 diffusion directions (Figures 4.19 and 4.22), our suggested method outperforms the Transformer-DTI [5] and performs similarly to the LLS fitting [4]. Figures 4.20 and 4.21 show that our model outperforms Transformer-DTI and LLS fitting for 5 diffusion directions, indicating that it is a useful tool for accurately estimating diffusion measures, particularly when there are fewer diffusion directions. Figures 4.21 and 4.22, respectively, show error plots of six diffusion components  $\bar{D}$  for 5 and 21 diffusion directional signals.

In conclusion, the integration of sparse diffusion measures in the proposed Swin-Transformer-based deep learning framework shows promise as a method for early FTD

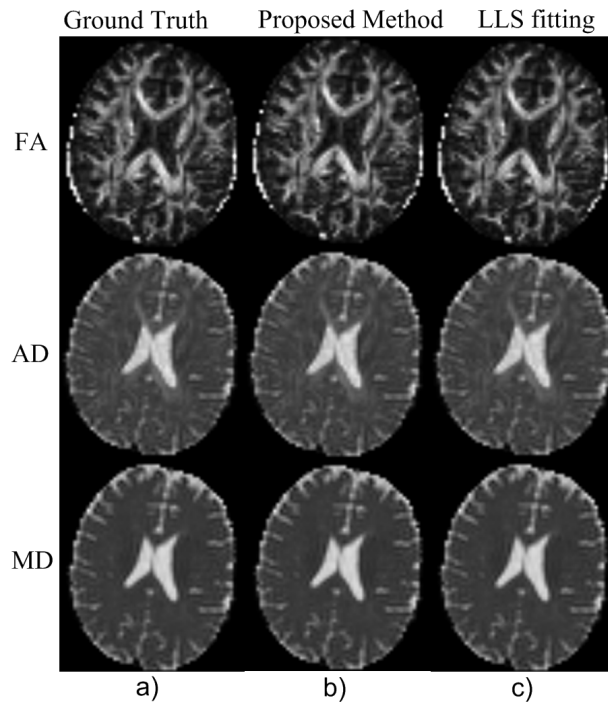


Figure 4.18: Comparison of 41 diffusion directions: Ground truth vs. Proposed method vs. LLS fitting [4]

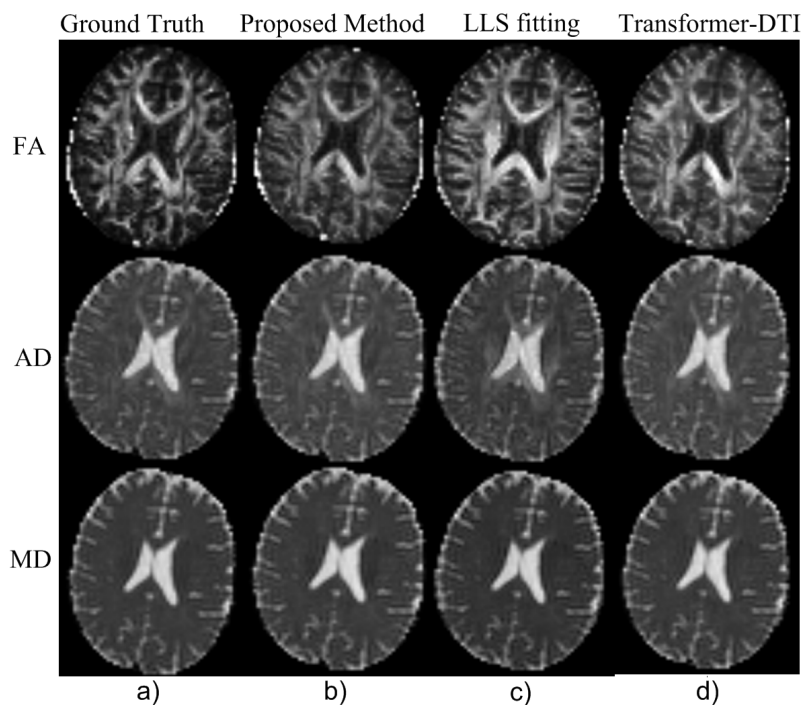


Figure 4.19: Comparison of 21 diffusion directions: Ground truth vs. Proposed method vs. LLS fitting [4] and Transformer-DTI [5]

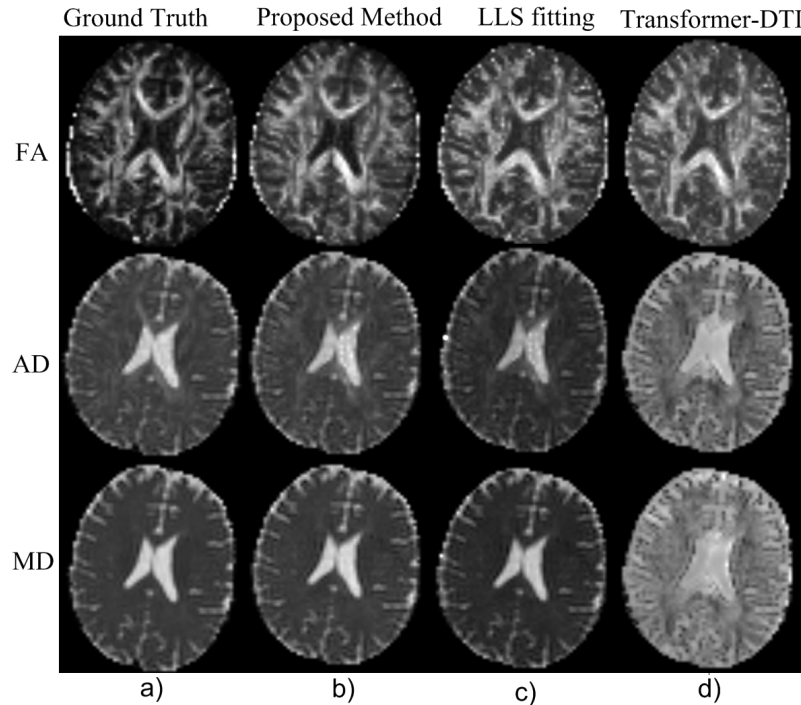


Figure 4.20: Comparison of 5 diffusion directions: Ground truth vs. Proposed method vs. LLS fitting [4] and Transformer-DTI [5]

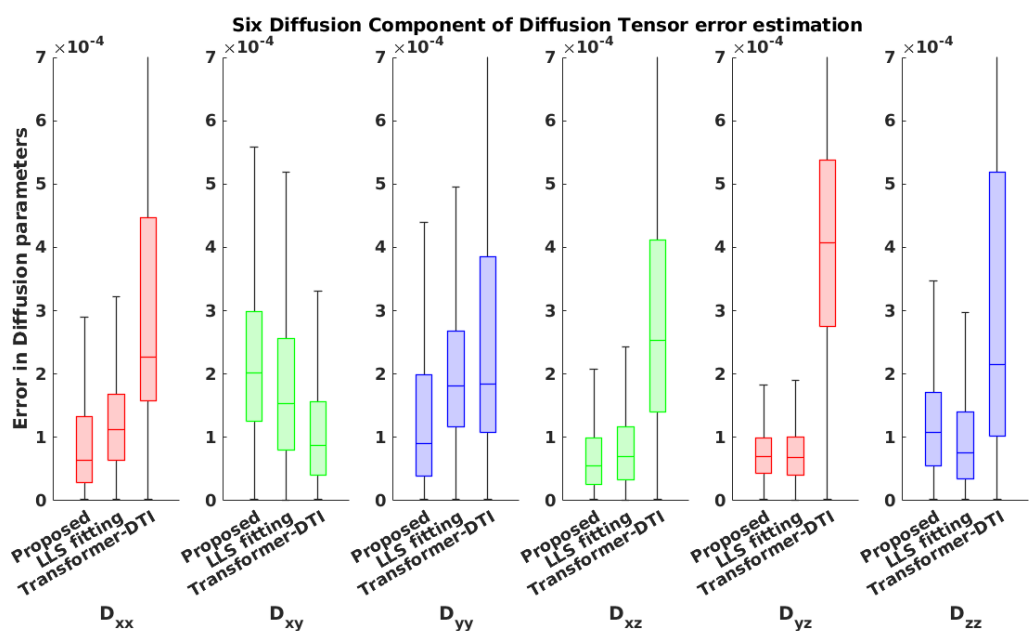


Figure 4.21: Six diffusion components of diffusion tensor for 5 diffusion directions

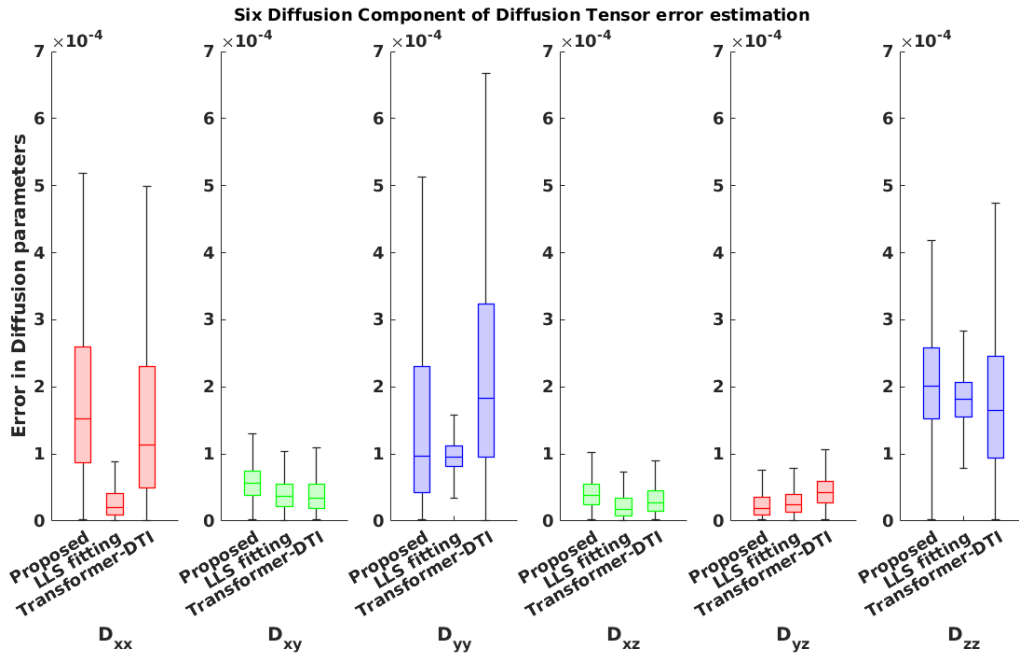


Figure 4.22: Six diffusion components of diffusion tensor for 21 diffusion directions

patient diagnosis. Our framework captures the underlying structural connectivity of the brain, which is a crucial characteristic in patients with frontotemporal dementia, by incorporating measures of sparse diffusion. The Swin-Transformer-based deep learning model effectively learns the complex relationships between brain connectivity patterns and disease status through this novel approach, enabling early and accurate diagnosis of FTD patients. The findings of this study support more research into the potential of the framework in extensive clinical trials, as it has the potential to make a substantial contribution to the diagnosis of neurodegenerative disorders. Subsequent investigations may also examine the efficacy of the framework in identifying FTD patients in different age categories, thus expanding its potential users. An exciting opportunity to improve FTD patients early diagnosis and potentially result in more successful interventions and better patient care—presents itself with our proposed Swin-Transformer-based deep learning framework.

#### 4.4 Experimental findings over ADNI

We used 40 DWI images of people from the ADNI dataset for our experiments. 20 images in this set belong to the cognitively normal (CN) group and the other 20 Mild Cognitive Impairment (MCI) group. 5 CN and 5 MCI images were chosen to train our model, and three CN and three MCI images were chosen for validation. Ultimately, 12 CN and 12 MCI images were placed aside for testing. The ground truth for our experiments has been the result of the fitting of the LLS over *ADNI – 41*.

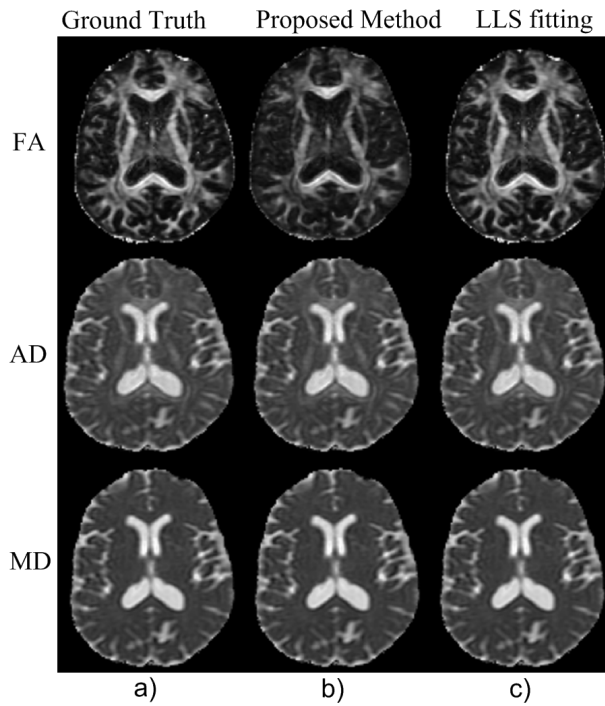


Figure 4.23: The results obtained from the ground truth, the proposed method, and LLS fitting [4] are compared, and it is observed that for 41 diffusion directions, the Proposed method shows comparability with both the ground truth and LLS fitting.

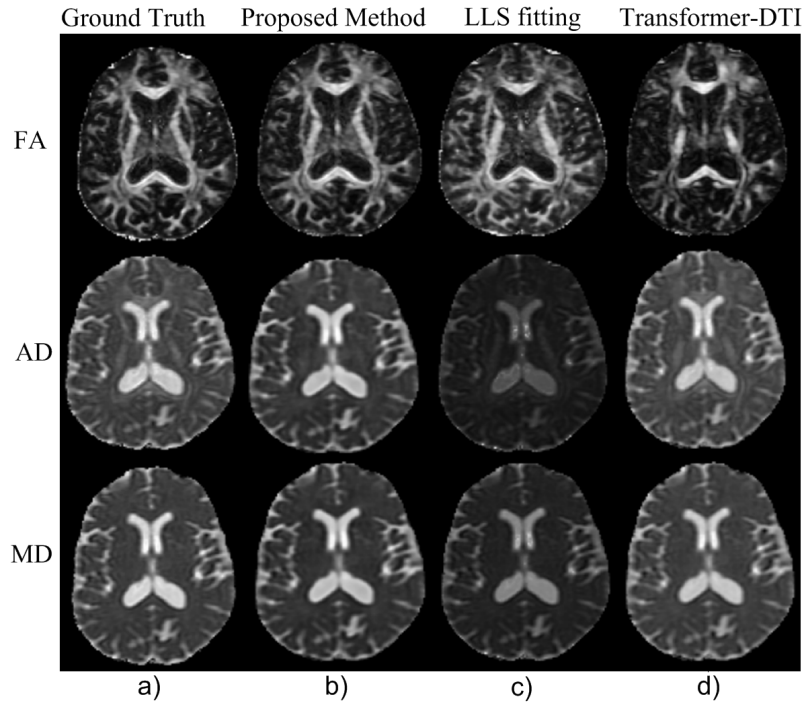


Figure 4.24: We compare the results obtained from the ground truth, the proposed method, LLS fitting [4], and Transformer-DTI [5]. We find that, for 21 diffusion directions, the Proposed method outperforms both LLS fitting [4] and Transformer-DTI [5].

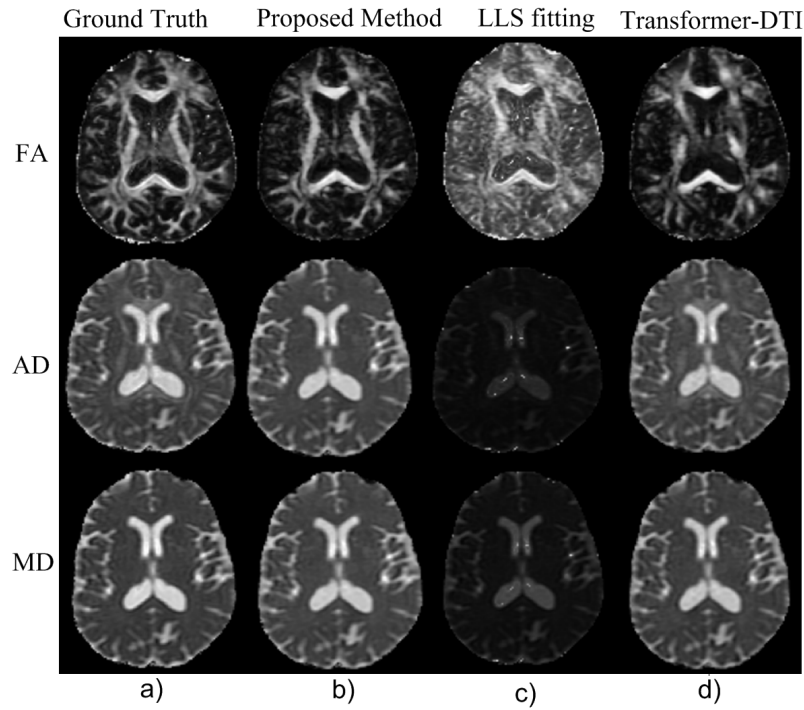


Figure 4.25: We compare results obtained from the ground truth, the proposed method, LLS fitting [4], and Transformer-DTI [5]. We find that, for 5 diffusion directions, the proposed method outperforms LLS fitting [4] and Transformer-DTI [5].

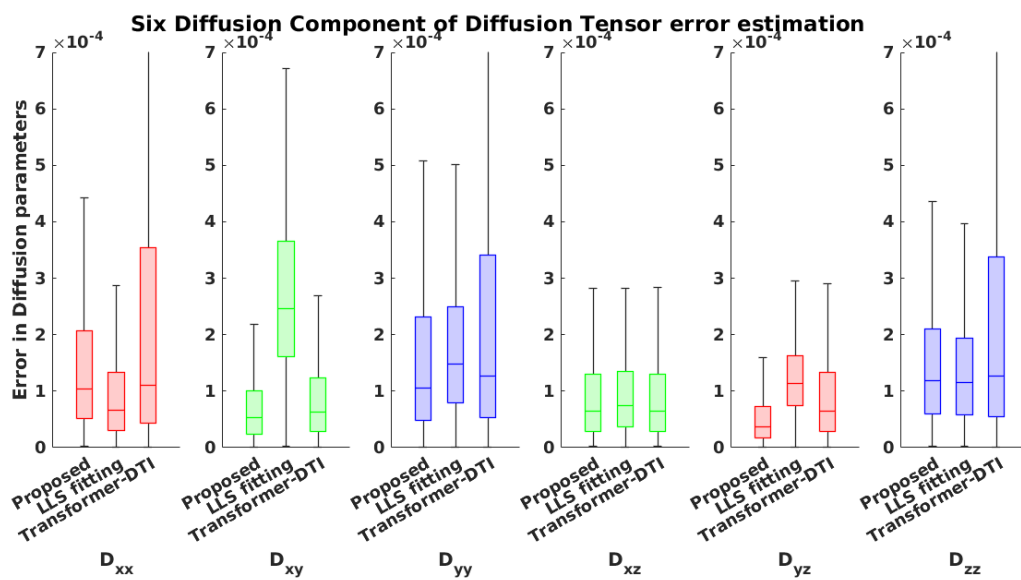


Figure 4.26: Six diffusion component of diffusion tensor for 5 diffusion directions

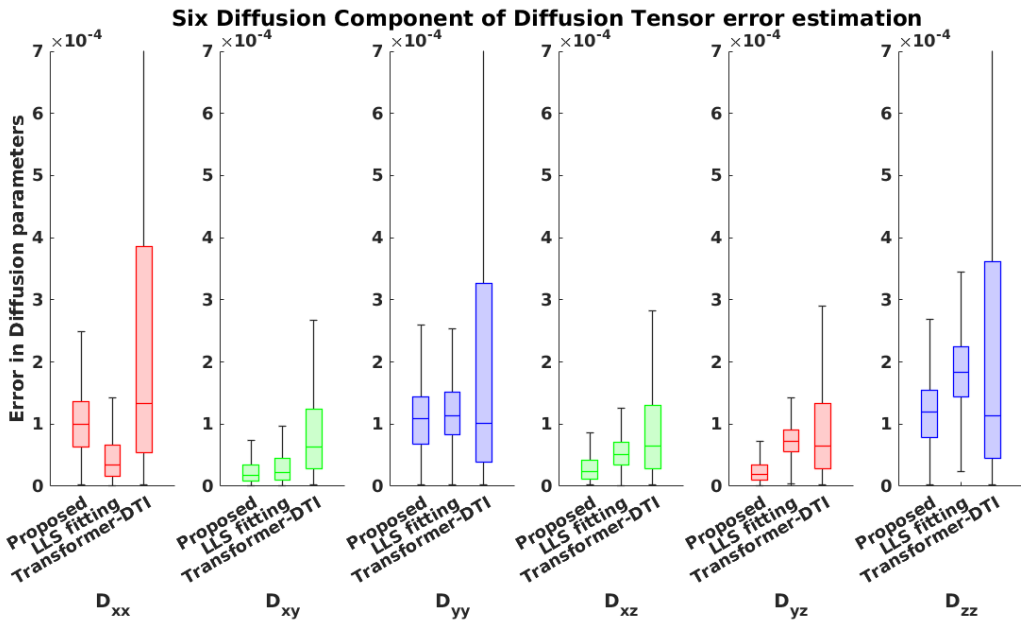


Figure 4.27: Six diffusion component of diffusion tensor for 21 diffusion directions

We evaluated the effectiveness of our suggested approach by contrasting the outcomes with LLS fitting and Transformer-DTI. Comparisons between the proposed method, ground truth, and LLS fitting for 41 diffusion directions are shown in Figure 4.23. The results indicate that the suggested approach is an equally good LLS fitting method. These results show that the diffusion tensor can be accurately estimated using the proposed approach. The results of using the suggested method, LLS fitting, and Transformer-DTI to compare the diffusion measures of 21 diffusion directional signals are shown in figure 4.24. The results of comparing the diffusion measures of five diffusion-directed signals using the suggested method, LLS fitting, and Transformer-DTI are shown in figure 4.25. In particular, as shown in figures 4.24 and 4.27, our suggested approach performs better than Transformer-DTI [5] for diffusion directions of 21 and is comparable to the LLS fitting [4]. According to the aforementioned figures 4.25 and 4.26, our suggested model performs better for 5 diffusion directional than both LLS fitting [4] and Transformer-DTI [5]. These findings demonstrate how well our approach estimates diffusion measures, especially when there are smaller diffusion directions. The findings are displayed in the error plots of the six diffusion components  $\bar{D}$  for the 5 and 21 diffusion directional signals, respectively, in figures 4.26 and 4.27.

In summary, a promising method for Alzheimer disease early diagnosis is the proposed Swin-Transformer-based deep learning framework that includes sparse diffusion measures. One important aspect of Alzheimer disease is the brain's structural connectivity, which is effectively captured by the proposed framework through the use of sparse diffusion measures. Based on the Swin Transformer architecture, we included a planned stride that allows us to strategically manipulate nearby windows in our suggested model. There were areas where the adjacent windows overlapped as a result of this intentional adjustment. The purpose of this deliberate

overlap was to improve intertoken attention. This improvement made it possible for tokens to connect meaningfully even when they are located in different windows. More opportunities for mutual influence were opened up by this dynamic interaction between the tokens, which encouraged the development of more detailed and complex representations. Early diagnosis of Alzheimer's disease is now possible thanks to the effective learning of neighboring patterns by the Swin-Transformer-based deep learning framework. These patterns intrinsically represent complex associations between brain connectivity and disease status. Further investigations can be conducted to examine this framework's potential in extensive clinical trials and to find out how well it works for identifying Alzheimer's in various populations.

# Chapter 5

## Tract-based spatial statistics(TBSS) Analysis

Tract-Based Spatial Statistics (TBSS) is a widely used neuroimaging technique to examine microstructural variations in white matter between different populations. However, TBSS has severe limitations when used on datasets with a single class, such as the Human Connectome Project (HCP) dataset.

White matter integrity metrics, which are usually obtained from diffusion-weighted imaging (DWI) data, are statistically compared voxel-wise in TBSS analysis. TBSS makes it easier to identify group differences in microstructural properties by aligning the data of individual subjects to a shared template and performing statistical inference at each voxel along the white matter skeleton. The fundamental idea behind TBSS is the comparison of white matter properties between various groups, like patients and controls or different disease cohorts. Because the HCP dataset is composed of a homogeneous population of healthy individuals, the standard TBSS analysis cannot be applied because there are no contrasting groups.

### 5.1 TBSS analysis over MICCAI Quad22

TBSS analysis was performed by Santiago Aja-Fernández et al.[1] on the MICCAI Quad22 Migraine dataset, which was a component of the MICCAI 2022 Challenge Quad22. Patient data containing cases of episodic migraine (EM) and chronic migraine (CM) were made available to 14 teams, as our team of Shiv Nadar University was team number 13. Our team received 39,256 points (the total number of voxels) with statistically significant differences in mean diffusivity (MD), axial diffusivity (AD), and fractional anisotropy (FA) across the FA skeleton in the raw TBSS data. The 14 teams contributions were combined by Santiago Aja-Fernández et al.[1] for TBSS analysis of the Migraine

dataset. They also provided the quantity of Regions of Interest (ROIs) for every metric in order to clarify statistically significant differences. Refer to the work of Santiago Aja-Fernández et al.[1] for a more thorough understanding of this subject.

## 5.2 TBSS analysis over NIFD

In addition, a t-test analysis was utilized in the research [176] to evaluate the statistical significance of our findings using the tract-based spatial statistics (TBSS) pipeline. Fractional anisotropy (FA) metrics were used in the analysis to compare two groups: healthy CN and FTD patients.

Using FNIRT from FSL [177], FA images were registered to the FMRIB-58 template in the MNI space. Because the white matter skeleton was obtained from a mean FA image with a 0.2 FA threshold, the data could be statistically interpreted with confidence. Axial and coronal brain slices with p-values from two sample t-tests highlighting the Cingulum and Uncinate fasciculus regions are displayed in Figures 5.1 and 5.2. According to previous research, the findings show a strong correlation between FTD patients and the Cingulum and Uncinate fasciculus regions [3, 178]. With sparse data, our suggested framework shows a similar relationship and considerably shortens the scanning time.

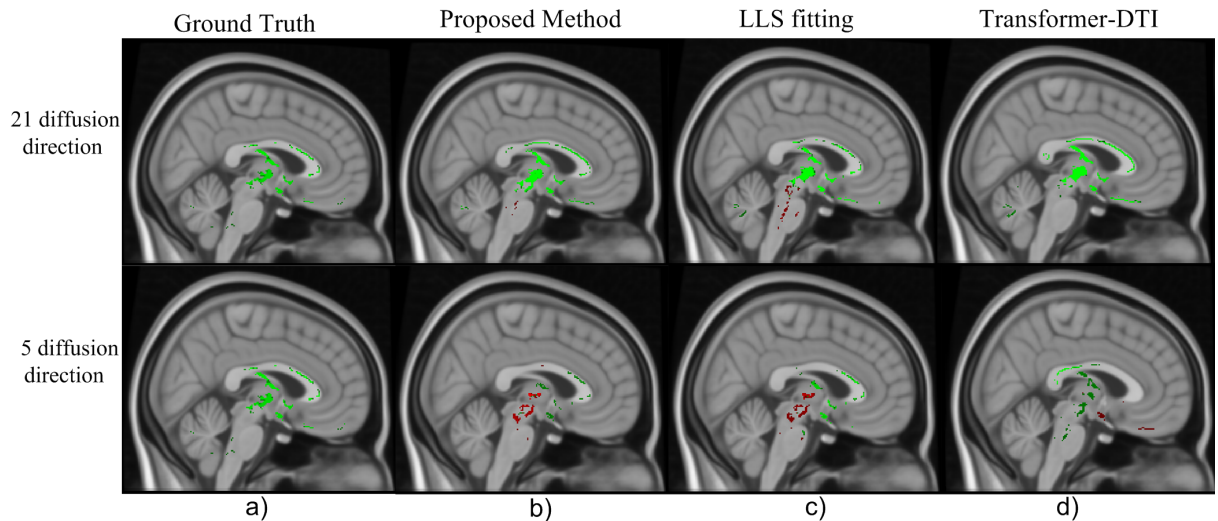


Figure 5.1: An axial brain slice showing the Cingulum region; the p-value from the two sample t-test ( $df=8$ ) is indicated. Green indicates that the tstat1 hypothesis test is a healthy CN > FTD patient; red indicates that the tstat2 hypothesis test is a healthy CN < FTD patient.

Changes in the microstructural integrity of these white matter tracts, which are important for a number of cognitive functions, may be associated with the onset of frontotemporal dementia (FTD). The number of pixels with p-values outside of confidence intervals for the two diffusion directions (5 Diff. and 21 Diff.) at 95% and 99% confidence intervals is compared in Table 5.1. In contrast to the LLS fitting and Transformer-DTI methods, which exhibit larger departures from the ground truth,

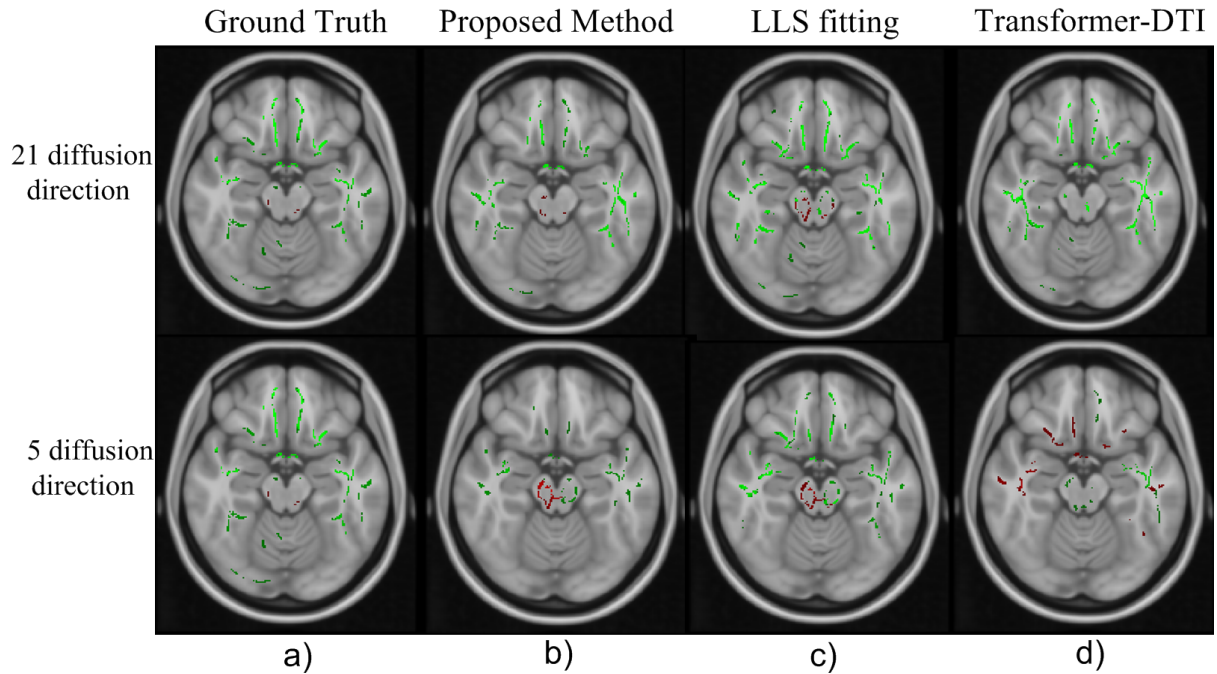


Figure 5.2: An illustration of the Uncinate fasciculus region in a coronal brain slice is shown with the p-value ( $df=8$ ) of the two sample t-test. Green hue indicates that tstat1-Healthy CN is the hypothesis being tested. Hypothesis testing tstat2 - Healthy CN  $<$  FTD patient, Red color.

Table 5.1: The Proposed Model, LLS fitting, and Transformer-DTI are examined for the number of pixels with p-values outside Confidence Intervals (95% and 99%) for the t-statistics (tstat1 and tstat2), where tstat1 compares Healthy CN > FTD patient and tstat2 compares Healthy CN < FTD patient.

P-Value	Ground Truth	Proposed Model		LLS fitting		Transformer-DTI	
		5 Diff.	21 Diff.	5 Diff.	21 Diff.	5 Diff.	21 Diff.
tstat1, 95 C.I.	15870	9924	14471	13844	18262	9481	17820
tstat2, 95 C.I.	4294	7527	5719	5391	4351	12162	4517
tstat1, 99 C.I.	3591	2418	3564	3585	4836	2510	4866
tstat2, 99 C.I.	837	1702	1450	1061	913	3818	1181

the results show that our suggested method maintains an equal number of pixels with significant differences.

### 5.3 TBSS analysis over ADNI

We used the tract-based spatial statistics (TBSS) pipeline [176] to perform a t-test analysis comparing two groups (Healthy CN and MCI) based on fractional anisotropy (FA) metrics in order to further evaluate the statistical significance of our results. Using the FNIRT tool from FSL [177], FA images were non-linearly registered to the FMRIB-58 template in the Montreal Neurological Institute (MNI) space, which includes averaged FA maps. A mean FA image produced with an FA threshold of 0.2 was thinned to identify the white matter skeleton and distinguish it from the gray matter.

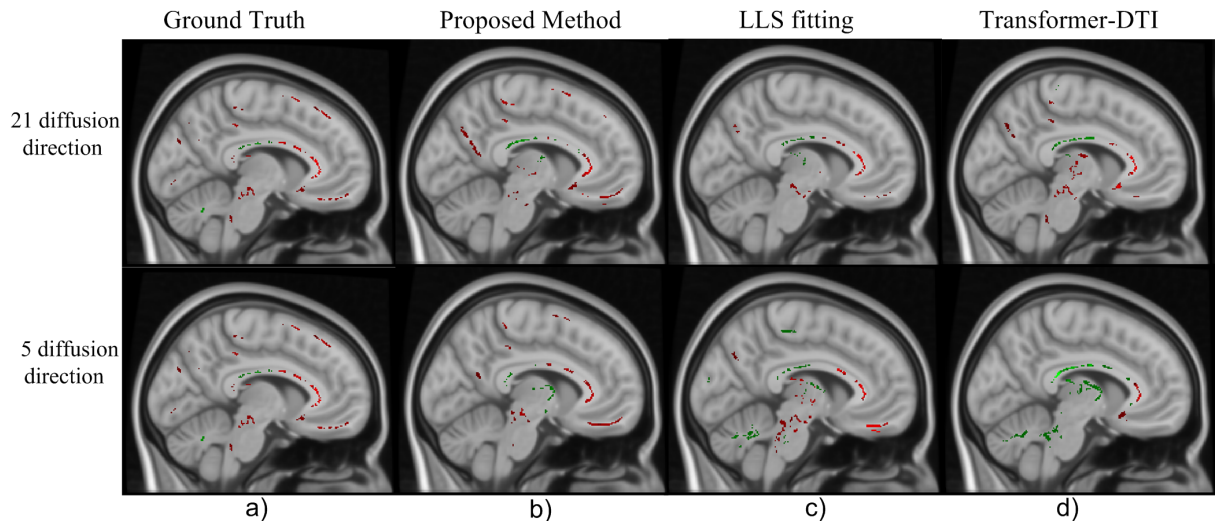


Figure 5.3: An axial brain slice showing the Cingulum region; the p-value from the two sample t-test ( $df=22$ ) is indicated. Green color: hypothesis testing  $tstat1 - \text{Healthy CN} > \text{MCI}$ , Red color: hypothesis testing  $tstat2 - \text{Healthy CN} < \text{MCI}$ .

An exhaustive comparison of the two groups was made possible by this methodical approach, which also enabled an accurate statistical interpretation of the data. A p-value from a two sample t-test with 22 degrees of freedom is used to highlight an axial brain slice in figure 5.3 that represents the Cingulum region. A coronal brain slice representing the Uncinate fasciculus region is highlighted similarly in Figure 5.4, with a p-value derived from a two-sample t-test with 22 degrees of freedom. These diagrams offer insightful data regarding the areas of the brain that might be impacted by the experimental setup and can be further examined in relation to the study's research question or hypothesis.

The Cingulum and Uncinate fasciculus are significantly associated with the development of Alzheimer's disease, according to the findings of research done by [3, 178]. With sparse data,

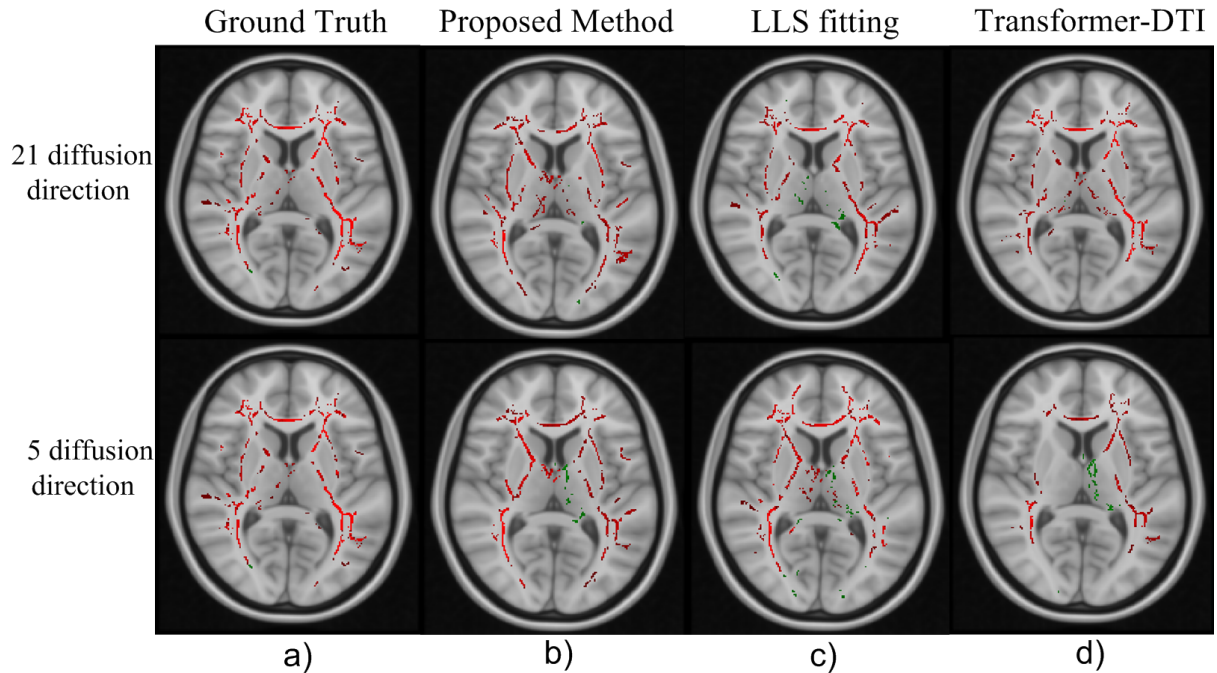


Figure 5.4: Uncinate fasciculus region represented by a coronal brain slice, with a two sample t-test p-value of ( $df=22$ ) indicated. Green color: hypothesis testing  $tstat1$  - Healthy CN  $>$  MCI, Red color: hypothesis testing  $tstat2$  - Healthy CN  $<$  MCI.

Table 5.2: Pixel count for t-statistics ( $tstat1$  and  $tstat2$ ) in the proposed model, LLS fitting, and Transformer-DTI that have p-values outside of the 95% and 99% confidence intervals. There are two hypotheses:  $tstat1$  (healthy CN  $>$  MCI) and  $tstat2$  (healthy CN  $<$  MCI).

P-Value	Ground Truth	Proposed Model		LLS fitting		Transformer-DTI	
		5 Diff.	21 Diff.	5 Diff.	21 Diff.	5 Diff.	21 Diff.
$tstat1$ , 95 C.I.	3775	3246	3146	4024	5568	5311	4646
$tstat2$ , 95 C.I.	7586	8154	7188	7836	5683	5259	7228
$tstat1$ , 99 C.I.	618	505	485	741	981	960	860
$tstat2$ , 99 C.I.	1352	1693	1330	1578	917	1012	1184

Figures 5.3 and 5.4 show similar relationships using our proposed framework, which significantly reduces scanning time. Essential white matter tracts in the brain, the cingulum and uncinate fasciculus, are involved in a variety of cognitive functions, such as memory, emotional regulation, and social behavior. The beginning of Alzheimer's disease may be associated with changes in the microstructural integrity of these tracts, according to recent research. P-values for the number of pixels outside of confidence intervals are shown in Table 5.2. The results for two distinct diffusion directions—5 Diff. and 21 Diff.—are displayed. In terms of confidence levels, it offers confidence intervals at 95% (95 C.I.) and 99% (99 C.I.). An equal number of pixels with significant differences in two groups compared to the ground truth are preserved by the suggested method, as shown by the results in Table 5.2. On the other hand, a greater number of pixels with notable differences in two groups are produced by the LLS fitting and Transformer-DTI methods, which depart even more from the ground truth.

# Chapter 6

## Conclusion and Future Directions

### 6.1 Summary of Research Findings

The SwinDTI technique effectively and robustly estimates diffusion-weighted DTI parameters (such as FA, AD, and MD) from sparse diffusion-weighted images. the current model possess ability to predict using as few as five diffusion directions, which is difficult for other state of the art(SOTA). Enhanced non-linearity, lower computational costs, and better parallelization are achieved by SwinDTI through the use of window self-attention and shifting mechanisms in the Swin Transformer architecture. In DTI parameter estimation and structural similarity index on the HCP Young Adult dataset, SwinDTI outperforms other techniques such as 3D U-Net, Transformer-DTI, and linear least square fitting. SwinDTI demonstrates that it can detect microstructural alterations in specific regions associated with neurological conditions and illnesses. Sparse diffusion measures are used in the proposed Swin-Transformer-based deep learning framework to diagnose Alzheimer's disease. It detects significant differences in brain regions between the groups with mild cognitive impairment and the healthy group, and it estimates DTI parameters with reduced diffusion directions with accuracy.

An additional proposal utilizing the neural network based on Swin-Transformer aims to diagnose frontotemporal dementia (FTD). This framework helps distinguish between healthy people and FTD patients by providing accurate estimates of important DTI parameters. Notable correlations have been discovered between particular brain regions and FTD patients, which may improve FTD diagnosis and shorten scanning times.

In another study, the impact of angular resolution on distinguishing between patients with episodic and chronic migraines is examined in relation to the application of deep learning techniques to improve the quality of diffusion MRI data in clinical studies. Although the techniques increased the number of false positives while also improving the detection of group differences, this suggests that applying AI-based techniques to heterogeneous clinical data may

carry a risk of generalization. When utilizing AI for clinical study data synthesis or harmonization, extreme caution is recommended because crucial data could be manipulated or falsified.

An exact and strong correlation between the diffusion signals and the estimated diffusion tensor parameters in nearby voxels is provided by the suggested method. Spatial correlation is therefore an important factor to consider, since the fiber orientation of the brain tissue micro-structures is not distributed randomly among adjacent voxels. The existing research clearly demonstrates a lack of studies focusing on spatial correction of nearby voxels[5, 69, 179], which may be related to the high processing cost of such work.

Interestingly, Transformer-DTI[5] does account for nearby voxels; however, the inclusion of 25 million trainable parameters suggests that computing requirements will increase. Using a conventional method based on the maximum likelihood estimate (MLE), a Log Euclidean framework, another formulation based on spatial prior[109] improves the spatial resolutions of DWI images without changing the number of diffusion directions. The problem with MLE-based techniques is that they require a lot of repeating calculations for each voxel, which slows down the estimation process. Compared to conventional convolution neural networks and recurrent neural networks, the attention-based transformer model is more resilient and performs better at learning the correlations between elements[67, 68].

The b-values are essential to the diffusion-weighted imaging (DWI) procedure in the proposed framework. The b-value is a crucial factor that influences how sensitive the DWI sequence is to the diffusion of water molecules within brain tissues, as Figure 3.1 illustrates. The effect of changing b-values on the content and quality of the diffusion-weighted images is shown in Figure 3.1. Greater sensitivity to restricted diffusion is made possible by higher b-values, which makes it possible to distinguish between various tissue types, such as gray and white matter. In contrast, lower b-values reveal more about the overall tissue microstructure because they are more sensitive to free diffusion.

In order to provide an accurate representation of the diffusion behavior in the brain, the selection of b values in the proposed framework is essential. This helps to improve the interpretation of the values of mean diffusivity (MD), axial diffusivity (AD), and fractional anisotropy (FA). We trained our developed model with the widely used clinical standard b-value of  $1000 \text{ s/mm}^2$ .

The main contributions using HCP dataset are as follows:

- Large-scale image recognition tasks are the main goal of the Swin Transformer[68]. With the use of the Swin Transformer block for parameter estimation (FA, AD, and MD), our proposed method SwinDTI, outperforms in predicting quantitative measurements in sparse data.
- Our proposed model SwinDTI is able to measure FA, AD, and MD simultaneously for a variety of diffusion directions  $N_{dir} = 5, 21, 32, 64$ .

- Even with just 5 diffusion directions, SwinDTI shows that it can predict FA, AD, and MD with reasonable accuracy. This demonstrates how well it can handle these difficult "ill-posed problems" by using backpropagation training to obtain internal prior knowledge.
- The proposed framework shows promise in precisely predicting FA, AD, and MD measures in particular regions of interest (ROIs) associated with various diseases.

The goal was to assess how well deep learning (DL) methods work in improving the quality of diffusion MRI (dMRI) data for use in clinical settings. The purpose of the research was to determine whether the application of artificial intelligence (AI) techniques to medical images could lead to the appearance of false information or the loss of important clinical data. A migraine clinical trial was conducted, specifically comparing patients with episodic and chronic migraine, to evaluate the angular resolution of dMRI. White matter analysis results were impacted by the number of gradient directions; statistically significant differences between groups were significantly reduced when 21 gradient directions were used instead of the original 61. The objective was to apply DL to improve the three diffusion metrics (FA, AD, and MD) derived from data collected with 21 gradient directions and a b-value of  $1000 \text{ s/mm}^2$ . The teams had to come from 14 different institutions to complete this task. Producing outcomes similar to those derived from 61 gradient directions was the aim. Using Tract-Based Spatial Statistics (TBSS) to compare patients with episodic and chronic migraines, the results were evaluated using both common image quality metrics. Although most DL techniques increased the number of false positives, the study's findings indicate that they also enhanced the ability to identify statistical differences between groups. The results demonstrated a continuous growth rate of false positives that was linearly proportional to the number of new true positives. This underscores the danger of generalizing AI-based tasks when evaluating heterogeneous clinical cohorts and training on data from a single group. Additionally, several of the methods displayed notable bias, and they performed differently when trying to replicate the data's original distribution. Finally, even though global metrics like peak signal-to-noise ratio or structural similarity seem to indicate otherwise, great care should be taken when using AI methods for harmonization or synthesis when processing heterogeneous data in clinical studies. This is because crucial information may be altered.

The main contributions using MICCAI Quad22 migraine dataset:

- Proposed deep learning framework aids in biomarker-based decision-making for chronic migraine (CM) and episodic migraine (EM).
- Proposed method predicted better quantitative measures FA, AD and MD compare to traditional method for 21 diffusion directional signal of chronic migraine and episodic migraine.

As part of the MICCAI 2022 Challenge Quad22, the MICCAI Quad22 Migraine Dataset was used in a research investigation led by Santiago Aja-Fernández et al.[1]. This dataset included patient

information from cases of both chronic migraine (CM) and episodic migraine (EM). It was made available to 14 teams that took part, including Team 13, which I am a member of. Our team developed a deep learning framework for the purpose of this research to examine quantitative metrics related to both EM and CM, including mean diffusivity (MD), axial diffusivity (AD), and fractional anisotropy (FA). In order to analyze the results, Santiago Aja-Fernández et al. [1] combined the contributions from each of the 14 teams. They also offered information on the number of Regions of Interest for each metric, which helped to find statistically significant discrepancies.

SwinTransformer-based deep learning framework was utilized to diagnose the incidence of Frontotemporal Dementia. By incorporating sparse diffusion measures, our framework effectively demonstrates the underlying structural connectivity of the brain, a critical feature in FTD patients. Through this approach, the Swin-Transformer-based deep learning model successfully learns the complex relationships between brain connectivity patterns and disease status, helping in accurate diagnosis of FTD patients at an early stage.

The main contributions using NIFD dataset are as follows:

- Effectively acquiring spatial correlation in adjacent voxels to enhance the robustness of DTI parameter estimations.
- Introducing a Framework to Estimate DTI Parameters with Sparse Measurements and Maintain Comparable Estimate Quality to Dense Measurements.
- The ability of the suggested model’s DTI parameter estimates to generate unique features for both healthy individuals and FTD patients is demonstrated.

The main contributions using ADNI dataset are as follows:

- A novel training strategy involving shifting window with overlapping strides is used to effectively learn spatial correlation in neighboring voxels and improve the robustness of diffusion tensor imaging parameters.
- The proposed method enables quick estimation of DTI parameters from sparse measurements.
- Demonstrated ability to use the proposed framework to measure diffusion parameters and identify Alzheimer’s disease in its early stages.

## 6.2 Limitations and Potential Improvements

Even with a sparse set of diffusion-weighted images, the SwinDTI method demonstrates remarkable accuracy in estimating diffusion tensor imaging (DTI) parameters, such as mean diffusivity (MD), axial diffusivity (AD), and fractional anisotropy (FA). Its resilience is especially remarkable, since it can manage different numbers of diffusion directions, even cases with as few as five diffusion directions, which is difficult for other methods to handle.

By combining window self-attention and shifting mechanisms, which facilitate effective parallelization, lower computing costs, and improved non-linearity in parameter estimation, SwinDTI builds on the advantages of the Swin Transformer architecture. As demonstrated by the method's improved structural similarity index on the HCP Young Adult dataset, this design decision helps it perform better than other approaches like 3D U-Net, Transformer-DTI, and linear least square fitting.

Additionally, as demonstrated by its ability to capture subtle microstructural alterations within particular regions of interest linked to a variety of neurological disorders and diseases, SwinDTI shows promise for use in clinical settings.

To further solidify its performance and applicability, the SwinDTI method may benefit from a few improvements despite its strengths. For example, investigating the incorporation of multi-scale feature extraction mechanisms or the integration of additional data augmentation techniques may enhance its capacity to extract complex structural information. Further development of the approach may concentrate on improving its robustness in managing data variability and its generalizability across various datasets, particularly in clinical settings.

Furthermore, it is critical to continuously validate the SwinDTI method across a variety of patient cohorts and incorporate rigorous validation protocols, given the dynamic nature of neuroimaging research and the growing complexity of clinical data. Its credibility as a useful tool for the early diagnosis and monitoring of neurological conditions would be strengthened by this process, which would also aid in evaluating its reliability in clinical decision-making.

In addition, the incorporation of interpretability measures and explainable AI techniques could improve the models clinical adoption and trustworthiness, leading to a better understanding of the underlying neurobiological processes in the context of the proposed Swin-Transformer-based framework for early diagnosis of Alzheimer's disease and the deep learning framework for diagnosing frontotemporal dementia.

The application of deep learning techniques to improve the quality of diffusion MRI data in clinical studies emphasizes the need to proceed with caution when utilizing AI techniques for data synthesis or harmonization in heterogeneous clinical datasets. In order to mitigate the risk of potential misinterpretation or manipulation of crucial clinical information, it would be imperative to develop customized data validation strategies and strong quality control measures. This would ensure the reliability and integrity of AI-based findings. To further promote trust and responsible AI-driven healthcare practices, it is imperative to establish transparency and accountability in the development and application of AI algorithms within clinical settings.

### 6.3 Future Research and Applications

Using sparse diffusion-weighted images, a new technique called SwinDTI shows excellent accuracy and robustness in estimating DTI parameters such as mean diffusivity (MD), axial diffusivity (AD), and fractional anisotropy (FA). An important limitation of current methods is overcome by SwinDTI, which can handle varying numbers of diffusion directions efficiently, even with as few as 5 directions. SwinDTI optimizes non-linearity, minimizes computational cost, and facilitates efficient parallelization by utilizing the benefits of window self-attention and shifting mechanism in the Swin Transformer architecture. Using the HCP Young Adult dataset, SwinDTI outperforms 3D U-Net, Transformer-DTI, and linear least square fitting techniques in terms of DTI parameter estimation and structural similarity index. Microstructural alterations in particular regions of interest associated with a range of neurological illnesses and disorders can be detected by SwinDTI.

The mean square error of the results shows that applying AI-based techniques to heterogeneous clinical data should be done with caution because there is a chance that crucial information may be changed or misrepresented. The future direction of our work will be focused on addressing problems with noise-induced robustness, solve crossing-fiber problems, and develop tract-based classification and localization methods.

### 6.4 Conclusion

We conclude that our proposed deep learning framework, SwinDTI, based on Swin-Transformers represents a significant advance in the field of diffusion tensor imaging (DTI). With sparse diffusion-weighted images, it performs exceptionally well in the estimation of important DTI parameters, including mean diffusivity (MD), axial diffusivity (AD), and fractional anisotropy (FA). Crucially, SwinDTI demonstrates its versatility by yielding dependable outcomes with as few as 5 diffusion directions—an accomplishment that other methods have not been able to achieve. The use of window self-attention and shifting mechanisms, which improve non-linearity while lowering computing costs and facilitating effective parallelization, has helped to achieve this result.

According to findings on the HCP Young Adult dataset, SwinDTI routinely outperforms well-known techniques like 3D U-Net, Transformer-DTI, and linear least square fitting in comparison evaluations against them in terms of DTI parameter estimation and structural similarity index. Beyond parameter estimation, SwinDTI also demonstrates its effectiveness in capturing microstructural changes in particular regions of interest that are pertinent to a range of neurological disorders and diseases.

Our framework is demonstrated to be highly accurate in estimating DTI parameters using sparse

diffusion measures in a related study on early diagnosis of Alzheimer's disease. Through statistical analysis, it detects significant differences in brain regions between healthy individuals and those with mild cognitive impairment, and it handles different diffusion directions with efficiency. Our approach presents a promising avenue for reducing scanning time and advancing early diagnosis and treatment of Alzheimer's disease. These findings have been validated on the Alzheimer's Disease Neuroimaging Initiative (ADNI) dataset.

As part of an additional investigation, we investigated how deep learning methods might improve the quality of diffusion MRI data used in clinical trials to identify differences between patients with episodic and chronic migraines. Based on our research, most approaches lead to a rise in false positives even though they are effective in enhancing group differentiation. This finding emphasizes the significance of using AI-based techniques with caution in clinical research, especially when dealing with heterogeneous data. As a consequence of the harmonization or synthesis process, critical information must be carefully considered to prevent its compromise or alteration.

In conclusion, our work highlights the difficulties and complexities involved in using AI techniques in clinical research, while also emphasizing the important contributions made by SwinDTI to the advancement of DTI parameter estimation and its potential for early diagnosis in neurological disorders.

# References

- [1] Santiago Aja-Fernández, Carmen Martín-Martín, Álvaro Planchuelo-Gómez, Abrar Faiyaz, Md Nasir Uddin, Giovanni Schifitto, Abhishek Tiwari, Saurabh J Shigwan, Rajeev Kumar Singh, Tianshu Zheng, et al. Validation of deep learning techniques for quality augmentation in diffusion mri for clinical studies. *NeuroImage: Clinical*, 39:103483, 2023.
- [2] Sarah M Jurick, Samantha N Hoffman, Scott Sorg, Amber V Keller, Nicole D Evangelista, Nicole E DeFord, Mark Sanderson-Cimino, Katherine J Bangen, Lisa Delano-Wood, Sean Deoni, et al. Pilot investigation of a novel white matter imaging technique in veterans with and without history of mild traumatic brain injury. *Brain injury*, 32(10):1255–1264, 2018.
- [3] Negar Fani, Tricia Z King, Emily Reiser, Elisabeth B Binder, Tanja Jovanovic, Bekh Bradley, and Kerry J Ressler. Fkbp5 genotype and structural integrity of the posterior cingulum. *Neuropsychopharmacology*, 39(5):1206–1213, 2014.
- [4] Cheng Guan Koay, Lin-Ching Chang, John D Carew, Carlo Pierpaoli, and Peter J Basser. A unifying theoretical and algorithmic framework for least squares methods of estimation in diffusion tensor imaging. *Journal of magnetic resonance*, 182(1):115–125, 2006.
- [5] Davood Karimi and Ali Gholipour. Diffusion tensor estimation with transformer neural networks. *Artificial Intelligence in Medicine*, page 102330, 2022.
- [6] Chuohao Yeo, Hui Li Tan, and Yih Han Tan. On rate distortion optimization using ssim. *IEEE Transactions on Circuits and Systems for Video Technology*, 23(7):1170–1181, 2013.
- [7] Pedro A Luque Laguna, Anna JE Combes, Johannes Streffler, Steven Einstein, Maarten Timmers, Steve CR Williams, and Flavio Dell’Acqua. Reproducibility, reliability and variability of fa and md in the older healthy population: A test-retest multiparametric analysis. *NeuroImage: Clinical*, 26, 2020.
- [8] World Health Organization. The world health report 2001: Mental health: new understanding, new hope. 2001.
- [9] Sheema Noorain, Maria Paola Scaparra, and Kathy Kotiadis. Mind the gap: a review of optimisation in mental healthcare service delivery. *Health Systems*, 12(2):133–166, 2023.

- [10] Charles B Truax and Robert Carkhuff. *Toward effective counseling and psychotherapy: Training and practice*. Transaction Publishers, 2007.
- [11] Tonya White, Miranda Nelson, and Kelvin O Lim. Diffusion tensor imaging in psychiatric disorders. *Topics in Magnetic Resonance Imaging*, 19(2):97–109, 2008.
- [12] Jason D Yeatman, Robert F Dougherty, Nathaniel J Myall, Brian A Wandell, and Heidi M Feldman. Tract profiles of white matter properties: automating fiber-tract quantification. *PloS one*, 7(11):e49790, 2012.
- [13] Bing Jian and Baba C Vemuri. A unified computational framework for deconvolution to reconstruct multiple fibers from diffusion weighted mri. *IEEE transactions on medical imaging*, 26(11):1464–1471, 2007.
- [14] Christine Stadelmann, Sebastian Timmler, Alonso Barrantes-Freer, and Mikael Simons. Myelin in the central nervous system: structure, function, and pathology. *Physiological reviews*, 99(3):1381–1431, 2019.
- [15] Arthur M Butt, Robert F Fern, and Carlos Matute. Neurotransmitter signaling in white matter. *Glia*, 62(11):1762–1779, 2014.
- [16] Derek K Jones, Thomas R Knösche, and Robert Turner. White matter integrity, fiber count, and other fallacies: the do’s and don’ts of diffusion mri. *Neuroimage*, 73:239–254, 2013.
- [17] Bai Lu, Guhan Nagappan, Xiaoming Guan, Pradeep J Nathan, and Paul Wren. Bdnf-based synaptic repair as a disease-modifying strategy for neurodegenerative diseases. *Nature Reviews Neuroscience*, 14(6):401–416, 2013.
- [18] Anne Isabelle Boullerne. The history of myelin. *Experimental neurology*, 283:431–445, 2016.
- [19] Pierre Morell and William T Norton. Myelin. *Scientific American*, 242(5):88–119, 1980.
- [20] Stéphanie Debette and HS Markus. The clinical importance of white matter hyperintensities on brain magnetic resonance imaging: systematic review and meta-analysis. *Bmj*, 341, 2010.
- [21] Marek Kubicki, CARL-FREDRIK WESTIN, ROBERT W McCARLEY, and Martha E Shenton. The application of dti to investigate white matter abnormalities in schizophrenia. *Annals of the New York Academy of Sciences*, 1064(1):134–148, 2005.
- [22] Nobutsugu Hirono, Hajime Kitagaki, Hiroaki Kazui, Mamoru Hashimoto, and Etsuro Mori. Impact of white matter changes on clinical manifestation of alzheimer’s disease: a quantitative study. *Stroke*, 31(9):2182–2188, 2000.
- [23] Nicolae Sarbu, Robert Y Shih, Robert V Jones, Iren Horkayne-Szakaly, Laura Oleaga, and James G Smirniotopoulos. White matter diseases with radiologic-pathologic correlation. *Radiographics*, 36(5):1426–1447, 2016.

- [24] Naama Barnea-Goraly, Vinod Menon, Mark Eckert, Leanne Tamm, Roland Bammer, Asya Karchemskiy, Christopher C Dant, and Allan L Reiss. White matter development during childhood and adolescence: a cross-sectional diffusion tensor imaging study. *Cerebral cortex*, 15(12):1848–1854, 2005.
- [25] Douglas C Dean, Jonathan O’Muircheartaigh, Holly Dirks, Nicole Waskiewicz, Lindsay Walker, Ellen Doernberg, Irene Piryatinsky, and Sean CL Deoni. Characterizing longitudinal white matter development during early childhood. *Brain Structure and Function*, 220:1921–1933, 2015.
- [26] Thomas R Knösche, Alfred Anwander, Matthew Liptrot, and Tim B Dyrby. Validation of tractography: comparison with manganese tracing. *Human brain mapping*, 36(10):4116–4134, 2015.
- [27] Robert H Garman. Histology of the central nervous system. *Toxicologic pathology*, 39(1):22–35, 2011.
- [28] Jay N Giedd. Structural magnetic resonance imaging of the adolescent brain. *Annals of the New York Academy of Sciences*, 1021(1):77–85, 2004.
- [29] Miguel Guevara, Pamela Guevara, Claudio Román, and Jean-François Mangin. Superficial white matter: A review on the dmri analysis methods and applications. *Neuroimage*, 212:116673, 2020.
- [30] George Bartzokis. Alzheimer’s disease as homeostatic responses to age-related myelin breakdown. *Neurobiology of aging*, 32(8):1341–1371, 2011.
- [31] Mehmet Yigit Avci, Ziyu Li, Qiuyun Fan, Susie Huang, Berkin Bilgic, and Qiyuan Tian. Quantifying the uncertainty of neural networks using monte carlo dropout for deep learning based quantitative mri. *arXiv preprint arXiv:2112.01587*, 2021.
- [32] Davood Karimi, Camilo Jaimes, Fedel Machado-Rivas, Lana Vasung, Shadab Khan, Simon K Warfield, and Ali Gholipour. Deep learning-based parameter estimation in fetal diffusion-weighted mri. *Neuroimage*, 243:118482, 2021.
- [33] Hongyu Li, Zifei Liang, Chaoyi Zhang, Ruiying Liu, Jing Li, Weihong Zhang, Dong Liang, Bowen Shen, Xiaoliang Zhang, Yulin Ge, et al. Superdti: Ultrafast dti and fiber tractography with deep learning. *Magnetic resonance in medicine*, 86(6):3334–3347, 2021.
- [34] Qiyuan Tian, Berkin Bilgic, Qiuyun Fan, Congyu Liao, Chanon Ngamsombat, Yuxin Hu, Thomas Witzel, Kawin Setsompop, Jonathan R Polimeni, and Susie Y Huang. Deepdti: High-fidelity six-direction diffusion tensor imaging using deep learning. *NeuroImage*, 219:117017, 2020.

- [35] Helmut Mehrer. History and bibliography of diffusion. *Diffusion in solids: Fundamentals, methods, materials, diffusion-controlled processes*, pages 1–23, 2007.
- [36] Bernard H Lavenda. *Statistical physics: A probabilistic approach*. Courier Dover Publications, 2016.
- [37] Denis Le Bihan and Heidi Johansen-Berg. Diffusion mri at 25: exploring brain tissue structure and function. *Neuroimage*, 61(2):324–341, 2012.
- [38] M Meyyappan, Biji Babu, M Anitha, Gopinath Ganesan, S Anita, Paarthipan Natarajan, M Meyyappan, Biji Babu Sr, and M Anitha. Role of diffusion tensor imaging in early diagnosis and characterization of movement disorders. *Cureus*, 16(2), 2024.
- [39] Herman Y Carr and Edward M Purcell. Effects of diffusion on free precession in nuclear magnetic resonance experiments. *Physical review*, 94(3):630, 1954.
- [40] Edward O Stejskal and John E Tanner. Spin diffusion measurements: spin echoes in the presence of a time-dependent field gradient. *The journal of chemical physics*, 42(1):288–292, 1965.
- [41] D Le Bihan and E Breton. In vivo magnetic resonance imaging of diffusion. *Comptes Rendus des Seances de l'Academie des Sciences. Serie 2*, 301(15):1109–1112, 1985.
- [42] Denis Le Bihan, Eric Breton, Denis Lallemand, Philippe Grenier, Emmanuel Cabanis, and Maurice Laval-Jeantet. Mr imaging of intravoxel incoherent motions: application to diffusion and perfusion in neurologic disorders. *Radiology*, 161(2):401–407, 1986.
- [43] Gesa Sophia Borgeest. *Lifestyle, Brain Structure and Cognitive Ageing*. PhD thesis, University of Cambridge, 2022.
- [44] Todd E Golde. Alzheimer’s disease—the journey of a healthy brain into organ failure. *Molecular Neurodegeneration*, 17(1):18, 2022.
- [45] Elizabeth R Sowell, Paul M Thompson, and Arthur W Toga. Mapping changes in the human cortex throughout the span of life. *The Neuroscientist*, 10(4):372–392, 2004.
- [46] Rik Ossenkoppele, Ellen H Singleton, Colin Groot, Anke A Dijkstra, Willem S Eikelboom, William W Seeley, Bruce Miller, Philip Scheltens, Janne M Papma, Gil D Rabinovici, et al. Research criteria for the behavioral variant of alzheimer disease: a systematic review and meta-analysis. *JAMA neurology*, 79(1):48–60, 2022.
- [47] Maxime Descoteaux, Rachid Deriche, Thomas R Knosche, and Alfred Anwander. Deterministic and probabilistic tractography based on complex fibre orientation distributions. *IEEE transactions on medical imaging*, 28(2):269–286, 2008.

- [48] Pratik Mukherjee, JI Berman, Stephen W Chung, CP Hess, and RG Henry. Diffusion tensor mr imaging and fiber tractography: theoretic underpinnings. *American journal of neuroradiology*, 29(4):632–641, 2008.
- [49] Rafael Neto Henriques, Richard Henson, Cam-CAN, and Marta Morgado Correia. Unique information from common diffusion mri models about white-matter differences across the human adult lifespan. *Imaging Neuroscience*, 2023.
- [50] Peter J Basser, James Mattiello, and Denis LeBihan. Mr diffusion tensor spectroscopy and imaging. *Biophysical journal*, 66(1):259–267, 1994.
- [51] Derek K Jones. Studying connections in the living human brain with diffusion mri. *cortex*, 44(8):936–952, 2008.
- [52] Marco Catani, Derek K Jones, Eileen Daly, Nitzia Embiricos, Quinton Deeley, Luca Pugliese, Sarah Curran, Dene Robertson, and Declan GM Murphy. Altered cerebellar feedback projections in asperger syndrome. *Neuroimage*, 41(4):1184–1191, 2008.
- [53] David Solomon Tuch et al. *Diffusion MRI of complex tissue structure*. PhD thesis, Massachusetts Institute of Technology, 2002.
- [54] Abhishek Tiwari and Rajeev Kumar Singh. Performance, trust, or both? covid-19 diagnosis and prognosis using deep ensemble transfer learning on x-ray images. pages 1–9, 2022.
- [55] Vladimir Golkov, Alexey Dosovitskiy, Jonathan I Sperl, Marion I Menzel, Michael Czisch, Philipp Sämann, Thomas Brox, and Daniel Cremers. Q-space deep learning: twelve-fold shorter and model-free diffusion mri scans. *IEEE transactions on medical imaging*, 35(5):1344–1351, 2016.
- [56] Eric K Gibbons, Kyler K Hodgson, Akshay S Chaudhari, Lorie G Richards, Jennifer J Majersik, Ganesh Adluru, and Edward VR DiBella. Simultaneous noddi and gfa parameter map generation from subsampled q-space imaging using deep learning. *Magnetic resonance in medicine*, 81(4):2399–2411, 2019.
- [57] Matthew Leming. Application of deep learning to brain connectivity classification in large mri datasets. 2020.
- [58] Qiyuan Tian, Ziyu Li, Qiuyun Fan, J. Polimeni, Berkin Bilgiç, David H. Salat, and Susie Yi Huang. Sdndti: Self-supervised deep learning-based denoising for diffusion tensor mri. *NeuroImage*, 253, 2021.
- [59] Fan Zhang, Tengfei Xue, Weidong (Tom) Cai, Yogesh Rathi, Carl-Fredrik Westin, and Lauren J. O'Donnell. Tractoformer: A novel fiber-level whole brain tractography analysis framework using spectral embedding and vision transformers. 2022.

- [60] Chantal M. W. Tax, Matteo Bastiani, Jelle Veraart, E. Garyfallidis, and M. Okan Irfanoglu. What’s new and what’s next in diffusion mri preprocessing. *NeuroImage*, 249:118830 – 118830, 2021.
- [61] Eric Aliotta, Hamidreza Nourzadeh, Jason Sanders, Donald Muller, and Daniel B Ennis. Highly accelerated, model-free diffusion tensor mri reconstruction using neural networks. *Medical physics*, 46(4):1581–1591, 2019.
- [62] Vishwesh Nath, Kurt G Schilling, Prasanna Parvathaneni, Colin B Hansen, Allison E Hainline, Yuankai Huo, Justin A Blaber, Ilwoo Lyu, Vaibhav Janve, Yurui Gao, et al. Deep learning reveals untapped information for local white-matter fiber reconstruction in diffusion-weighted mri. *Magnetic resonance imaging*, 62:220–227, 2019.
- [63] Simon Koppers, Christoph Haarburger, J Christopher Edgar, and Dorit Merhof. Reliable estimation of the number of compartments in diffusion mri. pages 203–208, 2017.
- [64] Simon Koppers and Dorit Merhof. Direct estimation of fiber orientations using deep learning in diffusion imaging. pages 53–60, 2016.
- [65] Zhichao Lin, Ting Gong, Kewen Wang, Zhiwei Li, Hongjian He, Qiqi Tong, Feng Yu, and Jianhui Zhong. Fast learning of fiber orientation distribution function for mr tractography using convolutional neural network. *Medical physics*, 46(7):3101–3116, 2019.
- [66] Simon Koppers, Matthias Friedrichs, and Dorit Merhof. Reconstruction of diffusion anisotropies using 3d deep convolutional neural networks in diffusion imaging. pages 393–404, 2017.
- [67] Ashish Vaswani, Noam Shazeer, Niki Parmar, Jakob Uszkoreit, Llion Jones, Aidan N Gomez, Łukasz Kaiser, and Illia Polosukhin. Attention is all you need. *Advances in neural information processing systems*, 30, 2017.
- [68] Ze Liu, Yutong Lin, Yue Cao, Han Hu, Yixuan Wei, Zheng Zhang, Stephen Lin, and Baining Guo. Swin transformer: Hierarchical vision transformer using shifted windows. pages 10012–10022, 2021.
- [69] Özgün Çiçek, Ahmed Abdulkadir, Soeren S Lienkamp, Thomas Brox, and Olaf Ronneberger. 3d u-net: learning dense volumetric segmentation from sparse annotation. pages 424–432, 2016.
- [70] Tim B Dyrby, Giorgio M Innocenti, Martin Bech, and Henrik Lundell. Validation strategies for the interpretation of microstructure imaging using diffusion mri. *Neuroimage*, 182:62–79, 2018.

- [71] Stephen Correia, Stephanie Y Lee, Thom Voorn, David F Tate, Robert H Paul, Song Zhang, Stephen P Salloway, Paul F Malloy, and David H Laidlaw. Quantitative tractography metrics of white matter integrity in diffusion-tensor mri. *Neuroimage*, 42(2):568–581, 2008.
- [72] Angelos Barmpoutis and Jiachen Zhuo. Diffusion kurtosis imaging: robust estimation from dw-mri using homogeneous polynomials. pages 262–265, 2011.
- [73] Gwenaëlle Douaud, Saâd Jbabdi, Timothy EJ Behrens, Ricarda A Menke, Achim Gass, Andreas U Monsch, Anil Rao, Brandon Whitcher, Gordon Kindlmann, Paul M Matthews, et al. Dti measures in crossing-fibre areas: increased diffusion anisotropy reveals early white matter alteration in mci and mild alzheimer’s disease. *Neuroimage*, 55(3):880–890, 2011.
- [74] Eloy Martinez-Heras, Francesco Grussu, Ferran Prados, Elisabeth Solana, and Sara Llufríu. Diffusion-weighted imaging: recent advances and applications. 42(5):490–506, 2021.
- [75] Paul A Taylor, A Alhamud, Andre van der Kouwe, Muhammad G Saleh, Barbara Laughton, and Ernesta Meintjes. Assessing the performance of different dti motion correction strategies in the presence of epi distortion correction. *Human brain mapping*, 37(12):4405–4424, 2016.
- [76] Mina Kim, Itamar Ronen, Kamil Ugurbil, and Dae-Shik Kim. Spatial resolution dependence of dti tractography in human occipito-callosal region. *Neuroimage*, 32(3):1243–1249, 2006.
- [77] Silvia De Santis, Derek K Jones, and Alard Roebroeck. Including diffusion time dependence in the extra-axonal space improves in vivo estimates of axonal diameter and density in human white matter. *NeuroImage*, 130:91–103, 2016.
- [78] Van J Wedeen, RP Wang, Jeremy D Schmahmann, Thomas Benner, Wen-Yih Isaac Tseng, Guangping Dai, DN Pandya, Patric Hagmann, Helen D’Arceuil, and Alex J de Crespigny. Diffusion spectrum magnetic resonance imaging (dsi) tractography of crossing fibers. *Neuroimage*, 41(4):1267–1277, 2008.
- [79] Maxime Descoteaux. High angular resolution diffusion imaging (hardi). *Wiley encyclopedia of electrical and electronics engineering*, pages 1–25, 1999.
- [80] Hui Zhang, Torben Schneider, Claudia A Wheeler-Kingshott, and Daniel C Alexander. Noddi: practical in vivo neurite orientation dispersion and density imaging of the human brain. *Neuroimage*, 61(4):1000–1016, 2012.
- [81] Christopher P Hess, Pratik Mukherjee, Eric T Han, Duan Xu, and Daniel B Vigneron. Q-ball reconstruction of multimodal fiber orientations using the spherical harmonic basis. *Magnetic Resonance in Medicine: An Official Journal of the International Society for Magnetic Resonance in Medicine*, 56(1):104–117, 2006.

- [82] Daniela Kuhnt, Miriam HA Bauer, Jan Egger, Mirco Richter, Tina Kapur, Jens Sommer, Dorit Merhof, and Christopher Nimsky. Fiber tractography based on diffusion tensor imaging compared with high-angular-resolution diffusion imaging with compressed sensing: initial experience. *Neurosurgery*, 72(0 1):165, 2013.
- [83] Vesna Prckovska, Tim HJM Peeters, Markus van Almsick, Bart ter Haar Romeny, and Anna Vilanova i Bartroli. Fused dti/hardi visualization. *IEEE Transactions on Visualization and Computer Graphics*, 17(10):1407–1419, 2010.
- [84] Nathan S White, Trygve B Leergaard, Helen D’Arceuil, Jan G Bjaalie, and Anders M Dale. Probing tissue microstructure with restriction spectrum imaging: histological and theoretical validation. *Human brain mapping*, 34(2):327–346, 2013.
- [85] Hongyang Du, Ruichen Zhang, Dusit Niyato, Jiawen Kang, Zehui Xiong, Dong In Kim, Xuemin Sherman Shen, and H Vincent Poor. Exploring collaborative distributed diffusion-based ai-generated content (aigc) in wireless networks. *IEEE Network*, 2023.
- [86] Dow-Mu Koh and David J Collins. Diffusion-weighted mri in the body: applications and challenges in oncology. *American Journal of Roentgenology*, 188(6):1622–1635, 2007.
- [87] Klaus H Maier-Hein, Peter F Neher, Jean-Christophe Houde, Marc-Alexandre Côté, Eleftherios Garyfallidis, Jidan Zhong, Maxime Chamberland, Fang-Cheng Yeh, Ying-Chia Lin, Qing Ji, et al. The challenge of mapping the human connectome based on diffusion tractography. *Nature communications*, 8(1):1349, 2017.
- [88] Matthew M Cheung, Edward S Hui, Kevin C Chan, Joseph A Helpern, Liqun Qi, and Ed X Wu. Does diffusion kurtosis imaging lead to better neural tissue characterization? a rodent brain maturation study. *Neuroimage*, 45(2):386–392, 2009.
- [89] Tianjia Zhu, Qinmu Peng, Austin Ouyang, and Hao Huang. Neuroanatomical underpinning of diffusion kurtosis measurements in the cerebral cortex of healthy macaque brains. *Magnetic resonance in medicine*, 85(4):1895–1908, 2021.
- [90] S Umesh Rudrapatna, Tadeusz Wieloch, Kerstin Beirup, Karsten Ruscher, Wouter Mol, Pavel Yanev, Alexander Leemans, Annette van der Toorn, and Rick M Dijkhuizen. Can diffusion kurtosis imaging improve the sensitivity and specificity of detecting microstructural alterations in brain tissue chronically after experimental stroke? comparisons with diffusion tensor imaging and histology. *Neuroimage*, 97:363–373, 2014.
- [91] Liu-Hong Zhu, Zhong-Ping Zhang, Fu-Nan Wang, Qi-Hua Cheng, and Gang Guo. Diffusion kurtosis imaging of microstructural changes in brain tissue affected by acute ischemic stroke in different locations. *Neural Regeneration Research*, 14(2):272, 2019.

- [92] Andrew B Rosenkrantz, Anwar R Padhani, Thomas L Chenevert, Dow-Mu Koh, Frederik De Keyzer, Bachir Taouli, and Denis Le Bihan. Body diffusion kurtosis imaging: basic principles, applications, and considerations for clinical practice. *Journal of Magnetic Resonance Imaging*, 42(5):1190–1202, 2015.
- [93] Rajikha Raja, Neelam Sinha, Jitender Saini, Anita Mahadevan, KVL Narasinga Rao, and Aarthi Swaminathan. Assessment of tissue heterogeneity using diffusion tensor and diffusion kurtosis imaging for grading gliomas. *Neuroradiology*, 58:1217–1231, 2016.
- [94] Ed X Wu and Matthew M Cheung. Mr diffusion kurtosis imaging for neural tissue characterization. *NMR in Biomedicine*, 23(7):836–848, 2010.
- [95] Trina Mitchell, Derek B Archer, Winston T Chu, Stephen A Coombes, Song Lai, Bradley J Wilkes, Nikolaus R McFarland, Michael S Okun, Mieniecia L Black, Ellen Herschel, et al. Neurite orientation dispersion and density imaging (noddi) and free-water imaging in parkinsonism. *Human brain mapping*, 40(17):5094–5107, 2019.
- [96] Maria Caranova, Júlia F Soares, Sónia Batista, Miguel Castelo-Branco, and João Valente Duarte. A systematic review of microstructural abnormalities in multiple sclerosis detected with noddi and dti models of diffusion-weighted magnetic resonance imaging. *Magnetic Resonance Imaging*, 2023.
- [97] Kouhei Kamiya, Masaaki Hori, and Shigeki Aoki. Noddi in clinical research. *Journal of neuroscience methods*, 346:108908, 2020.
- [98] Niall Colgan, Bernard Siow, James M O’Callaghan, Ian F Harrison, Jack A Wells, Holly E Holmes, Ozama Ismail, S Richardson, Daniel C Alexander, Emily C Collins, et al. Application of neurite orientation dispersion and density imaging (noddi) to a tau pathology model of alzheimer’s disease. *Neuroimage*, 125:739–744, 2016.
- [99] Amy FD Howard, Michiel Cottaar, Mark Drakesmith, Qiuyun Fan, Susie Y Huang, Derek K Jones, Frederik J Lange, Jeroen Mollink, Suryanarayana Umesh Rudrapatna, Qiyuan Tian, et al. Estimating axial diffusivity in the noddi model. *NeuroImage*, 262:119535, 2022.
- [100] Kadi Vaher, Paola Galdi, Manuel Blesa Cabez, Gemma Sullivan, David Q Stoye, Alan J Quigley, Michael J Thrippleton, Debby Bogaert, Mark E Bastin, Simon R Cox, et al. General factors of white matter microstructure from dti and noddi in the developing brain. *Neuroimage*, 254:119169, 2022.
- [101] Koji Kamagata, Taku Hatano, and Shigeki Aoki. What is noddi and what is its role in parkinson’s assessment? *Expert review of neurotherapeutics*, 16(3):241–243, 2016.

- [102] Fan Zhang, Anna Breger, Kang Ik Kevin Cho, Lipeng Ning, Carl-Fredrik Westin, Lauren J O'Donnell, and Ofer Pasternak. Deep learning based segmentation of brain tissue from diffusion mri. *Neuroimage*, 233:117934, 2021.
- [103] David B Douglas, Michael Iv, Pamela K Douglas, Anderson Ariana, Sjoerd B Vos, Roland Bammer, Michael Zeineh, and Max Wintermark. Diffusion tensor imaging of tbi: potentials and challenges. *Topics in magnetic resonance imaging: TMRI*, 24(5):241, 2015.
- [104] Liming Zhong, Tengfei Li, Hai Shu, Chao Huang, Jason Michael Johnson, Donald F Schomer, Ho-Ling Liu, Qianjin Feng, Wei Yang, and Hongtu Zhu. 2wm: tumor segmentation and tract statistics for assessing white matter integrity with applications to glioblastoma patients. *Neuroimage*, 223:117368, 2020.
- [105] Ting Gong, Qiqi Tong, Zhiwei Li, Hongjian He, Hui Zhang, and Jianhui Zhong. Deep learning-based method for reducing residual motion effects in diffusion parameter estimation. *Magnetic Resonance in Medicine*, 85(4):2278–2293, 2021.
- [106] William Consagra, Arun Venkataraman, and Zhengwu Zhang. Optimized diffusion imaging for brain structural connectome analysis. *IEEE Transactions on Medical Imaging*, 2022.
- [107] João P de Almeida Martins, Markus Nilsson, Björn Lampinen, Marco Palombo, Peter T While, Carl-Fredrik Westin, and Filip Szczepankiewicz. Neural networks for parameter estimation in microstructural mri: Application to a diffusion-relaxation model of white matter. *NeuroImage*, 244:118601, 2021.
- [108] Talia M Nir, Neda Jahanshad, Julio E Villalon-Reina, Arthur W Toga, Clifford R Jack, Michael W Weiner, Paul M Thompson, Alzheimer's Disease Neuroimaging Initiative (ADNI), et al. Effectiveness of regional dti measures in distinguishing alzheimer's disease, mci, and normal aging. *NeuroImage: clinical*, 3:180–195, 2013.
- [109] Vikash Gupta, Nicholas Ayache, and Xavier Pennec. Improving dti resolution from a single clinical acquisition: a statistical approach using spatial prior. pages 477–484, 2013.
- [110] Lauren J O'Donnell, Yannick Suter, Laura Rigolo, Pegah Kahali, Fan Zhang, Isaiah Norton, Angela Albi, Olutayo Olubiyi, Antonio Meola, Walid I Essayed, et al. Automated white matter fiber tract identification in patients with brain tumors. *NeuroImage: Clinical*, 13:138–153, 2017.
- [111] Maximilian Baust, Andreas Weinmann, Matthias Wieczorek, Tobias Lasser, Martin Storath, and Nassir Navab. Combined tensor fitting and tv regularization in diffusion tensor imaging based on a riemannian manifold approach. *IEEE Transactions on Medical Imaging*, 35:1972–1989, 2016.

- [112] Denis Le Bihan, Jean-François Mangin, Cyril Poupon, Chris A Clark, Sabina Pappata, Nicolas Molko, and Hughes Chabriat. Diffusion tensor imaging: concepts and applications. *Journal of Magnetic Resonance Imaging: An Official Journal of the International Society for Magnetic Resonance in Medicine*, 13(4):534–546, 2001.
- [113] James G Malcolm, Martha E Shenton, and Yogesh Rathi. Filtered multitensor tractography. *IEEE transactions on medical imaging*, 29(9):1664–1675, 2010.
- [114] Richard AI Bethlehem, Jakob Seidlitz, Simon R White, Jacob W Vogel, Kevin M Anderson, Chris Adamson, Sophie Adler, George S Alexopoulos, Evdokia Anagnostou, Ariosity Areces-Gonzalez, et al. Brain charts for the human lifespan. *Nature*, 604(7906):525–533, 2022.
- [115] Steen Moeller, Pramod Pisharady Kumar, Jesper Andersson, Mehmet Akcakaya, Noam Harel, Ruoyun Ma, Xiaoping Wu, Essa Yacoub, Christophe Lenglet, and Kamil Ugurbil. Diffusion imaging in the post hcp era. *Journal of Magnetic Resonance Imaging*, 54(1):36–57, 2021.
- [116] Andy Wai Kan Yeung, Shammi More, Jianxiao Wu, and Simon B Eickhoff. Reporting details of neuroimaging studies on individual traits prediction: a literature survey. *NeuroImage*, 256:119275, 2022.
- [117] Chase R Figley, Md Nasir Uddin, Kaihim Wong, Jennifer Kornelsen, Josep Puig, and Teresa D Figley. Potential pitfalls of using fractional anisotropy, axial diffusivity, and radial diffusivity as biomarkers of cerebral white matter microstructure. *Frontiers in Neuroscience*, 15:799576, 2022.
- [118] Ilana J Bennett, David J Madden, Chandan J Vaidya, Darlene V Howard, and James H Howard Jr. Age-related differences in multiple measures of white matter integrity: A diffusion tensor imaging study of healthy aging. *Human brain mapping*, 31(3):378–390, 2010.
- [119] Qiyuan Tian, Ziyu Li, Qiuyun Fan, Jonathan R Polimeni, Berkin Bilgic, David H Salat, and Susie Y Huang. Sdnndti: Self-supervised deep learning-based denoising for diffusion tensor mri. *NeuroImage*, 253:119033, 2022.
- [120] Jes Olesen. Headache classification committee of the international headache society (ihs) the international classification of headache disorders. *Cephalgia*, 38(1):1–211, 2018.
- [121] Catherine D Chong, Jacob Peplinski, Visar Berisha, Katherine Ross, and Todd J Schwedt. Differences in fibertract profiles between patients with migraine and those with persistent post-traumatic headache. *Cephalgia*, 39(9):1121–1133, 2019.
- [122] Andreas Kattem Husøy, Live Eikenes, Asta K Håberg, Knut Hagen, and Lars Jacob Stovner. Diffusion tensor imaging in middle-aged headache sufferers in the general population: a cross-sectional population-based imaging study in the nord-trøndelag health study (hunt-mri). *The Journal of Headache and Pain*, 20(1):1–15, 2019.

- [123] Álvaro Planchuelo-Gómez, David García-Azorín, Ángel L Guerrero, Santiago Aja-Fernández, Margarita Rodríguez, and Rodrigo de Luis-García. White matter changes in chronic and episodic migraine: a diffusion tensor imaging study. *The journal of headache and pain*, 21:1–15, 2020.
- [124] Gianluca Coppola, Antonio Di Renzo, Emanuele Tinelli, Barbara Petolicchio, Cherubino Di Lorenzo, Vincenzo Parisi, Mariano Serrao, Valentina Calistri, Stefano Tardioli, Gaia Cartocci, et al. Patients with chronic migraine without history of medication overuse are characterized by a peculiar white matter fiber bundle profile. *The Journal of Headache and Pain*, 21(1):1–8, 2020.
- [125] Rahil Rahimi, Mahsa Dolatshahi, Fatemeh Abbasi-Feijani, Sara Momtazmanesh, Giulia Cattarinussi, Mohammad Hadi Aarabi, and Lorenzo Pini. Microstructural white matter alterations associated with migraine headaches: a systematic review of diffusion tensor imaging studies. *Brain Imaging and Behavior*, 16(5):2375–2401, 2022.
- [126] Alvaro Planchuelo-Gomez, David Garcia-Azorin, Angel L Guerrero, Santiago Aja-Fernandez, Margarita Rodriguez, and Rodrigo de Luis-Garcia. Structural connectivity alterations in chronic and episodic migraine: A diffusion magnetic resonance imaging connectomics study. *Cephalgia*, 40(4):367–383, 2020.
- [127] Peter J Basser. Relationships between diffusion tensor and q-space mri. *Magnetic Resonance in Medicine: An Official Journal of the International Society for Magnetic Resonance in Medicine*, 47(2):392–397, 2002.
- [128] C-F Westin, Stephan E Maier, Hatsuhiko Mamata, Arya Nabavi, Ferenc A Jolesz, and Ron Kikinis. Processing and visualization for diffusion tensor mri. *Medical image analysis*, 6(2):93–108, 2002.
- [129] Yuchuan Qiao and Yonggang Shi. Unsupervised deep learning for fod-based susceptibility distortion correction in diffusion mri. *IEEE transactions on medical imaging*, 41(5):1165–1175, 2021.
- [130] Adnan Ahmad, Drew Parker, Suhani Dheer, Zahra Riahi Samani, and Ragini Verma. 3d-qcnet—a pipeline for automated artifact detection in diffusion mri images. *Computerized Medical Imaging and Graphics*, 103:102151, 2023.
- [131] Hemant K Aggarwal, Merry P Mani, and Mathews Jacob. Modl-mussels: Model-based deep learning for multishot sensitivity-encoded diffusion mri. *IEEE transactions on medical imaging*, 39(4):1268–1277, 2019.
- [132] Shreyas Fadnavis, Joshua Batson, and Eleftherios Garyfallidis. Patch2self: Denoising diffusion

- mri with self-supervised learning. *Advances in Neural Information Processing Systems*, 33:16293–16303, 2020.
- [133] Alyssa H Zhu, Daniel C Moyer, Talia M Nir, Paul M Thompson, and Neda Jahanshad. Challenges and opportunities in dmri data harmonization. pages 157–172, 2019.
- [134] Chantal MW Tax, Francesco Grussu, Enrico Kaden, Lipeng Ning, Umesh Rudrapatna, C John Evans, Samuel St-Jean, Alexander Leemans, Simon Koppers, Dorit Merhof, et al. Cross-scanner and cross-protocol diffusion mri data harmonisation: A benchmark database and evaluation of algorithms. *NeuroImage*, 195:285–299, 2019.
- [135] Daniel Moyer, Greg Ver Steeg, Chantal MW Tax, and Paul M Thompson. Scanner invariant representations for diffusion mri harmonization. *Magnetic resonance in medicine*, 84(4):2174–2189, 2020.
- [136] Stefano B Blumberg, Marco Palombo, Can Son Khoo, Chantal MW Tax, Ryutaro Tanno, and Daniel C Alexander. Multi-stage prediction networks for data harmonization. pages 411–419, 2019.
- [137] Eduardo HMSG de Figueiredo, Arthur FNG Borgonovi, and Thomas M Doring. Basic concepts of mr imaging, diffusion mr imaging, and diffusion tensor imaging. *Magnetic Resonance Imaging Clinics*, 19(1):1–22, 2011.
- [138] PJ Basser and C Pierpaoli. Microstructural features measured using diffusion tensor imaging. *J Magn Reson B*, 111(3):209–219, 1996.
- [139] David S Tuch, Timothy G Reese, Mette R Wiegell, and Van J Wedeen. Diffusion mri of complex neural architecture. *Neuron*, 40(5):885–895, 2003.
- [140] Antonio Tristán-Vega, Carl-Fredrik Westin, and Santiago Aja-Fernández. Estimation of fiber orientation probability density functions in high angular resolution diffusion imaging. *NeuroImage*, 47(2):638–650, 2009.
- [141] Evren Özarslan, Timothy M Shepherd, Baba C Vemuri, Stephen J Blackband, and Thomas H Mareci. Resolution of complex tissue microarchitecture using the diffusion orientation transform (dot). *NeuroImage*, 31(3):1086–1103, 2006.
- [142] Derek K Jones. The effect of gradient sampling schemes on measures derived from diffusion tensor mri: a monte carlo study. *Magnetic Resonance in Medicine: An Official Journal of the International Society for Magnetic Resonance in Medicine*, 51(4):807–815, 2004.
- [143] Maxime Descoteaux, Elaine Angelino, Shaun Fitzgibbons, and Rachid Deriche. Regularized, fast, and robust analytical q-ball imaging. *Magnetic Resonance in Medicine: An Official Journal of the International Society for Magnetic Resonance in Medicine*, 58(3):497–510, 2007.

- [144] Geng Chen, Bin Dong, Yong Zhang, Weili Lin, Dinggang Shen, and Pew-Thian Yap. Angular upsampling in infant diffusion mri using neighborhood matching in x-q space. *Frontiers in Neuroinformatics*, 12:57, 2018.
- [145] Geng Chen, Bin Dong, Yong Zhang, Weili Lin, Dinggang Shen, and Pew-Thian Yap. Xq-sr: joint xq space super-resolution with application to infant diffusion mri. *Medical image analysis*, 57:44–55, 2019.
- [146] David S Tuch. Q-ball imaging. *Magnetic Resonance in Medicine: An Official Journal of the International Society for Magnetic Resonance in Medicine*, 52(6):1358–1372, 2004.
- [147] Mengwei Ren, Heejong Kim, Neel Dey, and Guido Gerig. Q-space conditioned translation networks for directional synthesis of diffusion weighted images from multi-modal structural mri. pages 530–540, 2021.
- [148] Matthew Lyon, Paul Armitage, and Mauricio A Álvarez. Angular super-resolution in diffusion mri with a 3d recurrent convolutional autoencoder. pages 834–846, 2022.
- [149] Rui Zeng, Jinglei Lv, He Wang, Luping Zhou, Michael Barnett, Fernando Calamante, and Chenyu Wang. Fod-net: A deep learning method for fiber orientation distribution angular super resolution. *Medical Image Analysis*, 79:102431, 2022.
- [150] Bennett A Landman, Jonathan AD Farrell, Craig K Jones, Seth A Smith, Jerry L Prince, and Susumu Mori. Effects of diffusion weighting schemes on the reproducibility of dti-derived fractional anisotropy, mean diffusivity, and principal eigenvector measurements at 1.5 t. *Neuroimage*, 36(4):1123–1138, 2007.
- [151] Gonzalo Barrio-Arranz, Rodrigo de Luis-García, Antonio Tristán-Vega, Marcos Martín-Fernández, and Santiago Aja-Fernández. Impact of mr acquisition parameters on dti scalar indexes: a tractography based approach. *PloS one*, 10(10):e0137905, 2015.
- [152] Shayan Kolahkaj et al. A connectome-based deep learning approach for early mci and mci detection using structural brain networks. *Neuroscience Informatics*, page 100118, 2023.
- [153] Yida Qu, Pan Wang, Bing Liu, Chengyuan Song, Dawei Wang, Hongwei Yang, Zengqiang Zhang, Pindong Chen, Xiaopeng Kang, Kai Du, et al. Ai4ad: artificial intelligence analysis for alzheimer’s disease classification based on a multisite dti database. *Brain Disorders*, 1:100005, 2021.
- [154] Shangran Qiu, Matthew I Miller, Prajakta S Joshi, Joyce C Lee, Chonghua Xue, Yunruo Ni, Yuwei Wang, Ileana De Anda-Duran, Phillip H Hwang, Justin A Cramer, et al. Multimodal deep learning for alzheimer’s disease dementia assessment. *Nature communications*, 13(1):3404, 2022.

- [155] Benoit Scherrer and Simon K Warfield. Parametric representation of multiple white matter fascicles from cube and sphere diffusion mri. *PLoS one*, 7(11):e48232, 2012.
- [156] Shuangshuang Gao and Dimas Lima. A review of the application of deep learning in the detection of alzheimer’s disease. *International Journal of Cognitive Computing in Engineering*, 3:1–8, 2022.
- [157] Eman N Marzban, Ayman M Eldeib, Inas A Yassine, Yasser M Kadah, and Alzheimer’s Disease Neurodegenerative Initiative. Alzheimer’s disease diagnosis from diffusion tensor images using convolutional neural networks. *Plos one*, 15(3):e0230409, 2020.
- [158] Ayşe Demirhan, Talia M Nir, Artemis Zavaliangos-Petropulu, Clifford R Jack, Michael W Weiner, Matt A Bernstein, Paul M Thompson, and Neda Jahanshad. Feature selection improves the accuracy of classifying alzheimer disease using diffusion tensor images. pages 126–130, 2015.
- [159] Liang Zhan, Matt A Bernstein, B Borowski, Clifford R Jack, and Paul M Thompson. Evaluation of diffusion imaging protocols for the alzheimer’s disease neuroimaging initiative. pages 710–713, 2014.
- [160] Karim Aderghal, Karim Afdel, Jenny Benois-Pineau, and Gwénaëlle Catheline. Improving alzheimer’s stage categorization with convolutional neural network using transfer learning and different magnetic resonance imaging modalities. *Heliyon*, 6(12), 2020.
- [161] Sukrit Arora, Michael Lustig, and Stella Yu. Deep learning applications in computational mri: A thesis in two parts. 2021.
- [162] Zhenbing Liu, Haoxiang Lu, Xipeng Pan, Mingchang Xu, Rushi Lan, and Xiaonan Luo. Diagnosis of alzheimer’s disease via an attention-based multi-scale convolutional neural network. *Knowledge-Based Systems*, 238:107942, 2022.
- [163] M Tanveer, MA Ganaie, Iman Beheshti, Tripti Goel, Nehal Ahmad, Kuan-Ting Lai, Kaizhu Huang, Yu-Dong Zhang, Javier Del Ser, and Chin-Teng Lin. Deep learning for brain age estimation: A systematic review. *Information Fusion*, 2023.
- [164] Prajit Ramachandran, Niki Parmar, Ashish Vaswani, Irwan Bello, Anselm Levskaya, and Jon Shlens. Stand-alone self-attention in vision models. *Advances in neural information processing systems*, 32, 2019.
- [165] Han Hu, Zheng Zhang, Zhenda Xie, and Stephen Lin. Local relation networks for image recognition. pages 3464–3473, 2019.
- [166] Eleftherios Garyfallidis, Matthew Brett, Bagrat Amirbekian, Ariel Rokem, Stefan Van Der Walt, Maxime Descoteaux, Ian Nimmo-Smith, and Dipy Contributors. Dipy, a library for the analysis of diffusion mri data. *Frontiers in neuroinformatics*, 8:8, 2014.

- [167] Jelle Veraart, Dmitry S Novikov, Daan Christiaens, Benjamin Ades-Aron, Jan Sijbers, and Els Fieremans. Denoising of diffusion mri using random matrix theory. *Neuroimage*, 142:394–406, 2016.
- [168] Jesper LR Andersson and Stamatiou N Sotiroopoulos. An integrated approach to correction for off-resonance effects and subject movement in diffusion mr imaging. *Neuroimage*, 125:1063–1078, 2016.
- [169] Stephen M Smith, Mark Jenkinson, Mark W Woolrich, Christian F Beckmann, Timothy EJ Behrens, Heidi Johansen-Berg, Peter R Bannister, Marilena De Luca, Ivana Drobniak, David E Flitney, et al. Advances in functional and structural mr image analysis and implementation as fsl. *Neuroimage*, 23:S208–S219, 2004.
- [170] Yongyue Zhang, Michael Brady, and Stephen Smith. Segmentation of brain mr images through a hidden markov random field model and the expectation-maximization algorithm. *IEEE transactions on medical imaging*, 20(1):45–57, 2001.
- [171] J-Donald Tournier, Robert Smith, David Raffelt, Rami Tabbara, Thijs Dhollander, Maximilian Pietsch, Daan Christiaens, Ben Jeurissen, Chun-Hung Yeh, and Alan Connelly. Mrtrix3: A fast, flexible and open software framework for medical image processing and visualisation. *Neuroimage*, 202:116137, 2019.
- [172] Thijs Dhollander, David Raffelt, and Alan Connelly. Unsupervised 3-tissue response function estimation from single-shell or multi-shell diffusion mr data without a co-registered t1 image. 5(5), 2016.
- [173] Mark Jenkinson, Christian F Beckmann, Timothy EJ Behrens, Mark W Woolrich, and Stephen M Smith. Fsl. *Neuroimage*, 62(2):782–790, 2012.
- [174] Susumu Mori, Kenichi Oishi, Hangyi Jiang, Li Jiang, Xin Li, Kazi Akhter, Kegang Hua, Andreia V Faria, Asif Mahmood, Roger Woods, et al. Stereotaxic white matter atlas based on diffusion tensor imaging in an icbm template. *Neuroimage*, 40(2):570–582, 2008.
- [175] Zhou Wang, Alan C Bovik, Hamid R Sheikh, and Eero P Simoncelli. Image quality assessment: from error visibility to structural similarity. *IEEE transactions on image processing*, 13(4):600–612, 2004.
- [176] Stephen M Smith, Mark Jenkinson, Heidi Johansen-Berg, Daniel Rueckert, Thomas E Nichols, Clare E Mackay, Kate E Watkins, Olga Ciccarelli, M Zaheer Cader, Paul M Matthews, et al. Tract-based spatial statistics: voxelwise analysis of multi-subject diffusion data. *Neuroimage*, 31(4):1487–1505, 2006.

- [177] Daniel Rueckert, Luke I Sonoda, Carmel Hayes, Derek LG Hill, Martin O Leach, and David J Hawkes. Nonrigid registration using free-form deformations: application to breast mr images. *IEEE transactions on medical imaging*, 18(8):712–721, 1999.
- [178] John S Duncan. Imaging in the surgical treatment of epilepsy. *Nature Reviews Neurology*, 6(10):537–550, 2010.
- [179] Yu-Qi Yang, Peng-Shuai Wang, and Yang Liu. Interpolation-aware padding for 3d sparse convolutional neural networks. pages 7467–7475, 2021.